ENGINEERING OF AN IMMUNOMODULATIVE NANODRUG FOR THERANOSTICS AND
BIOMEDICAL APPLICATIONS

By

Kay Elaine Hadrick

A DISSERTATION

Submitted to
Michigan State University
in partial fulfillment of the requirements
for the degree of

Biomedical Engineering – Doctor of Philosophy

2025

ABSTRACT

The immune system plays a critical role in many disease processes, and when it is functioning

properly, it provides robust protection from both internal and external threats. However, when

the immune system behaves inappropriately, chronic and potentially deadly diseases can occur.

The treatment of these diseases, which range from rheumatoid arthritis to solid tumor cancers,

is complicated by the fact that though the immune system is implicated, the mechanism of

action is different between conditions. Specifically, some diseases are characterized by

inflammation while others are characterized by immune suppression. Current treatments for

inflammatory and anti-inflammatory conditions are insufficient to overcome the burden of

these diseases since many patients either do not respond to treatment or suffer from severe

side effects. However, nanomedicine, which remains underutilized, shows remarkable promise

as an option for treating these diseases. Nanoceria, with its unique enzymatic properties, small

size, and highly tunable synthesis, makes a promising candidate for the treatment of conditions

in which macrophages play a major role. The focus of this project was the development of a

nanoceria-based immunomodulative drug capable of driving the polarization of macrophages

toward either a pro or anti-inflammatory state. Use of albumin and single-walled carbon

nanotube substrates and variations in synthetic conditions allowed for the development of

multiple formulations of the nanodrug with different properties including enzymatic activity,

STAT3 inhibition, and targeting. Further modification of these particles can allow for the

inclusion of fluorescence and photoacoustic contrast. Thus, by characterizing these nano-

formulations and testing their effects *in vitro* and *in vivo*, we can develop highly effective

immunomodulatory theranostics. We explore the potential of nanoceria as a diagnostic and

treatment for endometriosis, a chronic inflammatory condition. Additionally, since nanoparticles offer high diagnostic specificity, it is possible to create novel imaging agents based on fluorescent silica nanoparticles, for diseases such as colorectal cancer which require enhanced imaging options. Ultimately, by utilizing the tunable properties of nanomaterials, we can create new diagnostics and therapeutics capable of improving the health of patients and enhancing their quality of life.

I would like to dedicate this dissertation to Meghan Hill, Leah Terrian, and Jacob Reynolds. Without the three of you, I would not have had the strength to achieve all that I have in graduate school. You have been with me on the entire journey, and I am incredibly grateful.

TABLE OF CONTENTS

LIST OF ABBREVIATIONS

Arg-1 – Arginase-1

AuNR – Gold Nanorod

CAR – Center for Animal Resources

CD – Cluster of Differentiation

CEA – Carcinoembryonic Antigen

CIA – Collagen Induced Arthritis

CRC – Colorectal Cancer

CT – Computerized Tomography

DCFDA – 2',7'-dichlorodihydrofluorescein Diacetate

DDI – Double-Distilled Water

DLS – Dynamic Light Scattering

DMSO – Dimethyl Sulfoxide

DNA – Deoxynucleic Acid

DSPE – 1, 2-Distearoyl-sn-glycero-3-phosphoethanolamine

EPR – Enhanced Permeability and Retention Effect

FBS – Fetal Bovine Serum

FCC – Face Centered Cubic

FDA – Food and Drug Administration

FSN – Fluorescent Silica Nanoparticles

H_2O_2 – Hydrogen Peroxide

H&E – Hematoxylin and Eosin

HRTEM – High Resolution Transmission Electron Microscopy

IACUC - Institutional Animal Care and Use Committee

ICG – Indocyanine Green

ICP – Inductively Coupled Plasma

ICP-OES – Inductively Coupled Plasma Optical Emission Spectrometry

IF – Immunofluorescence

IFN – Interferon

IHC – Immunohistochemistry

IL – Interleukin

IONP – Iron Oxide Nanoparticle

IR – Infrared

IV – Intravenous

JAK – Janus Family Kinase

LITT – Laser Interstitial Thermal Therapy

LPS – Lipopolysaccharide

MPI – Magnetic Particle Imaging

MPTMS – (3-mercaptopropyl) Rrimethoxysilane

MRI – Magnetic Resonance Imaging

mRNA – Messenger Ribonucleic Acid

MSOT - Multispectral Optoacoustic Tomographic Imaging System

MTT - 3-(4,5-Dimethylthiazol-2-yl)-2,5-diphenyltetrazolium bromide

NAC – N-acetylcysteine

NIR – Near-Infrared

NIRF – Near-Infrared Fluorescence Imaging

NIR II – Second Near-Infrared

NSAID – Nonsteroidal Anti-Inflammatory Drug

OCT – Optimal Cutting Temperature

PBS – Phosphate Buffered Saline

PDI – Polydispersity Index

PEG – Poly-Ethylene Glycol

PFA – Paraformaldehyde

PLGA – Poly Lactic-co-Glycolic Acid

pSTAT3 – Phosphorylated Signal Transducer and Activator of Transcription 3

Purpald – 4-amino-3-hydrazino-5-mercapto-1,2,4-traizole

RITC – Rhodamine Isothiocyanate

RNA – Ribonucleic Acid

ROS – Reactive Oxygen Species

SBF – Simulated Body Fluid

SOD – Superoxide Dismutase

SPION – Super Paramagnetic Iron Oxide Nanoparticle

STAT3 – Signal Transducer and Activator of Transcription 3

SWCNT – Single Wall Carbon Nanotube

TAM – Tumor Associated Macrophage

TEM – Transmission Electron Microscopy

TNF – Tumor Necrosis Factor

UV – Ultraviolet

XPS – X-ray Photoelectron Spectroscopy

Chapter 1: Introduction

1.1 General Overview of Nanoparticles and Nanomedicine

Despite the incredible progress made over the last century in the realm of modern medicine, many conditions have either no available treatment or an imperfect solution. Cancers, inflammatory, and autoimmune conditions are particularly challenging, often requiring treatments with severe side effects that may not resolve or even improve the condition they are used for[1, 2]. In some cases, the medication used to treat cancers can decrease quality of life more than the cancer itself[1] while medications used to treat immune conditions can either suppress the immune system leaving patients vulnerable to infectious diseases or over activate the immune system leading to chronic inflammation and pain[2, 3]. In many cases, patients with serious conditions must consider whether they would like to have more time with a lower quality of life or less time with a higher quality of life. This is never an easy choice, and in many cases can be devastating, leading to poor mental health and worse outcomes for patients[4, 5]. For this reason, medical scientists have been exploring a myriad of solutions to these critical problems. One such solution involves the use of nanomaterials in medical applications. While medical applications of nanoparticles are a relatively new phenomenon, humans have been creating and using nanomaterials since Roman times. One of the earliest and best-known examples is the Lycurgus cup which appears green in direct light but red if light is shined through the inside of the glass thanks to silver and gold composite particles (~ 30:70)[6] (Figure 1). Though it is unlikely that the ancient Romans intentionally synthesized nanoparticles, they were aware of their unique optical properties and took advantage of them to create, undeniably, one of the most impressive works of ancient glass. Fascinatingly, despite the loss of

a lot of Roman knowledge leading into the Middle Ages, the ability to make colorful glass by using what we now know are nanoparticles was preserved. The striking stained-glass windows found in churches, and fortunately preserved to the current day, contain silver and gold nanoparticles of varying sizes and shapes lending them their long-lasting color[6, 7] (Figure 1). However, historic use of nanomaterials was not relegated to glass work. In the realm of renaissance art, we see the use of glimmering ceramic glazes adopted from Islamic tradition that get their stunning effect from silver or copper nanoparticles embedded in the glaze prior to firing[8] (Figure 1). In a strikingly less artistic application, so called "Damascus blades," developed with techniques from the Ottoman Empire, employed what we now know were nanowires and nanotubes to create unusually strong and sharp swords for the time[6, 9] (Figure 1).

Figure 1: A timeline of early nanomaterials with representative images. The timeline runs from the 4th to the 19th century. In the mid-19th century, the modern era of nanomaterials began thanks to the development of novel analysis techniques. (Images adapted from Bayda et al. 2020[6], Chari et. al 2022[10], and Ghosal and Chakraborty 2015[11]).

It wasn't until we were able to intentionally synthesize and characterize nanomaterials in more detail that precision applications became possible. In the 1960s and 1970s, scientists began considering what "nanomedicine" could be. Armed with new tools like TEM for visualizing objects on the nanometer scale[12] (Figure 2), ICP for accurate elemental analysis[13], and XPS for evaluating surface chemistry[14], these pioneers considered a wide variety of applications before settling on drug delivery as the first step towards modern nanomedicine[6, 15]. By taking advantage of their small size and modifiable surface, scientists began nanoparticles to specific disease processes. For example, drug-loaded mesoporous silica nanoparticles can be routinely synthesized in standard laboratory conditions and can be further modified to include molecular targeting capabilities through the conjugation of antibodies or peptides[16]. Polymer based nanoparticles, like those made of PLGA, are capable of controlled release allowing for continuous release of a drug over time avoiding the need for multiple doses of medication overtime[17, 18], and lipid based particles are exceptionally biocompatible preventing toxic side effects of small molecule drugs encapsulated within[19]. This work on drug delivery eventually led to the discovery and 1995 FDA approval of Doxil (Figure 2), a liposome based chemotherapeutic comprised of a liposome containing doxorubicin capable of more accurately targeting tumors through the EPR effect[20]. After the success of Doxil, medical applications of nanoparticles have become even more prevalent with over 500 clinical trials underway at the end of 2022[21]. Alongside drug delivery applications, nanoparticles have been heavily explored as imaging agents providing contrast to enhance medical imaging. In MRI, SPIONs (Figure 2) and gadolinium-based materials are used to provide enhanced contrast (Table 1) especially in applications where it can be difficult to distinguish between healthy and diseased tissues[22]. One

such application is the detection of small, metastatic lesions present in advanced cancers. Though these smaller tumors may not be immediately distinguishable using intrinsic contrast, they "light up" on imaging when nanoparticles localize to them allowing for easy detection and more accurate cancer staging[23]. In photoacoustic imaging, nanoparticles amplify the light-in, sound-out effect responsible for the generation of high-quality images (Table 1). Perhaps the best-known nano-photoacoustic contrast agent are AuNRs which exhibit plasmonic resonance due to their unique shape and high aspect ratio[24, 25]. The use of these particles allows for both enhanced image quality and depth allowing for the clinical translation of this emerging imaging modality. There are also novel imaging techniques which require nanoparticle contrast agents to function. MPI, chief among these, has no background from tissue and generates all its signal from SPIONs injected prior to imaging[26] (Table 1). This allows for functionally unlimited imaging depth and extremely high resolution even in tissue deep in the body especially when used in connection with CT imaging[27].
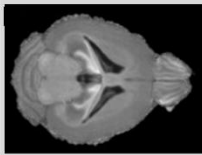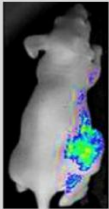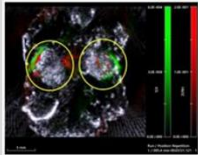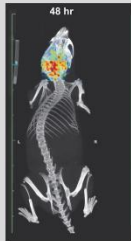
	MRI	Fluorescence	Photoacoustic Imaging	MPI	CT
Pros	• High contrast imaging • Detailed anatomical information • Unlimited imaging depth	• High sensitivity • Excellent specificity • Tunable ex/em • Cheap	• Excellent temporal Resolution • Minimal optical scattering	• No background from tissue • Unlimited imaging depth • Certain detection of contrast agent	• Good temporal resolution • Lower cost • Excellent hard tissue detail
Cons	• Poor temporal resolution • High Cost	• Extremely limited depth • NIR dyes expensive	• Limited imaging depth • Emerging tech	• Poor temporal resolution • Emerging tech • High Cost • No anatomical detail	• Exposure to radiation • Poor soft tissue resolution
Image Example					

Table 1: A table describing the pros and cons of various nano-enhanced imaging modalities. (Images adapted from Arbabi et. al 2022[28], Huang et. al 2019[29], Kalashnikova et. al 2020[30], Wu et. al 2019[31], and Beaucage et. al 2016[32].

Finally, for the purposes of this dissertation, there are nanoparticles which can be used directly to treat disease. These can be nanoparticle drugs that act directly like Prussian Blue nanoparticles which are FDA approved to treat heavy metal poisoning[33] and silver nanoparticles incorporated into bandages used to prevent infection[34]. They can also be nanoparticles that enhance or allow for other treatments such as AuNRs in laser ablation[35] or SPIONs in magnetic hyperthermia[36]. Overall, nanoparticles have a storied history, and modern scientists have learned to employ them for a multitude of medical purposes. With more nanoparticles being synthesized, investigated, and approved, nanomedicine is sure to be a key component of a healthier population in the 21st century and beyond.
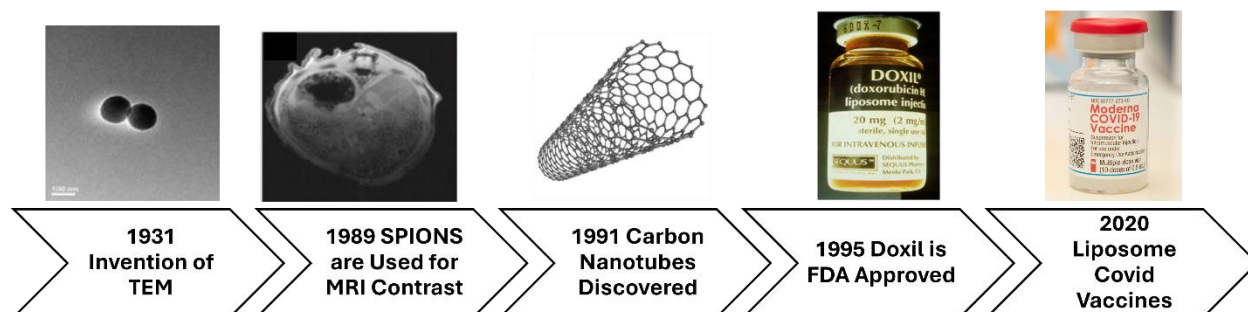
Figure 2: A timeline showing major moments in the progression of nanomedicine in the modern era. (Images adapted from Chung et. al 2024[37], Li et. al 2013[38], Goldmann et. al 2021[39], and Barenholz 2012[20]).

1.2 Overview of Inflammation and Immune Suppression

Inflammation and immune suppression are both key processes in a healthy individual. The immune system is a complex network of cells, signaling molecules, and pathways that keeps the body safe from external threats like microorganisms and foreign objects while simultaneously preventing the cells key to these processes from attacking healthy tissue. In most people, the immune system is balanced between pro-inflammatory and anti-inflammatory processes allowing for unique responses to different situations that arise in the body. Most people are familiar with the sensation of inflammation. On the macro level, inflammation is easy to identify by its distinctive characteristics. Swelling, heat, altered function, redness, and pain are the common symptoms of inflammation. Referred to in Latin as *tumor, calor, rubor,* and *dolor* or by the first aid acronym SHARP, inflammation comes in two main types[40]. The first, acute inflammation, is characterized by short term response from the innate immune system while

the second, chronic inflammation, takes place on a much longer time scale and has greater

involvement from the adaptive immune system[41].

Acute inflammation is a common process that is vital to survival and healing. In response to

stimuli, commonly unique molecules from invading organisms like LPS or intercellular proteins

in the extracellular environment due to injury, the innate immune system activates. Though

mast cells, the body's sentries that initially detect disruption, begin the signaling cascade[42], the

inflammatory process really starts with the neutrophils: phagocytes which take up and destroy

foreign material and damaged cells while simultaneously signaling for other cells through

endocrine secretion of cytokines[43]. Macrophages and T cells, after arriving at the site of injury,

begin to differentiate and secrete their own chemokines and cytokines contributing to the

overall acute, adaptive immune response[44] (Figure 3). Specifically, CD8 and CD4 T cells and M1

macrophages mediate the next stage of response to inflammation. While CD8 cells mainly

produce cytotoxic chemicals, CD4 cells instead recruit and control the balance of other immune

cells in the inflammatory environment[45]. CD4 T cells are in large part responsible for sending the

chemical signals that drive the behavior of other immune cells in the area. For macrophages,

they are responsible for mediating the modulation of the cells towards a desired state. In cases

where inflammation is ongoing, macrophages receive molecular signals such as IFN-γ from CD4

T cells and become pro-inflammatory M1 macrophages. These macrophages further signal

neutrophils creating a positive feedback loop that drives inflammatory response[44].

However, to allow for healing and prevent long periods of inflammation, the same cytokine

signaling pathways can be used to trigger an anti-inflammatory response. As CD4 T cells are

secreting IFN-γ and activating macrophages, the same cytokine is attracting and activating anti-

inflammatory B cells[44]. B cells, which secrete growth factors and anti-inflammatory cytokines, are critical to resolving acute inflammation[46] (Figure 3). They counteract the positive feedback loop described above by producing potent anti-inflammatories which in turn signal the macrophages to become M2 anti-inflammatory. IL-10 in particular plays a key role in this process by signaling to mast cells to stop recruiting neutrophils, to the CD4 T cells to stop participating in the positive feedback loop of producing pro-inflammatory cytokines, and to the macrophages to change from M1 to M2 cells[44]. As the inflammation resolves and an anti-inflammatory environment arises, cytokines promoting angiogenesis and blood flow, like TNFα[47], become more prevalent allowing the body to heal and return to its pre-injury state.
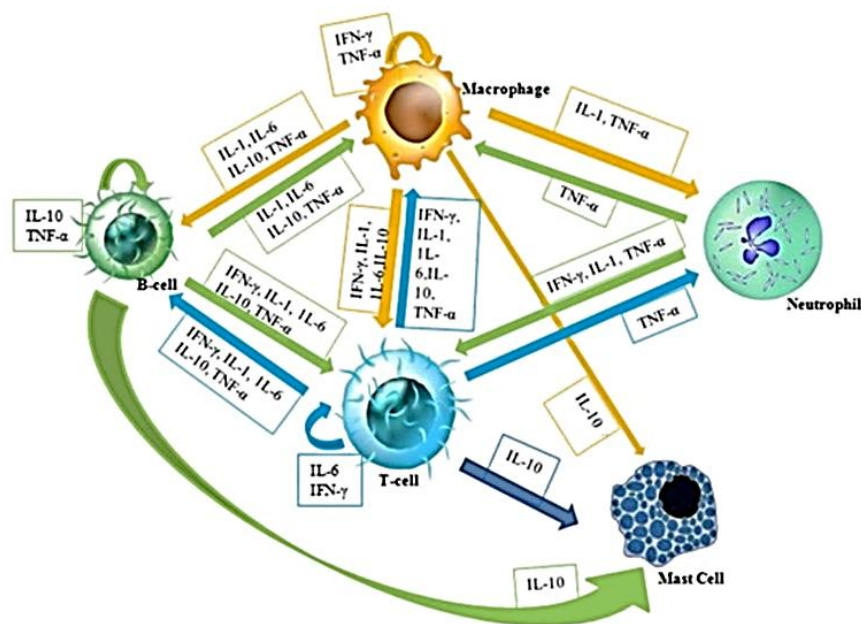

Figure 3: A graphic representing the cytokine signaling between cells involved in the innate immune response including the development and resolution of acute inflammations. (Figure from Megha et. al 2021[44]).

When this critical immune balance fails, people develop a wide variety of different conditions.

Many are familiar with chronic inflammatory conditions. Known for their characteristic pain and

sometimes life-long duration, common diseases like rheumatoid arthritis, which affects around

1% of the global population[48], are perhaps the easiest inflammatory conditions to highlight.

However, there are many chronic inflammatory conditions. These conditions can be relatively

minor as in some cases of psoriasis that leave patients with irritated skin and flakey, dry patches

but ultimately will not kill or even seriously injure a patient[49]. However, they can also be

devastating and potentially fatal. Cardiovascular diseases including high blood pressure and

heart disease are known to result from chronic inflammation and can contribute to heart attack

and stroke which are debilitating if not deadly[50]. Lung diseases like asthma, which is

characterized by inappropriate eosinophil response[51], and chronic obstructive pulmonary

disease cause more than 300,000 hospitalizations a year in adults alone[52], and asthma is far

more prevalent in children with 6.7% of children under the age of 18 being diagnosed[53]. Chronic

inflammation has even been implicated in neurodegenerative conditions like Alzheimer's and

dementia[54] which, while ultimately fatal, have devastating effects on living patients as they

struggle to perform basic tasks, manage their emotions, and remember their lives and loved

ones.

Since chronic inflammation has such a devastating effect, many people fail to consider the risks

associated with inappropriate anti-inflammatory response. Though chronic inflammation is

associated more closely with distressing symptoms like pain or trouble breathing, anti-

inflammatory immune behavior can prevent the body from launching appropriate responses to

both internal and external threats. Perhaps the best known inappropriate anti-inflammatory

response is found in solid tumor cancers. In cancers like breast, kidney, and liver cancer, tumors have M2 anti-inflammatory macrophages in their tumor microenvironment. These cells, called TAMs, secrete cytokines including IL-10, a particularly potent anti-inflammatory, and TNFα which promotes angiogenesis. These cytokines are responsible both for promoting the growth of the tumors and for allowing them to escape immune detection granting them a privileged status and leading to many of the difficulties associated with their treatment[55]. Additionally, in immune compromised environments pathogens and foreign bodies may not be dealt with effectively allowing them to proliferate and cause much more damage than they would in a healthy individual[56].

Right now, treatments for inflammation are oxymoronically robust and inadequate. Most people are familiar with NSAIDs which are available either over the counter or by prescription. The drugs typically work by acting on the COX-1 and/or COX-2 enzymes[57]. Advil (ibuprofen), Aspirin (acetylsalicylic acid), and Aleve (naproxen) are all readily available at any pharmacy in the United States alongside Tylenol (acetaminophen) which is categorized as an atypical NSAID[58] but shares many characteristics with the other medications in this section. All of these common medications are capable of reducing pain, fever, swelling, and other common symptoms of inflammation. In fact, in the case of acute inflammation like the pain of a sprained ankle, over the counter NSAIDs are known to be very effective in giving patients some much needed relief from their symptoms[59]. However, these drugs, while widely available, are associated with some concerning side effects. Ibuprofen is known to cause ulcers in prolonged or high dose uses with kidney failure and bleeding from the gut being much rarer but more dangerous side effects[60]. Acetaminophen is known to cause liver failure when taken at high enough doses and causes

around 500 deaths a year in the United States[61]. Acetylsalicylic acid is a known blood thinner which can enhance the risk of bleeding especially in those who are vulnerable[62], and naproxen can, ironically, cause inflammation of the gut and bowels leading to pain, vomiting, and bleeding[60]. For this reason, many alternative treatment options, especially for patients requiring long term relief from inflammation, have been explored.

The next class of anti-inflammatories is steroids. As a general term, steroid refers to a molecule containing 4 rings of carbon and can encompass hormones, vitamins, and synthetic drugs such as those discussed below[63]. The proper name for the subclass of synthetic steroids that can be used as anti-inflammatories is corticosteroids[64]. Many common medications including hydrocortisone available over the counter as anti-itch cream and prednisone available as a prescription drug are corticosteroids, and they have pronounced benefits in a number of conditions. In the case of hydrocortisone topical applications, they can be used in the treatment of eczema[65], psoriasis[49], and even common insect bites[66]. Known for its remarkable ability to reduce redness, itch, and pain, many outdoorspeople carry a tube of this steroid in their first aid kit. Luckily, the external use of low dose, over the counter hydrocortisone creams is known to be extremely safe with only a few side effects such as unexpected hair growth being considered common, but in higher dose prescription formulations topical hydrocortisone can rarely cause more severe side effects[67]. Since topical use of corticosteroids, especially at low dose, is insufficient to treat more severe ailments or internal conditions, oral steroids are often prescribed. These oral medications, like prednisone, are known to be much more effective with a corresponding greater risk of side effects. Prednisone works by suppressing the immune response through the inhibition of polymorphonuclear leukocytes (neutrophils, basophils, and

eosinophils) and the reduction of capillary permeability[68, 69]. It is a very effective anti-inflammatory used both short and long term to address conditions ranging from asthma flare-ups (short course)[70] to rheumatoid arthritis (ongoing treatment)[71]. However, prednisone has several side effects associated with its use. These range from the relatively minor like development of acne to the much more severe like Cushing Syndrome (increased fat around the torso, neck, and midsection associated with unusual hair growth and thinning skin) or even psychological concerns like hypomania or psychosis[72]. Patients who use steroids over long periods of time also develop a specific appearance, called "moon face[73]," due to the associated swelling which can further affect self-esteem and mental health.

A third class of drug that warrants discussion here, while not anti-inflammatory, are the opioid pain killers. These drugs do not affect the inflammatory signaling or pathways in the body; rather they change the way the body processes pain signals to reduce discomfort and enhance feelings of well-being[74]. These drugs are particularly useful in extreme or traumatic situations which inflammation can be beneficial such as during or after surgery, or after a major injury like a broken femur. They are also often used alongside anti-inflammatories for a more robust pain inhibiting effect[75]. From the perspective of those hoping to more effectively control immune response, there are two main problems associated with the use of these drugs. First, and most obviously in this context, opioids merely inhibit pain signals[74]. They do not actually affect the immune system directly and do not resolve the root cause of pain associated with inflammation. Second, these drugs have immense potential for abuse. Opioids, unlike NSAIDs or corticosteroids, are addictive and over time require greater and greater doses to achieve the same effect. They are also known to produce a "high" in patients which feeds the cycle of

addiction as they seek more drugs to maintain this feeling[76]. From 1999-2017, almost 400,000

deaths in the United States could be attributed to opioid overdose[77]. These death statistics can

be used as a proxy for the severity of the opioid abuse epidemic in the United States making the

search for effective anti-inflammatory drugs capable of addressing chronic inflammation and

associated pain even more critical than in the past.

	Non-Steroidal Anti-inflammatory Drugs (NSAIDs)	Steroids (Corticosteroids)	Opioid Pain Killers
Pros	• Simple to access • Very effective short term • Low cost	• Available in many formulations • Well characterized mechanism • Effective short and long term	• Do not interfere with healthy inflammation • Prevents shock and in some cases death from trauma • Work with anti-inflammatories
Cons	• High doses cause side effects • Possible overdose • Can cause more inflammation	• Prolonged use results in severe side effects • Rare side effects make them unusable for some patients	• Not anti-inflammatory • Highly addictive • Inadequate for chronic conditions
Examples	• Ibuprofen (Advil) • Acetaminophen (Tylenol) • Acetylsalicylic Acid (Aspirin)	• Hydrocortisone • Prednisone • Beclomethasone	• Oxycodone • Hydrocodone • Morphine

Table 2: A table explaining various treatments for inflammation including pros, cons, and
examples of each subtype.

For the treatment of inappropriate anti-inflammatory behavior, there are fewer options. As this

problem is not typically associated with the same noticeable, negative symptoms as

inflammation, treatments for anti-inflammatory conditions have been far less studied and

understood. The simplest type of inflammatory agent used medically is the adjuvant. Common

in vaccines, adjuvants are chemicals known to elicit an inflammatory response, typically by

triggering the innate immune system and an acute inflammatory process[78]. There are many

different immune signal strengthening adjuvants including aluminum salts (found in vaccines for

over 70 years) or virosomes[79]. These molecules trigger a robust immune response in situations

where there would typically be no or limited response to allow for the development of immunity. Similar molecules have been employed in anti-tumor applications where injections of an adjuvant are used to trigger an immune response to an otherwise privileged tumor, but the results are mixed[80]. Another option for the reversal of anti-inflammatory states is in the use of immunotherapy. Immunotherapies, which broadly strengthen the body's immune response, include checkpoint inhibitors, oncolytic viruses, and monoclonal antibody treatments. These therapies have been employed in a wide variety of conditions including diabetes, cancer, and allergies with different applications enjoying different rates of success[81-83]. In allergies, for example, immunotherapy is generally quite effective with patients seeing improvement in their symptoms within 2-4 months. However, the therapy occurs over 3-5 years and must be consistently complied with to ensure results[82]. In the case of diabetes, immunotherapy can be a double-edged sword. While immunotherapy has been shown to slow the progression of the disease, no known option completely reverses or halts its course[83]. Additionally, some immunotherapies are ironically known to trigger diabetes in some patients due to immune response to insulin producing β-cells[84]. In cancers, immunotherapy is very effective when it works but only has a success rate of around 30% which can vary a bit depending on the patient's age, disease progression, and overall health[81, 85].

	Adjuvants	Immunotherapy
Pros	• Simple mechanism • Common • Many available	• Highly tunable • Useful for many diseases • Can treat away from site of administration
Cons	• Must be administered directly to site of interest • Limited effects • Low tunability	• Long timeframes • Unpredictable side effects • Limited efficacy
Examples	• Aluminum Salts • Virosomes	• Allergy shots • Type-1 Diabetes Delay • Reversal of tumor immune privilege

Table 3: A table explaining various treatments for inappropriate anti-inflammatory response including pros, cons, and examples of each subtype.

Despite the large number of available treatments, aberrant immune behavior remains remarkably difficult to adequately treat. Between treatments that are insufficient to overcome all the symptoms of a condition and treatments with life altering side effects, it is clear that, while we have been successful in developing tools for that improve immune balance, there is a strong need for novel treatments that resolve diseases without significantly impacting a patient's quality of life.

1.3 Theranostic Application of Nanoparticles

Nanoparticles are known to be fantastic diagnostics allowing for complex, multimodal imaging. Taking advantage of strategies as diverse as NIR fluorescence imaging, photoacoustic imaging, and MRI, nanoparticles can be used as contrast agents for diagnostic imaging allowing for more sensitive detection even in tissues which would otherwise prove challenging to image[86]. For example, MRI contrast provided by SPIONs allows for high-resolution imaging and the detection of small tumors that may otherwise be challenging to visually distinguish from surrounding

tissue[22]. Likewise, fluorescence imaging is well suited to the detection of abnormalities located near the imaged surface such as early-stage skin cancers[87].

However, nanoparticles do not need to be either diagnostic or therapeutic. Theranostics, which have both capabilities, are an area of intense interest in the nanomedicine community[88]. The appeal of theranostics from a medical perspective is straightforward. Having one product that is capable of simultaneously diagnosing a disease and beginning its treatment cuts the time from diagnosis to start of treatment to zero. This would allow for more efficient treatment and prevent disease progression that can occur during the time between diagnostic and treatment appointments. Additionally, the continued use of theranostics over a treatment course allows for long term disease tracking alongside treatment[88]. This disease treating and tracking combination would allow for more specialized treatment of diseases ultimately improving patient outcomes (Figure 4).
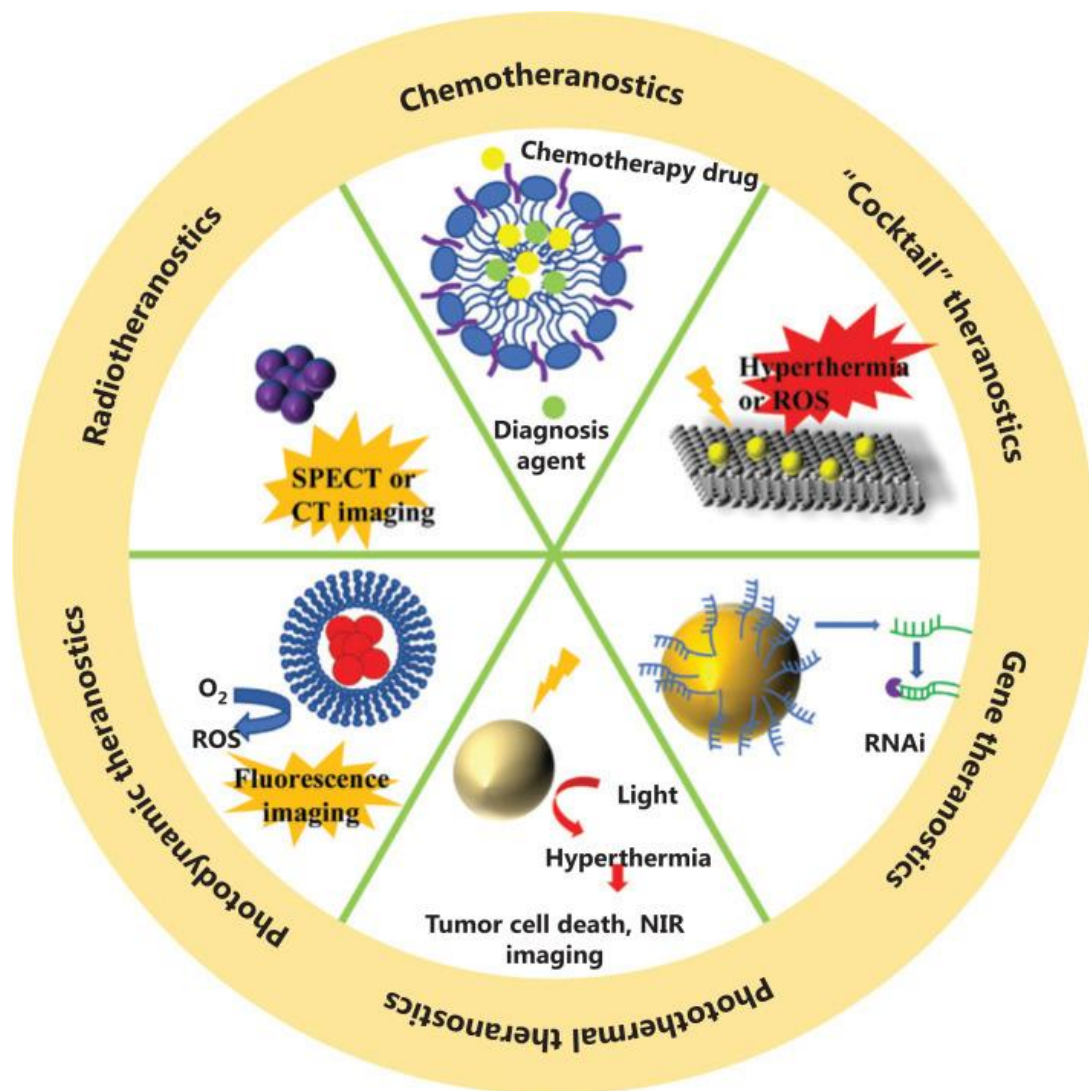
Figure 4: A graphic showing the different kinds of theranostic nanomedicine used in the treatment of cancers. (Figure from Xue et. al 2021).

Perhaps the most straightforward category of theranostic particles is the contrast agent conjugated nanoparticle. These particles, which can be drug loaded or intrinsically active, are prepared as needed to perform their intended therapeutic effect then subsequently tagged with a contrast agent to allow for easy visualization of the therapeutic particle in the body. Commonly, SPIONs may be conjugated to polymer or lipid nanoparticles to make them detectable by MRI and give long term information about their distribution and effect[89]. However, as MRI takes a long time and is very costly, other options for theranostic imaging are often used. Fluorescent dyes facilitate fluorescence imaging which is extremely quick. However, imaging depth is a major challenge in the use of fluorescence within the body[90]. One option for overcoming this challenge is to take advantage of the biological transparency window otherwise known as the NIR and NIR II regions. Dyes which absorb and fluoresce in this region, like ICG, are subject to less scattering and absorbance by surrounding tissue allowing for fluorescence imaging at greater depths[91, 92]. However, fluorescence imaging is still impractical for deeper tissue applications as even NIR light has a maximum depth of tissue penetration on the multi-centimeter scale. Taking advantage of the improved temporal resolution as compared to MRI and the enhanced imaging depth as compared to fluorescence, photoacoustic (light in sound out) imaging which has been FDA approved for breast cancer diagnostics[93] and is currently under investigation for other clinical applications including detailed imaging of skin cancer[94], of conjugated contrast agents like ICG or AuNR can be used for enhanced theranostics in cases where other diagnostic methods are impractical[95]. By choosing an appropriate combination of therapeutic and diagnostic for the target disease, these particles can be specially tuned for maximum efficacy.

The second category of theranostic nanoparticles we will discuss here are the nanoparticles which are inherently theranostic. These nanoparticles are typically metal or metal oxide based, and their properties on the nanoscale make them suitable both for imaging and treatment. One example of this is the use of SPIONs in both MRI and magnetic hyperthermia. Both applications of the particle rely on superparamagnetism and thus allow for minimal interference from endogenous molecules. MRI can be used to image and pinpoint an area of interest like a tumor then magnetic hyperthermia can be applied to ablate the region allowing for consecutive or even concurrent diagnosis/visualization and treatment[22]. SPIONs are also useful for MPI imaging which can also be combined with magnetic hyperthermia[22]. A major advantage of using MPI over MRI or other imaging modalities is that background signal is essentially zero allowing for extremely sensitive and specific imaging[26]. Another particle with similar theranostic potential is Prussian Blue. Relying on photoacoustic contrast, these nanoparticles are both excellent contrast agents and stable particles for use in photothermal therapy[96]. This means that light-in sound-out can be used to image regions of interest while light-in heat-out can be used to treat them. This allows for near simultaneous visualization and treatment of disease states. Perhaps the most promising use of these particles as a theranostic is in LITT used to ablate tumors. Using the particles both to identify the tumor boundaries and to induce cell death allows for clean surgical margins and destruction of any residual tumor cells improving patient outcomes[96].

In many cases, it is possible to further enhance existing theranostics to enhance their diagnostic potential their therapeutic potential or both. AuNRs, for example, are both excellent photoacoustic contrast agents and excellent photothermal therapy agents, but they suffer from limited stability when exposed to laser light[35]. As exposure time increases, the efficacy of the

particles decreases due to them changing from rod-shaped to spherical reducing their plasmonic resonance[97]. To overcome this, engineers have begun to experiment with surface modifications that improve the stability of AuNRs under light exposure. Silica coating the particles has been shown to preserve their aspect ratio and thus their diagnostic and therapeutic properties[98]. This alone makes silica coating a viable strategy for improving the theranostics of AuNR, but the silica coating can also be further modified. The silica can be modified to be fluorescent allowing for multimodal imaging[99]. The silica can also be conjugated to targeting molecules like antibodies allowing for greater specificity in targeting and thus better imaging and treatment outcomes[37].

1.4 Nanoparticles for Immune Application

Careful engineering of nanomaterials makes it possible to tailor them to a specific application. The unique properties of nanoscale materials make nanoparticles interesting candidates for the treatment of conditions controlled by the immune system. In cases where traditional therapeutics fall short, nanomedicines show remarkable potential for addressing inflammatory and anti-inflammatory conditions. Thanks in large part to their tunable properties, different classes of nanoparticles are suited to different applications, and refinement of particles allows for superior treatments. While nanoparticle immune therapies are a relatively recent invention, there are a surprisingly large number of them showing promise in the field[100].

The first, and perhaps most traditional method of using nanoparticles to address these concerns involves using nanoparticles for drug delivery (Figure 5). There are many drugs available to address immune concerns as described in section 1.2, but nearly every drug applied for these conditions has some side effects or off target effects that must be mitigated to improve patient

experience. The wide variety of different nanoparticles that can be used for drug delivery can help to overcome many of the problems associated with traditional drug therapy[101]. Broadly, there are three categories of nanoparticles. There are polymeric nanoparticles which are comprised of polymers, inorganic nanoparticles (a broad category including all inorganics including silica and metal oxides), and lipid nanoparticles which are, unsurprisingly, made of lipids[102]. Under each category, there are many subtypes of particles which could hypothetically be used for drug delivery. For polymer-based nanomaterials, the most common type of particle used in drug delivery is the nanocapsule. These particles are made of a polymer shell with a hollow core and can contain either hydrophilic or hydrophobic drugs[103]. Nanocapsules are used primarily due to the ease of tuning them during synthesis and the ability to make them locally responsive allowing for precision targeting of diseases without the usual risks of systemic delivery. For inorganics, silica nanoparticles are commonly used for drug delivery[16]. These particles are simple to synthesize even in large quantities thanks to the highly repeatable Stöber method[104]. Through exposure to acidic ethanol, solid silica nanoparticles can be etched to become either mesoporous greatly enhancing their surface area to volume ratio[105] and providing places for the particle to "store" small molecules like drugs[16]. The porous nature of the silica prevents burst release of drugs instead allowing them to be slowly released over time. Additionally, surface coatings, like PEG, can further enhance the efficacy of the particles by reducing premature release and enhancing circulation time[106]. Finally, liposomes are similar in structure to extracellular vesicles and cell membranes produced naturally by cells in living organisms[107]. These particles are composed of phospholipids which can form mono, bi, and multi-layer vesicles allowing for the encapsulation and transport of both hydrophilic and

lipophilic drugs[108]. The appeal of using liposomes over other drug delivery options comes from the biomimicry aspect. As liposomes are very similar to existing structures and can be modified to include additional molecules embedded within or conjugated to the surface, they are long circulating and do not get cleared as easily as many other nanoparticles[109]. Additionally, liposomes can be targeted to specific tissues much like extracellular vehicles, allowing for relatively straightforward targeting of diseases including cancers[110].

Though drug delivery nanoparticles can certainly be immunomodulatory and used to address some of the concerns associated with traditional drug use in the treatment of immune conditions, they cannot fully overcome issues associated with toxicity or off target effects of these drugs[111]. For this reason, the use of nanoparticles in directly therapeutic applications has become an area of interest for many in the field (Figure 5). Inorganic nanoparticles are of particular interest for these applications due to their diverse and inherent properties[112]. However, not all these treatment options are appropriate for immune conditions, and care must be taken when considering which treatment modality to use. Here, we discuss three immunomodulatory treatments that can be facilitated by inorganic nanoparticles.

Magnetic hyperthermia and photothermal therapy are treatments which have been primarily used to treat solid tumor cancers[113, 114]. However, they have a wide variety of potential applications including ablation of plaques in coronary artery disease[115] or destruction of dangerous biofilms formed by bacteria on implants and medical devices[116]. Magnetic hyperthermia involves the injection of superparamagnetic nanoparticles either systemically or directly into sites of interest. Then, pulsed magnetic fields cause rapid heating of the particles ultimately destroying tissues with high concentrations of particle[22]. Photothermal therapy is

22

fairly similar, but instead of requiring superparamagnetic particles and a pulsed magnetic field, it requires photoactive particles and laser light exposure[35]. Both have two mechanisms of action. The first is a direct destructive effect resulting from the heat generated by the particles. This heat, which is generally around 40°C, is sufficient to induce cell death causing the death of tissue directly exposed to the particle treatment[117]. However, the second effect is a pro-inflammatory immunomodulatory effect. This effect is provoked by the cell death generated in the first mechanism. Dead cells release intercellular material into the extracellular matrix[118] triggering the innate immune response described in section 1.2. This causes an acute inflammatory response which in turn allows the body to respond to the areas that have received treatment as though they are pathogenic or injurious[118]. This effect is especially valuable and pronounced in tumors treated with these therapies as magnetic hyperthermia and photothermal therapy can help trigger immune response to tumors that are otherwise immune privileged[98].

Nanoparticles themselves can also be immunostimulatory (Figure 5). Lipid nanoparticles in particular are well suited to this application[119]. As biomimetic nanoparticles similar to a cell membrane, these particles can both contain adjuvants and antigens within their liquid core and incorporate them into the membrane of the particles[120]. This allows nanoparticles to activate the immune system in a quasi-natural way eliciting potent innate immune response[121]. One application of nanoparticles as immunostimulatory agents that has garnered attention in recent years is the use of liposome carriers in mRNA vaccines like the COVID-19 vaccines produced by Pfizer and Moderna. The liposomal formulation contains multiple adjuvants and antigens[122] including the mRNA required to produce antibodies to the disease. When it interacts

23

successfully with cells, this mRNA is translated via ribosome and allows for robust immune response from the innate and adaptive immune systems[123]. This effective strategy allows for reduced use of attenuated viral vaccines which occasionally pose risks to patient populations[124] allowing for better whole-population vaccination rates.

The final class of nanoparticles that are of particular interest in immunomodulatory applications are nanozymes (Figure 5). The term nanozyme describes nanoparticles that are capable of replacing or supplementing enzymes[125]. There are two broad categories of nanozyme application. The first is the use of nanozymes in sensors. Nanozymes, with their ability to facilitate reactions, are useful in the development of diagnostic tools. In the presence of this analyte, they can facilitate simple yes-no tests for bedside diagnostics[126]. For example, there are tests for cholesterol that are facilitated by detection of the production of H_2O_2 generated through its interaction with catalase[127]. However, while nanozymes are useful for diagnostics, they are potentially even more powerful when used as therapeutics. Nanozymes are efficient ROS scavengers making them attractive for therapeutic applications[128]. Generally, as with most ROS scavenging treatments, nanozymes are used as anti-inflammatories[129]. Cerium oxide nanoparticles, which can act as SOD, catalase, and peroxidase, and IONPs, which have intense peroxidase activity, have been explored for the treatment of several conditions that are known to be mediated by ROS activity[130]. These conditions range from neurodegenerative conditions like Parkinson's and Alzheimer's[131] to traditional inflammatory conditions like rheumatoid arthritis[30], and cardiovascular conditions like heart attack and stroke[132]. Aside from nanoceria, Prussian blue nanoparticles can be used as nanozymes to reduce local inflammation in photothermal therapy, and IONPs can be used as efficient peroxidase mimics during and after

MRI imaging[96, 133]. Nanozymes have also been used to alleviate hypoxia in conditions where a hypoxic environment is detrimental to treatment and recovery. The best example of this is the use of nanozymes alongside radiation therapy in solid tumor cancers. As radiation acts to destroy the tumor, the nanozymes act to relieve the hypoxia in the tumor environment allowing for much more efficient radiation treatment and better outcomes for patients[134].
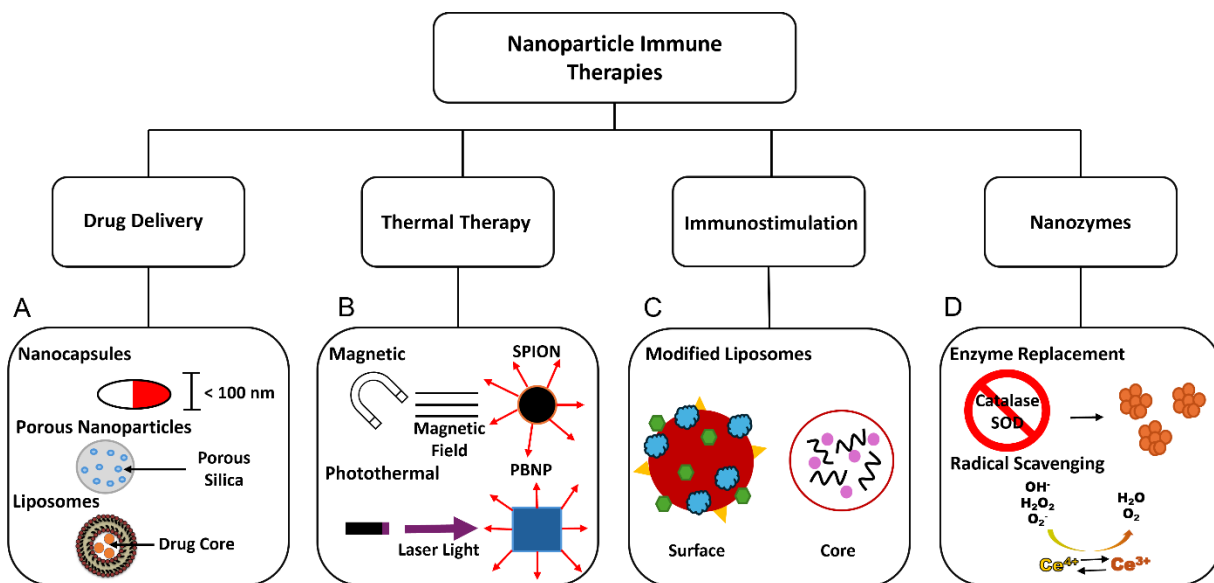
Figure 5: Graphic showing the most common types of nanoparticle immune therapies categorized by treatment approach. A) Drug delivery-based nanoparticle immune therapies include polymeric nanocapsules, porous nanoparticles like silica, and liposomes with a drug core. B) Thermal therapy options include magnetic hyperthermia where superparamagnetic nanoparticles are heated through application of a magnetic field and photothermal therapy where laser light is used to heat certain nanoparticles, like Prussian blue nanoparticles, to induce apoptosis or necrosis. C) Modified liposomes can be used for immunostimulant with surface and core modifications both serving to deliver stimulatory molecules to target areas. D) Nanozymes, nanoparticles with inherent enzymatic properties, can be used in either enzyme replacement or radical scavenging applications to modify the microenvironment and affect the immune system.

Chapter 2: Surface Valence and Substrate Tuned Nanoceria

2.1 Introduction

Cerium, number 58 on the periodic table, is a rare earth metal and lanthanide. In its pure, solid

state, cerium is a light grey, soft metal known for reacting easily with surrounding species[135].

Like many other metals, cerium can form oxides. These oxides are CeO_2 formed with Ce^{4+} and

Ce_2O_3 formed with Ce^{3+} [136]. These distinct subtypes of cerium oxide share some properties but

are known to differ in meaningful ways. Most obviously to the layperson, CeO_2 is very light

yellow in color appearing nearly white in powdered form while Ce_2O_3 is a deeper and more

vibrant yellow-gold color[137]. CeO_2 is the more abundant oxide, however even within bulk CeO_2

there exists Ce^{3+} present allowing for potent catalytic activity[138]. Cerium oxide nanoparticles,

also known as nanoceria, have long been considered for medical application due to their unique

properties. The combination of Ce^{3+} and Ce^{4+} found on their surface lends them unique

enzymatic and anti-inflammatory properties[139]. They are able to act as an SOD, catalase, and

peroxidase[30]. They do this, at least in part, through their ability to "recycle" their surface

valence between a Ce^{3+} and Ce^{4+} depending on the ROS they are faced with[132]. This allows

nanoceria to act as potent and reliable scavengers of ROS in their environment that are long

lasting and stable when compared to traditional drugs allowing for long term ROS scavenging

and relief of oxidative stress (Figure 6). These properties allow nanoceria to act as a potent anti-

inflammatory and have sparked a decade of research into their medical potential[140].

However, nanoceria has major shortcomings when it comes to biomedical applications.

Nanoceria has notable toxicity in biological systems; more specifically, it is cytotoxic, genotoxic,

and neurotoxic[140] (Figure 6). While the acute toxicity of the particles may be low, prolonged

exposure can cause significant harm. During prolonged exposure to intravenous or inhaled nanoceria, fibrosis develops in the lungs and granuloma develops in the lungs and liver. Additionally, and somewhat paradoxically, long term exposure to nanoceria can have an inflammatory effect and increase oxidative stress in some tissues[141]. The tissues susceptible to inflammation from long term nanoceria exposure even include the brain where, even after there is no longer detectable cerium, oxidative stress persists causing critical neurotoxicity[141]. Additionally, the small size of the nanoceria can lead to extremely rapid clearance by the kidneys[142]. Often, when considering the use of nanoparticles in biomedical applications, rapid clearance is seen as positive, especially in particles which have a risk of toxicity. However, for long-acting nanoparticles, like cerium oxide nanozymes, rapid clearance can result in limited treatment efficacy. When the particles are cleared from the environment before they are able to act, they are unable to effectively treat conditions. Unfortunately, the problems facing the use of nanoceria in medical applications can be attributed to the same properties that make nanoceria a particularly interesting candidate material for biological applications. Namely, their small size, powerful ROS scavenging capabilities, and recyclable surface cause both the benefits and harms of nanoceria use[143].
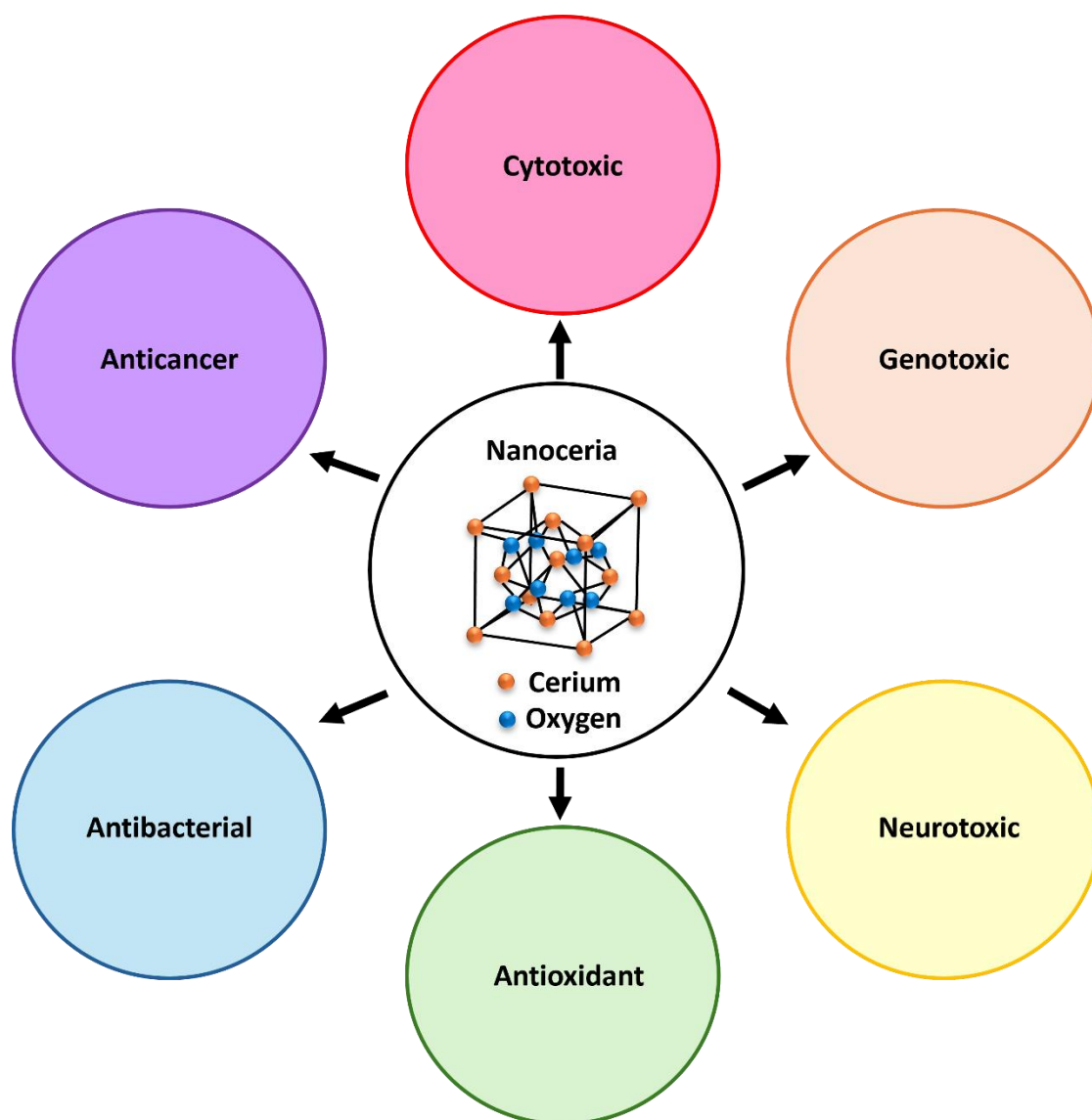
Figure 6: A graphic showing the different effects of nanoceria on biological systems. The FCC structure of a cerium-oxide crystal is shown in the center circle.

For this reason, nanoengineering of nanoceria is uniquely critical. Enhanced targeting and biocompatibility are the key challenges that must be overcome before nanoceria can be considered for clinical application[140]. Perhaps the most straightforward method of preventing toxicity and enhancing targeting is to create nanocomposites where nanoceria crystals are included in larger nanostructures comprised of a substrate material. One particularly promising choice for substrate is albumin, a common blood protein[30]. Albumin has been used as a substrate for several nanoparticles to enhance their biological use[144]. Comprising about 65% of total blood proteins, albumin is highly biocompatible and avoids provoking unwanted immune response in circulation[145]. It also improves circulation time of nanomaterials through both enhancing their size and slowing down the body's ability to identify them as foreign materials[146]. Albumin is well suited for use as a substrate for nanoceria due to its ability to not simply coat but integrate the nanoclusters during synthesis via a biomineralization process preventing leeching of the smaller nanoclusters in the body[30]. Additionally, albumin has been shown to have innate inflammation targeting properties as it accumulates in locations with swelling and disorganized vasculature which would allow albumin-nanoceria to efficiently accumulate in areas it would be most effective in[147].

However, while albumin is a conventional choice for a nanoceria substrate, another very interesting option is SWCNT. SWCNT are extremely high aspect ratio particles which have a diameter of ~1 nm and a length of up to several micrometers[148]. They are strong, flexible, and highly hydrophobic making them an interesting choice for many applications including drug delivery NIR II imaging[149, 150]. However, SWCNTs require modification prior to biological application due to their innate hydrophobicity and size. While it is possible to intuit why the

particles require hydrophilic modification prior to biological application, it may not immediately be obvious why their aspect ratio and flexibility can prove dangerous. However, in tissues where SWCNTs are known to accumulate, like the lungs, they cause mechanical damage to cells and as a result generate ROS[151]. One relatively easy way to mitigate these effects is to shorten the SWCNTs. SWCNTs of size 100-300 nm are not known to cause physical damage to cells and are highly biocompatible especially as compared to μm scale particles[151, 152]. Additionally, if during the process of shortening, PEG is conjugated to the particles, they can become hydrophilic allowing them to circulate safely in the body[153]. As the SWCNTs require significant modification prior to use in the body, it is important to highlight the reasons they make strong candidates for use as a substrate for nanoceria. First, after PEGylation, they enhance circulation time and prevent premature clearance associated with the small size of the nanoceria. However, this alone would not be enough to justify their use. 100-300 nm SWCNT are known to target monocytes and macrophages in the body, and macrophages are prevalent in inflamed tissue and in actively anti-inflammatory regions[154]. This means that, through conjugation of nanoceria to SWCNTs, nanoceria could be delivered directly to the sites where large populations of macrophages reside which are the same sites in which nanoceria would have its therapeutic effect. Though the mechanism of this targeting is not yet known, this effect may be critical to avoiding off target effects of nanoceria while simultaneously enhancing its treatment effectiveness.

One final and key aspect of nanoceria is its tunable surface oxygen valence. As stated above, Ce^{3+} and Ce^{4+} coexist on the surface of nanoceria[139]. However, their ratio is not constant. As in the macroscale cerium oxides, in nanoceria solutions, greater Ce^{3+} is associated with a darker

golden color while greater Ce^{4+} is associated with a pale-yellow color[155]. However, unlike in the case of the bulk material, in nanoceria, the ratio of the two can be carefully engineered. This leads not only to a variety of appearances, but also a variety of effects from the nanoceria. In particles with enhanced Ce^{3+}, SOD activity is known to be enhanced while in those with enhanced Ce^{4+} enhanced catalase activity is expected[156]. This implies that the ratio between the two is somehow key to the effects the particles have on biological systems. Following this logic, it is possible to extrapolate further and consider whether different formulations of nanoceria have different, pro and anti-inflammatory, effects on biological systems.

Here, we develop novel nanoceria formulations with albumin and SWCNT substrates and evaluate the differences between these particles. Additionally, we synthesize different, surface valence tuned, varieties of albumin-nanoceria through the use of catalysts and pH changes during synthesis. Through the development of robust, repeatable protocols that produce consistent particle products, we aim to develop a new class of immunomodulatory nanodrugs capable of addressing both pro and anti-inflammatory conditions (Figure 7). Changes in particle effect due to their synthetic condition will allow for greater understanding of nanoceria and appropriate choice of nanomaterial for biological application.
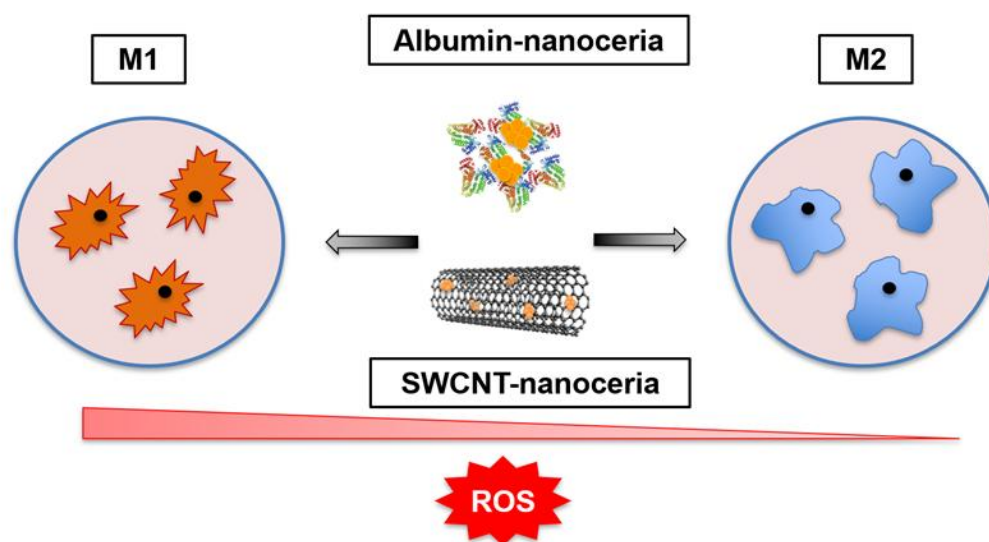
Figure 7: A graphical abstract showing the aims of tuning nanoceria formulation for macrophage modulation.

2.2 Methods

2.2.1 Synthesis of Nanoparticles

2.2.1.1 Albumin-nanoceria

Albumin-nanoceria was synthesized using a biomineralization process. A 20 mg/mL solution of

heated to 40°C and allowed to stir until albumin was fully dissolved. Then 0.5 mL of 1 mM

cerium (III) nitrate was mixed with the albumin solution, and this solution stirred for 15 minutes.

Then, the pH was adjusted using 2 M NaOH. For Ce^{3+} enhanced particles and Ce^{4+} enhanced

particles, the desired pH was between 8.5 and 9. For the intermediate albumin nanoceria, a pH

of 11 was required. For Ce^{3+} enhanced particles, 600 μL of 30% H_2O_2 was added immediately as

a catalyst. For Ce^{4+} enhanced particles and intermediate particles, no H_2O_2 was added. All

solutions were then stirred for 2 hours. After reaction, the solutions are clear (not cloudy) with

colors ranging from light yellow to deep orange depending on surface valence. The particles

were subsequently filtered via centrifugation through a 100 kDa membrane at 3240 rpm and the filtrate was discarded. The remaining particle solution was kept, diluted to a volume of 2 mL if required, and underwent dialysis through a 10 kDa membrane at 4°C. The final particles were stored at 4°C.

2.2.1.2 Conjugation of ICG to Albumin-Nanoceria

A 0.5 mg/mL ICG-NHS ester solution was prepared in water. This solution was combined with the product of 2.2.1.1 at a ratio of 1:100 ICG to albumin (mg:mg). The solution was rotated overnight at 4°C. These particles then underwent dialysis as described in 2.2.1.1. Following dialysis, excess water was removed using a 100 kDa membrane centrifugal filter, and the particle product was adjusted to the desired concentration. Particles were stored at 4°C.

2.2.1.3 Albumin-ICG

Albumin-ICG particles were made by desolvation. A 2 mL solution of 40 mg/mL BSA and 1.5 mg/mL ICG-NHS ester in water was prepared and stirred for 15 minutes to allow for the completed dissolvation of BSA. After 15 minutes, 6 mL of ethanol was added to the stirring solution dropwise. During this process, the solution should become very cloudy and ICG should completely dissolve. The resulting solution was stirred for 30 minutes at room temperature. The resulting particles were then washed by centrifugal filtration through a 100 kDa membrane at 3240 rpm. The supernatant was collected and underwent dialysis in a 10 kDa membrane overnight at 4°C. The final product was collected and stored at 4°C.

2.2.1.4 Synthesis of SWCNT-Nanoceria

Synthesis of SWCNT-Nanoceria occurred through a two-step process. First, the hydrophobic SWCNTs were solubilized through PEGylation. Briefly 10 mg of SWCNTs were weighed out in a

20 mL glass vial then combined with 8 mL of water. Then, the SWCNTs were sonicated at 4°C for 30 minutes. During this initial sonication, 50 mg of DSPE-PEG was weighed out and dissolved in 2 mL of water. Then, the PEG solution is combined with the SWCNTs and the combination is further sonicated for 6 hours. After sonication, the solution is stored overnight at 4°C. Following overnight storage, the PEGylated SWCNTs are washed the same way as the albumin-nanoceria (method described in 2.2.1.1). Second, after washing, the PEGylated SWCNT are resuspended at 0.1 mg/mL in water, heated to 40°C, and 0.5 mL of 1 mM cerium (III) nitrate is added. After 15 minutes, the pH is adjusted to 8.5. pH control at this step is critical as higher pH causes particle aggregation. Then, the pH adjusted solution stirs for 2 hours. It is then washed as previously described.

2.2.1.5 Conjugation of SWCNT-Nanoceria to ICG

For the synthesis of ICG conjugated SWCNT-nanoceria, ICG conjugated PEG is made by overnight mixing of 1 mg aminated PEG and 1 mg ICG NHS-ester. This allows the NHS-ester, amine bonding to proceed passively and form a stable product. This product is then used at a 1:9 ratio with DSPE-PEG during the PEGylation stage of 2.2.1.3. Otherwise, the synthesis proceeds as described in 2.2.1.3.

2.2.2 Characterization of nanoceria

Dynamic light scattering (DLS, Zeta Sizer Nano, Malvern Instruments) was used to evaluate the hydrodynamic diameter and polydispersity of the nanoparticles produced in section 2.2.1. A 2200FS high-resolution transmission electron microscope (HRTEM, JEOL) evaluated the size, shape, and crystallinity of cerium oxide nanoclusters and size and shape of SWCNT. Samples for XPS were prepared by lyophilization and XPS spectrum was acquired using an AXIS SUPRA+

system (KratosAnalytical Ltd.). Albumin concentration was determined by bicinchoninic acid assay (BCA, Thermo Scientific), and ICG quantification was performed using absorbance relative to a standard curve at 390 nm. Cerium concentration was evaluated using inductively coupled plasma-optical emission spectroscopy (ICP-OES, Varian 710-ES Axial ICP-OES).

2.2.3. Cell viability test

Cell viability was assessed using a 3-(4,5-Dimethylthiazol-2-yl)-2,5-Diphenyltetrazolium Bromide (MTT) assay. Briefly, J774 cells were seeded in a 96-well plate at 50k cells/well, incubated overnight at 37°C and 5% humidity, and the following day were treated with albumin-nanoceria or SWCNT-nanoceria at 0, 5, 10, 50, 100, or 200 μg Ce/mL. After an additional overnight incubation, the supernatant is discarded and replaced with MTT solution. Following a 4-hour incubation, the MTT solution is removed, and the resulting formazan crystals are dissolved in DMSO. Absorbance was collected using a SoftMax Pro plate reader (Molecular Devices, CA) at 570 nm. Background used for calculations was collected at 610 nm from the same plate on the same plate reader.

2.2.4 Enzymatic Assays

2.2.4.1 SOD Assay

SOD assay kit was purchased from Cayman Chemical (706002) and performed according to the included instructions. Briefly, 200 μl of Radical Detector was added to each well of a 96 well plate. Then, 10 μl of either standard or sample was added to each of these wells. The reaction was then initiated by adding 20 μl of Xanthine Oxidase to the wells. The plate was then briefly shaken to ensure even mixing and incubated for 30 minutes at room temperature. The

absorbance was read at 450 nm on a plate reader. Data was analyzed according to the instructions provided.

2.2.4.2 Catalase Assay

Catalase assay kit was purchased from Cayman Chemical (707002) and performed according to the included instructions. Briefly, 100 µl of Catalase Assay Buffer and 30 µl of methanol were added to each well of a 96 well plate. Then, 20 µl of standard, sample, or positive control was added to the appropriate well. The reactions were then initiated through the addition of 20 µl dilute H_2O_2 and incubated on a shaker for 20 minutes. Then, 30 µl of potassium hydroxide was added to terminate the reaction and Purpald, a chromogen, was added. This was followed by 10 minutes of incubation on the shaker. Finally, 10 µl of Potassium Periodate was added, and the plate was incubated for an additional 5 minutes. Absorbance was taken at 540 nm.

2.2.5 Cell Uptake Experiments

To determine the immune cell targeting capabilities of the particles, cell uptake experiments were performed. J774 and THP-1 cells were plated in 6-well plates at 500k cells/well. The cells were then incubated overnight at 37°C and 5% CO_2. The following day, the cells were either left untreated, treated with SWCNT, SWCNT-nanoceria, Albumin-nanoparticles, or Albumin-nanoceria at 30 µg/mL. The following day, after incubation, the cells were washed in PBS, stained with DAPI, washed again, and immediately imaged on a KEYENCE Fluorescence Microscope.

2.2.6 Statistical Analysis

Statistical analysis was performed in Origin Pro.. Comparisons of means were performed using a Student's t-test, and are presented as mean plus or minus standard deviation in graphs.

36

Statistical significance is defined as $p < 0.05$ for the purposes of this study unless otherwise stated.

2.3 Results/Discussion

Albumin-nanoceria was successfully synthesized by biomineralization while SWCNT-nanoceria was successfully synthesized *via* the two-step process described above. In the albumin-nanoceria synthesis, surface valence was altered through varying pH and inclusion or exclusion of hydrogen peroxide during synthesis. As shown in Figure 8 we see that all formulations of albumin-nanoceria and SWCNT-nanoceria contain small, highly crystalline cerium-oxide nanoclusters (~5 nm) as confirmed by HRTEM. For SWCNT-nanoceria, morphology of the SWCNT was confirmed *via* TEM as well (Figure 8). For albumin-nanoceria, visualization of the larger particle by TEM was difficult due to the protein substrate, so DLS was used in place to evaluate the particle's hydrodynamic diameter. For the albumin-nanoceria, we see that the particles are uniform and monodisperse with size around 25 nm for all synthetic conditions (Figure 8). We also evaluated the hydrodynamic diameter of our SWCNT-nanoceria and saw a characteristic two peaked distribution at 50 and 300 nm due to their exceptionally high aspect ratio (Figure 8). These sizes are well suited to our application as the albumin-nanoceria size is in line with previous reports from our lab[30] and the SWCNT-nanoceria are between 100 and 300 nanometers, which is the size range in which SWCNT are safest for biomedical applications[151].
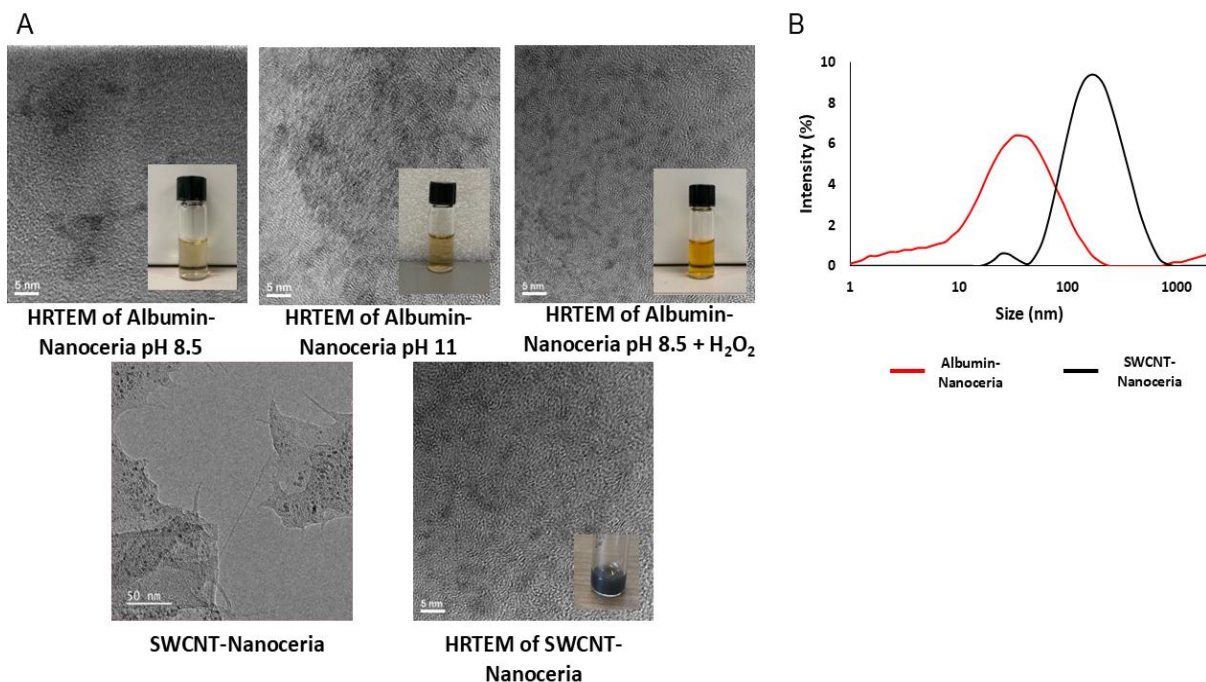
Figure 8: A) TEM images showing the morphology and size of the particles. HRTEM of all nanoceria formulations (Scale Bar = 5 nm) show small (<5 nm) highly crystalline cerium nanoclusters. TEM of SWCNT-nanoceria (Scale Bar = 50 nm) shows nanotubes remain intact during synthesis. Inlaid images show the color and dispersity of the particles. B) DLS of albumin-nanoceria (size 21.6 nm) and SWCNT-nanoceria (size 164.2 nm). All formulations of albumin-nanoceria were the same size (within 5 nm). The SWCNT-nanoceria shows a distinctive two peak distribution due to its high aspect ratio.

To further characterize these particles, XPS was used to evaluate the ratio of Ce^{3+}/Ce^{4+} on the surface of the particles. For the albumin-nanoceria, the ratio of Ce^{3+}/Ce^{4+} is dependent on the synthetic condition. We see a ratio of 2.2:7.8 for particles synthesized at a pH of 8.5, a ratio of 3.9:6.1 for those synthesized at a pH of 11, and a ratio of 5.4:4.6 for those synthesized at pH 8.5 in the presence of H_2O_2 (Figure 9). This indicates that increased pH and increased peroxide radicals during synthesis enrich the Ce^{3+} found in the particles. We also see that the ratio is 1.7:8.3 in the SWCNT-nanoceria most closely mimicking those synthesized at pH 8.5 without the inclusion of H_2O_2 though having a slightly lower ratio than those particles (Figure 9).
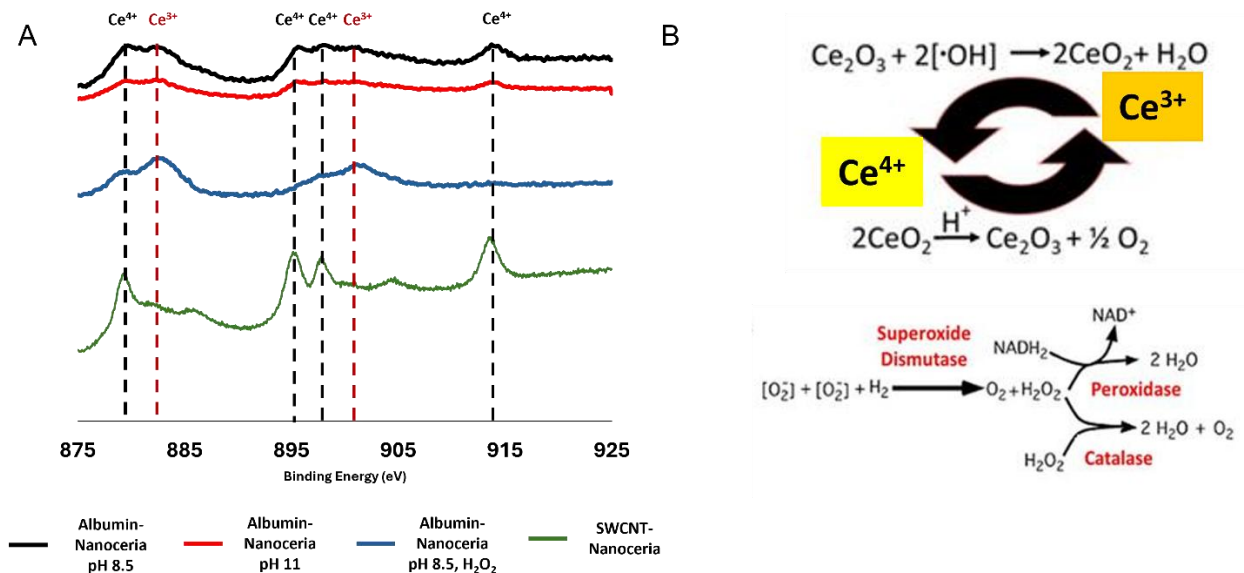
Figure 9: A) XPS of albumin and SWCNT-nanoceria formulations used to calculate the ratios of Ce^{3+}/Ce^{4+} that show that increasing pH and addition of H_2O_2 increase the ratio in albumin-nanoceria. This plot also shows the Ce^{4+} dominance on the surface of the SWCNT-nanoceria B) A schematic showing the mechanism of valence switching that allows for and prolonged enzymatic activity in the body. (Figure 9B Adapted from Kalashnikova et. al 2020[30]).

To evaluate the cytotoxicity of the particles and ensure they are biocompatible, we performed an MTT assay (Figure 10). Incredibly, at concentrations as high as 200 µg Ce/mL (as determined by ICP-OES), there is no significant toxicity from the albumin-nanoceria formulations or the SWCNT-nanoceria. This indicates the particles are not cytotoxic and are safe for biological application. To ensure that the enzymatic activity of the nanoceria is preserved in its substrate conjugated form, we performed SOD and Catalase assays on the particle formulations. Both albumin-nanoceria and SWCNT-nanoceria showed both SOD and catalase activity characteristic of nanoceria. However, we notice that the SWCNT-nanoceria showed reduced SOD activity and enhanced catalase activity as compared with the albumin-nanoceria formulations (Figure 11). This indicates there is a substrate dependent effect on the catalytic activity of the particles. This

finding demonstrates that the particles have a tunable enzymatic activity associated with their

synthetic conditions.
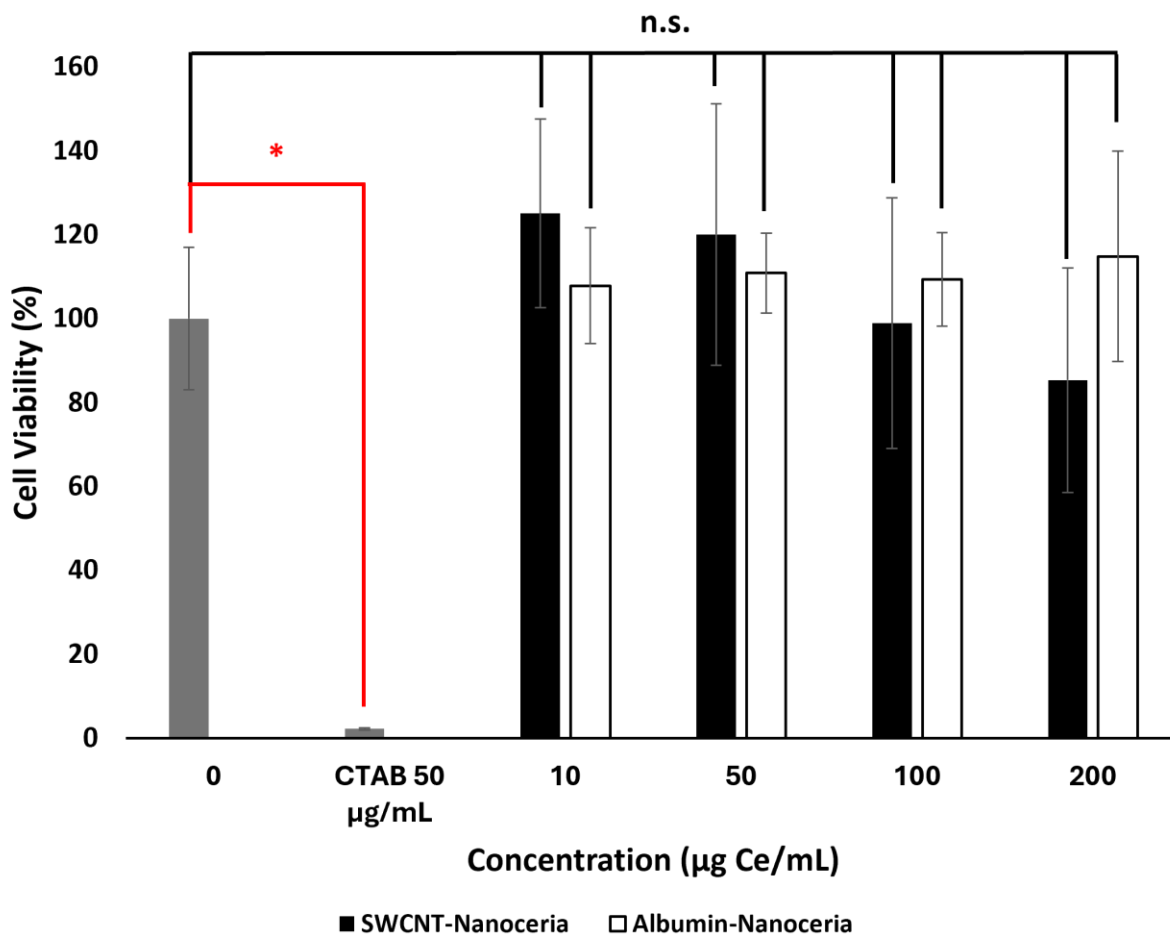
Figure 10: A) Results of an MTT Assay showing that in concentrations of up to 200 µg Ce/mL there is no statistically significant toxicity from either nanoceria formulation. CTAB at a concentration of 50 µg/mL is included as a control demonstrating that the assay is working properly as in the CTAB treated cells there is a significant reduction in viability (* $p<0.05$) (n=6 wells).
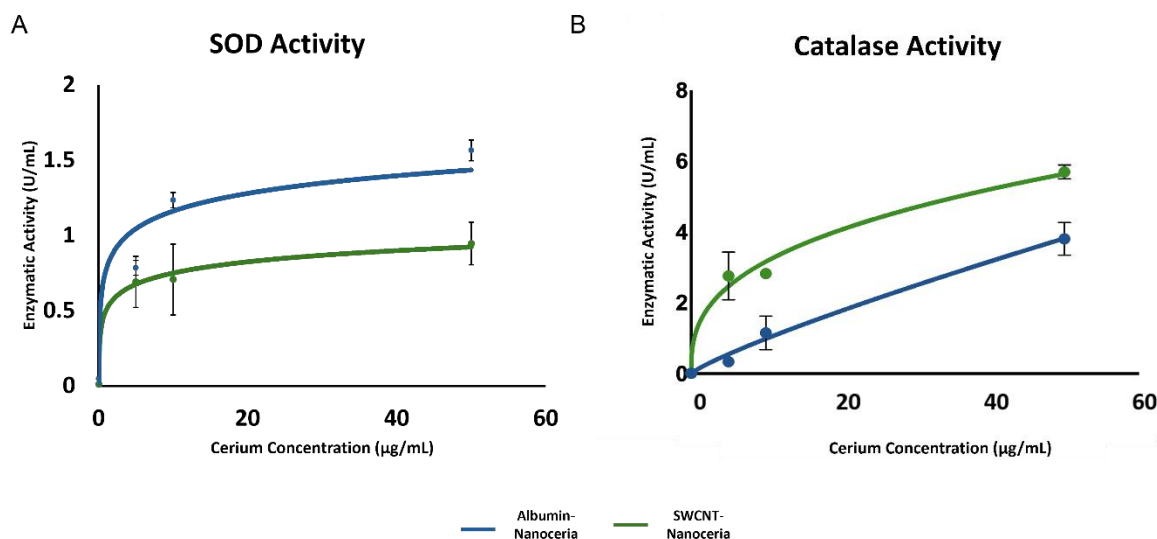
Figure 11: A) SOD and B) Catalase assays for the particle formulations demonstrating their ROS scavenging capabilities and a notable substrate dependent effect. For both assays readings for multiple wells (n=4) were averaged and compared to known standards error bars represent standard deviation.

To address the question of cell specific targeting and interactions between the cells and the particles, cell uptake assays were performed in J774 cells. In cells treated with RITC conjugated albumin particles and PEGylated SWCNT-nanoceria, the cells show a significantly higher uptake of the SWCNT than of the albumin-nanoceria particles even though J774 cells are phagocytic and uptake from the environment readily (Figure 12). This indicates that the SWCNTs in fact exhibit preferential uptake by the macrophage cells and would likely be a strong candidate for active immune cell targeting during systemic administration of nanoceria.
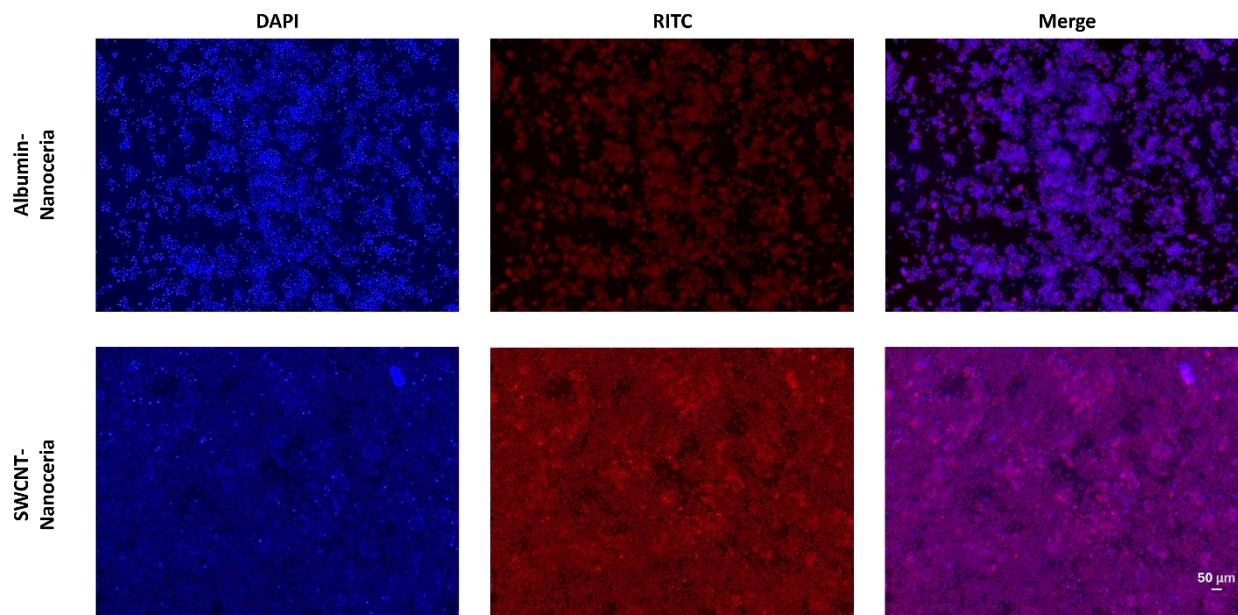
Figure 12: Cell uptake of albumin-nanoceria and SWCNT-nanoceria showing preferential uptake of SWCNT-nanoceria by J774 cells validating the immune targeting capabilities of the SWCNT substrate. (Scale Bar = 50 μm).

Here, we successfully synthesized three distinct albumin-nanoceria particles and one SWCNT-nanoceria formulation, characterized them, and validated their enzymatic properties. It has been well established in the literature that cerium-oxide nanocrystals have potent ROS scavenging effects[137], however, in many cases the particles are used with little to no surface modification making them difficult and dangerous to use in the body. To overcome these shortcomings, we take advantage of two distinct, biocompatible substrates. The first, albumin, is a protein and thus is exceptionally biocompatible with long circulation time[146]. The second, PEGylated SWCNT, requires much more careful preparation to avoid mechanical damage to tissue but comes with additional advantages like immune cell targeting[154]. While these substrates were chosen for their specific advantages, other substrates could be explored to broaden the capabilities of the nano-formulations.

We know that from the literature and from their ROS scavenging behavior that nanoceria can act as a potent anti-inflammatory[143], however, there is some evidence that nanoceria can have lasting pro-inflammatory effects under certain conditions[141]. It is demonstrated in this study that it is possible to tune the surface valence and enzymatic properties of the nanoparticles through relatively straightforward modifications during synthesis which represents a step forward in the engineering of nanoceria for medical applications. For this reason, we believe that it would be possible to tune the particles to specifically enhance their pro or anti-inflammatory properties. Use of catalysts, pH, and substrate all contribute to the behavior of nanoceria. One avenue that warrants further discussion and research is the use of SWCNT-nanoceria as a pro-inflammatory. SWCNT are known to have a pro-inflammatory effect on the body when not modified for to avoid this outcome[157]. Combining this inherent pro-inflammatory effect with the lasting pro-inflammatory effect of some nanoceria formulations could be beneficial for the treatment of immune suppressed conditions like solid tumor cancers. Finally, while the particles used here were primarily therapeutic, either formulation is more than capable of being conjugated to a fluorescent dye to allow for real time fluorescence imaging. Dyes, like the RITC used for the cell uptake experiment, can be covalently bonded directly to the albumin substrate in the albumin-nanoceria without disrupting the biomineralization process[30, 158]. For the SWCNT, dyes can instead be conjugated to the PEG used during the PEGylation step[159]. While the conjugation of the dye to the PEG is covalent in this case, the conjugation of the PEG to the SWCNT relies on hydrophobic interactions. For biological applications, this is sufficient as the general environment is water rich. This dye conjugation can make the particles fluorescent in the visible region, allowing for easy visualization in topical

applications or during surgical procedures or in the NIR region to take advantage of the
biological transparency window. However, SWCNT-nanoceria may not require further
modification as SWCNTs are known to be effective NIR II fluorescent and photoacoustic imaging
agents on their own which further justifies their use as a substrate for nanoceria[160, 161].

2.4 Conclusions

In this study, we successfully synthesized a variety of nanoceria formulations with different
properties dependent on their synthetic conditions. In terms of substrate, we were able to
successfully synthesize both albumin-nanoceria and SWCNT-nanoceria which are both highly
biocompatible demonstrating no cytotoxicity and which have different uptake efficiencies in
immune cells. Additionally, through XPS and enzymatic assays, we successfully demonstrated
the tunability of oxygen surface valence and resulting enzymatic activity of nanoceria not only
due to substrate changes but also due to changes in synthetic conditions. These differences in
the properties of nanoceria indicate that different formulations may be better suited to different
applications, and show that through relatively simple changes in synthesis, we can potentially
create a whole new class of immunomodulatory drugs capable of addressing pro and anti-
inflammatory conditions.

Chapter 3: Immunomodulatory Applications of Formulated Nanoceria

3.1 Introduction

Though it is clearly possible to create multiple nanoceria formulations that take advantage of different substrates and catalysts to achieve different properties, to see whether they have medical merit, *in vitro, in vivo,* and *ex vivo* validation beyond validation of enzymatic properties and targeting is needed. Specifically, as macrophages are critical in the pro and anti-inflammatory processes, we need to evaluate the effects of the particles on macrophages and associated immune processes.

Macrophages, which are derived from monocytes, are a key player in both pro and anti-inflammatory response thanks to their ability to be polarized towards either an M1 pro-inflammatory or M2 anti-inflammatory state from an M0 undifferentiated state[162]. Each type of macrophage has a unique role to play. M0 macrophages can be seen as "neutral" as they are phagocytes that arrive at sites and serve as a precursor to the M1 and M2 cells discussed throughout this dissertation[163]. However, upon being exposed to pro-inflammatory cytokines, M0 cells can become M1 cells[164]. These M1 cells are known for their ability to perpetuate the inflammatory response and recruit other immune cells through cytokine signaling specifically with IL-6 and IFN-γ acting as potent inflammatory agents both recruiting other immune cells and perpetuating a positive feedback loop in the macrophages themselves[44]. M2 macrophages serve a similar but nearly inverse purpose. Where M1 macrophages attract other immune cells and have a pro-inflammatory feedback loop, M2 macrophages suppress other immune cells and create an anti-inflammatory feedback loop through the excretion of anti-inflammatory cytokines like IL-4 and IL-10[44, 162].

Incredibly, macrophages that have been polarized towards a pro-inflammatory state can be repolarized to an anti-inflammatory state and vice versa[165]. This means that, even in chronic conditions where macrophages have been in an inappropriate state for a long time, they can change and alter the signaling cascade with them. For this reason, immunomodulatory agents capable of transitioning macrophages between pro and anti-inflammatory states have been a topic of intense study in drug development for autoimmune and chronic inflammatory diseases[162]. Perhaps the best known of the immunomodulatory agents used in this way are the drugs designed to target TAMs in many cancers[166]. However, these drugs are susceptible to the same concerns that plague all systemically administered drugs that affect the immune system. Side effects and off target effects are common, but they are also devastating. In the case of the drugs described above, inappropriate targeting of healthy M2 macrophages can cause unwanted inflammation requiring additional treatment[167]; while in the case of an immune modulator targeting M1 macrophages, off target effects could cause immune suppression in areas where inflammation would be beneficial such as in acute injury or illness[168]. Additionally, drugs often only modulate in one direction meaning that for each new application, a new drug must be developed and brought to market which is expensive, inefficient, and time consuming. For this reason, nanomedicine is well suited to immunomodulatory applications, and perhaps the best suited candidate material is nanoceria. Thanks to its powerful ROS scavenging capabilities and recyclable surface oxygen valence, nanoceria has been applied in inflammatory conditions as variable as arthritis and ischemic stroke[30, 132]. However, despite promising data, nanoceria has been underused for medical applications due to concerns about toxicity and poor understanding of the risks and benefits of the use of these particles in living organisms[140].

However, there is not merely one type of cerium-oxide and thus not only one kind of nanoceria[130, 169]. Specifically, it is possible to synthesize nanoceria with a variety of surface valences depending on the synthetic conditions[169]. In chapter 2, we explored the tunability of nanoceria through use of catalysts, pH, and substrates and saw that each synthetic condition provided notable differences in surface valence and resulting catalytic activity. Additionally, the use of a substrate can further alter the behavior of the overall particle by enhancing circulation time, targeting, biocompatibility, or even immunomodulatory effect. Previous research indicates enhanced Ce^{3+} is associated with greater anti-inflammatory effect of nanoceria while enhanced Ce^{4+} is less effective[170]. Based on this information, we hypothesize that modulating towards a Ce^{4+} dominant structure could allow us to enhance the proinflammatory effects of nanoceria. This information allows us to infer that nanoceria could be synthesized with properties that give it the desired effect on the body.

In this study, we investigated the effects of the nanoceria formulations developed in chapter 2 *in vitro* on mouse macrophage analogues and *in vivo* and *ex vivo* in a CIA model. We see that differently synthesized particles have different effects ranging from the expected strong anti-inflammatory effect to a more pro-inflammatory effect depending on surface valence and substrate. These results indicate that engineered nanoceria could be used as a novel immunomodulatory agent capable of being used as either a pro or anti-inflammatory depending on synthetic conditions. This would allow for specialized treatment of many diseases with one class of nanoparticles overcoming many of the downsides associated with traditional drug therapies.

3.2 Methods

3.2.1 Particle Preparation

3.2.1.1 Albumin-Nanoceria

Albumin-nanoceria was synthesized using a biomineralization process. A 20 mg/mL solution of heated to 40°C and allowed to stir until albumin was fully dissolved. Then 0.5 mL of 1 mM cerium (III) nitrate was mixed with the albumin solution, and this solution stirred for 15 minutes. Then, the pH was adjusted using 2 M NaOH. For Ce^{3+} enhanced particles and Ce^{4+} enhanced particles, the desired pH was between 8.5 and 9. For the intermediate albumin nanoceria, a pH of 11 was required. For Ce^{3+} enhanced particles, 600 μL of 30% hydrogen peroxide (H_2O_2) was added immediately as a catalyst. For Ce^{4+} enhanced particles and intermediate particles, no H_2O_2 was added. All solutions were then stirred for 2 hours. After reaction, the solutions are clear (not cloudy) with colors ranging from light yellow to deep orange depending on surface valence. The particles were subsequently filtered via centrifugation through a 100 kDa membrane at 3240 rpm and the filtrate was discarded. The remaining particle solution was kept, diluted to a volume of 2 mL if required, and underwent dialysis through a 10 kDa membrane at 4°C. The final particles were stored at 4°C.

3.2.1.2 Conjugation of ICG to Albumin-Nanoceria

A 0.5 mg/mL ICG-NHS ester solution was prepared in water. This solution was combined with the product of 2.2.1.1 at a ratio of 1:100 ICG to albumin (mg:mg). The solution was rotated overnight at 4°C. These particles then underwent dialysis as described in 2.2.1.1. Following dialysis, excess water was removed using a 100 kDa membrane centrifugal filter, and the particle product was adjusted to the desired concentration. Particles were stored at 4°C.

3.2.1.3 Synthesis of SWCNT-Nanoceria

Synthesis of SWCNT-Nanoceria occurred through a two-step process. First, the hydrophobic SWCNTs were solubilized through PEGylation. Briefly 10 mg of SWCNTs were weighed out in a 20 mL glass vial then combined with 8 mL of water. Then, the SWCNTs were sonicated at 4°C for 30 minutes. During this initial sonication, 50 mg of DSPE-PEG was weighed out and dissolved in 2 mL of water. Then, the PEG solution is combined with the SWCNTs and the combination is further sonicated for 6 hours. After sonication, the solution is stored overnight at 4°C. Following overnight storage, the PEGylated SWCNTs are washed the same way as the albumin-nanoceria (method described in 2.2.1.1). Second, after washing, the PEGylated SWCNT are resuspended at 0.1 mg/mL in water, heated to 40°C, and 0.5 mL of 1 mM cerium (III) nitrate is added. After 15 minutes, the pH is adjusted to 8.5. pH control at this step is critical as higher pH causes particle aggregation. Then, the pH adjusted solution stirs for 2 hours. It is then washed as previously described.

3.2.1.4 Conjugation of SWCNT-Nanoceria to ICG

For the synthesis of ICG conjugated SWCNT-nanoceria, ICG conjugated PEG is made by overnight mixing of 1 mg aminated PEG and 1 mg ICG NHS-ester. This allows the NHS-ester, amine bonding to proceed passively and form a stable product. This product is then used at a 1:9 ratio with DSPE-PEG during the PEGylation stage of 3.2.1.3. Otherwise, the synthesis proceeds as described in 3.2.1.3.

3.2.2 Fluorescence-Activated Cell Sorting (FACS)

J774 cells were seeded in 150 mm tissue culture dishes at 1×10^6 cells per dish and incubated overnight at 37°C and 5% humidity. The next day, cells received cytokine treatment if

appropriate. LPS and IFN-γ (10 ng/mL) were used to induce a pro-inflammatory response in the cells, IL-4/IL-13 treatment (40 ng/mL each), on the other hand, was used to induce an anti-inflammatory response. The cells were incubated overnight. Following incubation, cell in our experimental group were treated with each of the three albumin-nanoceria formulations or our SWCNT-nanoceria formulation at 60 μg Ce/mL. All dishes were incubated overnight. The next day, the cells were detached, permiablized with 0.5% Triton X-100, stained with APC-CD80, PE-Arg-1, and Zombie green fixable viability dye, washed, and fixed in 4% PFA overnight at 4°C. The following day, the fixed cells were washed again, resuspended in flow buffer, and passed through a 70 μm filter prior to FACS. The fixed cells were run on an Accuri c6 flow cytometer. Data was analyzed using FCS Express analysis software.

3.2.3 Collagen Induced Arthritis Model

All animal studies were approved by IACUC of Michigan State University. To initialize CIA, Complete Freund's Adjuvant (1 mg/mL) and Bovine type II collagen (2 mg/mL) were mixed in equal volumes and homogenized on ice. Then, 100 μL of this emulsion was injected into the base of the tail of 6-8 week old DBA/1J mice. After subcutaneous injection, the mice were monitored for 30 days to allow for the development of inflammation. After this monitoring period, a booster is used to complete the induction of CIA. Incomplete Freund's Adjuvant (2mg/mL) and Bovine type II collagen (2 mg/mL) were mixed in equal volumes and homogenized on ice to produce a booster injection. Then, 100 μL of this emulsion is injected at the base of the tail at a different location than the first injection. The mice were then monitored for 10-14 days and the development of arthritis was confirmed.

3.2.4 *in vivo* Particle Treatment

After arthritis has had time to develop, mice are prepared for treatment. Prior to injection, particle solutions were prepared at a concentration of 1.2 mg Ce/mL for injection allowing for injections of 60 µg Ce (50 µL solution), or 30 µg Ce (25 µL solution) directly into the paw of the mouse. Mice were anesthetized under 2% isoflurane and oxygen to allow for pain-free injection. After injection, mice were allowed to recover and return to their cage. Doses were administered 3 times a week over the course of a weeklong study. At the end of the study, arthritis was scored using a scale of 0-4 for the severity of CIA, and mice were sacrificed. Arthritic paws were collected from the mice for future study.

3.2.5 *ex vivo* Immunofluorescence Staining

Arthritic hind legs collected during 3.2.5 were embedded in OCT and sectioned on a cryostat at a thickness of 10 µm. OCT was removed from the slides through 5 minutes of gentle washing in DDI water. Then, tissue was permeabilized in PBS Triton X-100 (5%) for 5 min then blocked for 1 h at room temperature with 1:30 normal goat serum to prevent non-specific binding. After blocking, CD3 - Alexa Fluor 647 (T cell) and F80 - Alexa Fluor 488 (macrophage) primary, fluorescent antibodies were diluted 1:100 in the goat serum and allowed to incubate overnight at 4°C. The following day, the slides were washed twice for 5 minutes in DDI water to remove excess antibody and allowed to dry slightly. Then, slides were coverslipped with DAPI fluoromount and imaged on a Keyence fluorescence microscope.

3.2.6 Statistical Analysis

Statistical analysis was performed in Origin Pro with analysis of the flow cytometry data being analyzed primarily through the FCS Express software. Comparisons of means were performed

using a Student's t-test, and are presented as mean plus or minus standard deviation in graphs.

Statistical significance is defined as p<0.05 for the purposes of this study unless otherwise

stated. For power analysis, effect size was set at 0.5, significance level was set at 0.05, and

statistical power was set at 0.80.

3.3 Results/Discussion

Particles for these experiments were successfully synthesized and characterized as seen in

Figure 8. Following successful synthesis, the particles were used to treat J774 cells, and results

were compared to pro-inflammatory, anti-inflammatory, and undifferentiated control. FACS was

performed using the CD80 as a pro-inflammatory marker (Figure 13) and Arg-1 as an anti-

inflammatory marker (Figure 13). In the study, we see differences in the expression of pro and

anti-inflammatory markers dependent on the particles used in treating the cells. Specifically, the

higher the ratio of Ce^{3+} present in the albumin-nanoceria particles, the lower the expression of

CD80 pro-inflammatory surface marker (Figure 13) and the higher the expression of Arginase-1

(Figure 13). The effect on CD80 expression is much more pronounced showing undeniable visual

evidence that macrophages can have their M1 state modulated by the presence of nanoceria

(Figure 13). However, Arg-1 expression changes in statistically significant ways due to exposure

to nanoceria as well (Figure 13). Specifically, high ratios of Ce^{3+}/Ce^{4+} in the albumin-nanoceria

are associated with higher Arg-1 expression lending credence to the idea that changing the

surface valence of the particles has a strong effect on their immunomodulatory effects.

Interestingly, the trend does not hold for the SWCNT-nanoceria which, based on surface valence

alone, we would expect to have a less pronounced effect on CD80 expression than any albumin-

nanoceria formulation. However, as SWCNT-nanoceria have innate macrophage targeting

capabilities, the strong effect we see on our J774 cells (Figures 13) could be a product of more efficient particle localization to the cells. This result shows that surface valence and substrate tuned nanoceria has remarkable promise as an immunomodulatory agent capable of innately affecting the differentiation of macrophages.
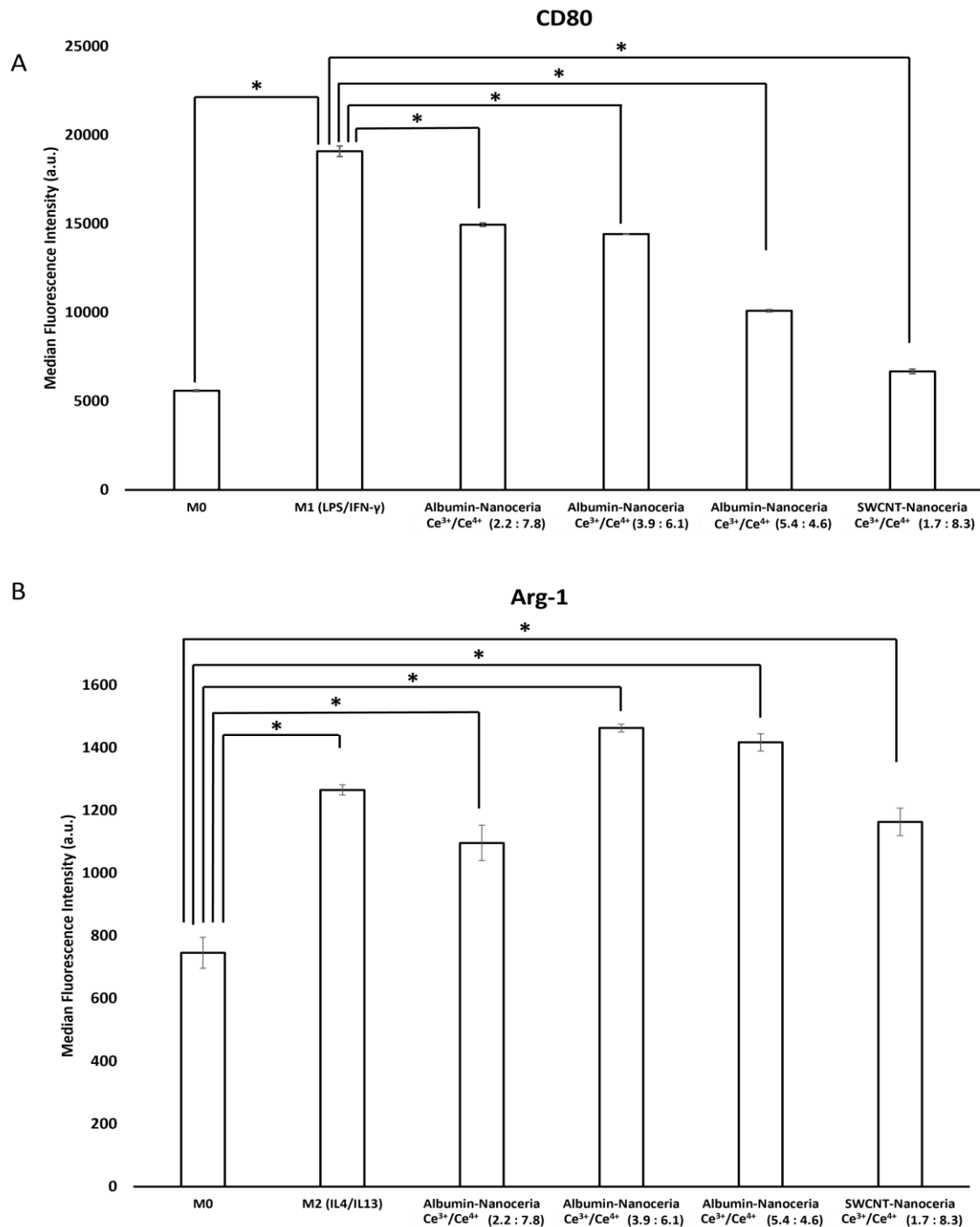
Figure 13: For all particle treated groups, cells were first treated with a pro-inflammatory cytokine cocktail (LPS/IFN-γ). Ratios presented with particle type on the x-axis are the ratio of Ce3+/Ce4+ as determined by XPS. A) Graph of the relative CD80 expression as determined by median fluorescence intensity in our treatment groups. All groups were significant when compared with a pro-inflammatory control (n = 3) (* p<0.05). B) Graph of the relative Arginase-1 expression as determined by median fluorescence intensity in our treatment groups. All groups were significant when compared to an untreated control (n = 3) (* p<0.05).

Our preliminary *in vivo* work was designed to evaluate the anti-inflammatory efficacy of our most anti-inflammatory albumin-nanoceria formulation and our SWCNT-nanoceria on CIA. Prior studies in our lab showed that albumin-nanoceria has promise as a treatment for arthritis[30]. As particles with more Ce^{3+} were shown to be more efficient anti-inflammatories, we selected the albumin-nanoceria with the highest ratio as one of our treatments and we selected the SWCNT-nanoceria as the other in order to evaluate the substrate effect. The results here show that the paw of a mouse treated with a high dose of Ce^{3+} enhanced albumin-nanoceria is visually indistinguishable from a healthy mouse's paw (Figure 14). However, we also see an interesting effect of the SWCNT-nanoceria *in vivo;* our preliminary results seemingly indicate that the SWCNT-nanoceria enhances inflammation rather than act as an anti-inflammatory (Figure 14). This indicates that the SWCNT-nanoceria synthesized has a pronounced substrate effect *in vivo* where it interacts with the wider microenvironment despite showing an anti-inflammatory effect *in vitro* (Figures 13 and 14). This pro-inflammatory effect is likely due to the combination of the lower ratio of Ce^{3+} to Ce^{4+} which was correlated with lower anti-inflammatory efficacy in our *in vitro* experiments and the known inflammatory properties of SWCNT[171].
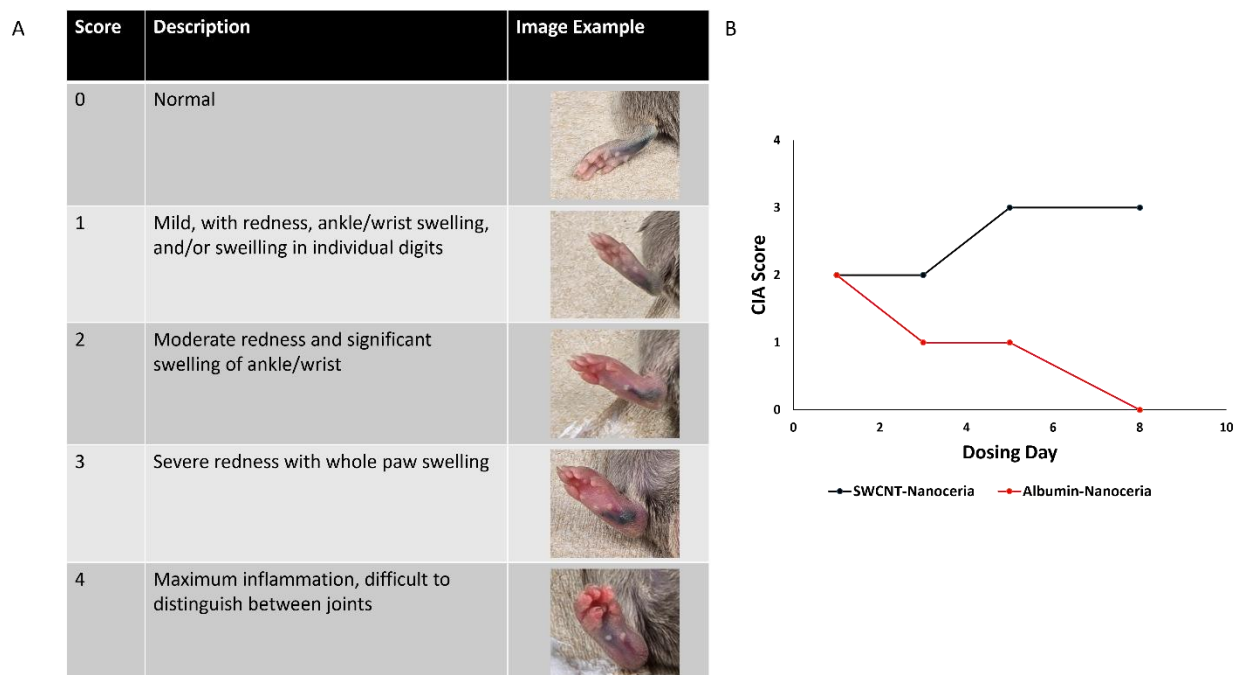
Figure 14: A) A table explaining the CIA scoring scale with images taken from our mice B) A graph showing the effect of particle treatment at 60 µg Ce/mL on CIA in mouse paws (n=1 for each treatment condition). No statistical significance can be determined from this data.

Ex vivo IF staining was used to examine the immune cell populations present in the treated paw of the experimental animal. Specifically, the populations T cells and macrophages were of interest. T cells are instrumental in pro-inflammatory signaling and the M1 polarization of macrophages and are recruited as part of the acute immune response. Thus, high levels of T Cells are correlated with greater inflammation. Macrophages, with their ability to polarize towards M1 and M2 subtypes, are critical in both pro and anti-inflammatory signaling and serve as our target cell for the effects of our nanoceria. We see that in the paw of the animal treated with Albumin-nanoceria with Ce^{3+} enhancement a reduced population of T-Cells with a high population of macrophages (Figure 15) which indicates an anti-inflammatory effect as previous work from our lab indicates that those macrophages are likely to be M2[30]. This is further backed

up by the change from pro to anti-inflammatory phenotype demonstrated in figures 13 and 14.

However, in the SWCNT-nanoceria treated paw, we see that T-Cells are highly expressed and it is

difficult to see the macrophages as the fluorescence is quenched by the SWCNT in the cells[172]

(Figure 15). The high presence of T cells as compared to both the albumin-nanoceria treated

group and the control serve to validate the pro-inflammatory effect shown in the arthritis

scoring.
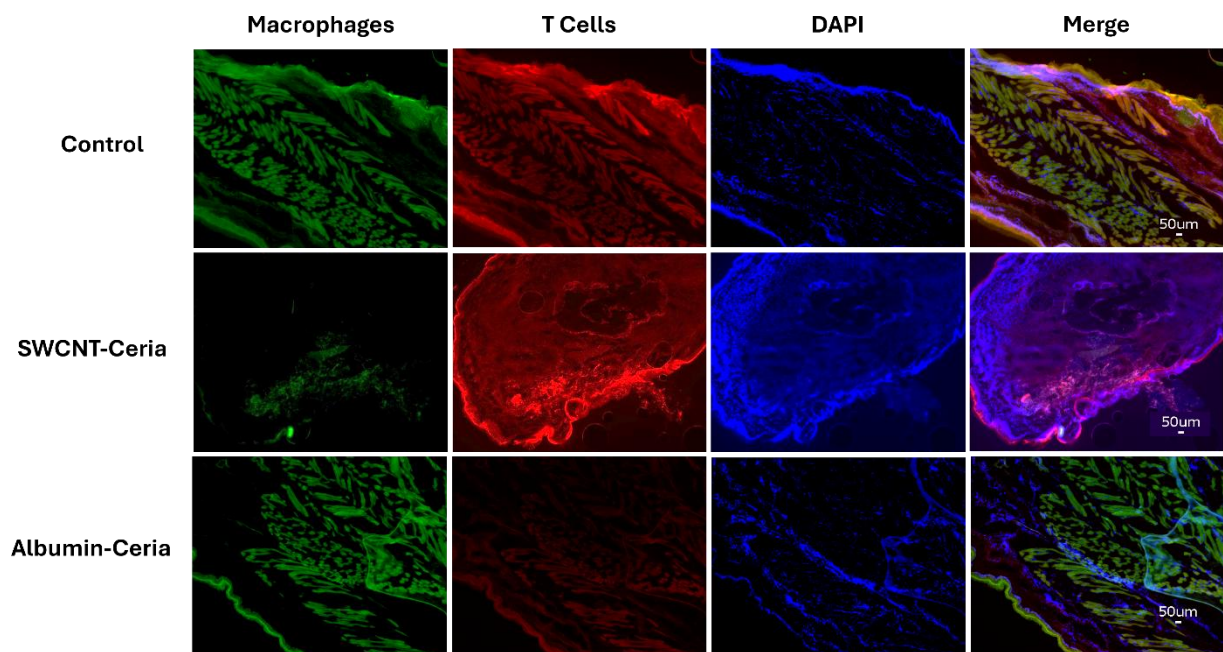
Figure 15: IF staining of sectioned mouse paws taken from the mice described in Figure 14. The control paw is inflamed as expected in CIA. Though it is anti-inflammatory *in vitro* the SWCNT-nanoceria seems to have a pro-inflammatory effect on the paws *ex vivo*. The albumin-ceria shows an anti-inflammatory effect as expected. (Scale Bar = 50 µm) (n=1 mouse paw per condition). Prior studies in our lab show that the populations of macrophages associated with albumin-nanoceria treatment are anti-inflammatory[30].

Here we were able to explore the pro and anti-inflammatory potential of our nanoceria formulations in depth in the *in vitro* stage. However, there are additional FACS studies which would lend more credibility to the claims made in this chapter and round out the data set. First, use of bone marrow derived macrophage cells instead of macrophage analogue cell lines would give us a more realistic model to evaluate the immunomodulatory effects of the nanoceria[173]. While J774 cells are generally effective for modeling macrophage behavior, they are known to have different phenotypes than bone marrow derived or primary macrophages when exposed to the same pathogens or cytokines[174]. Though the flow cytometry data presented in this section is significant and shows the trend we expect, the use of bone marrow derived macrophages would allow us to more accurately determine what phenotypic changes are occurring as a result of exposure to our particles. This would ultimately provide more robust evidence of the effects we see here. Second, studying the effects of our nanoceria on both differentiated and undifferentiated monocytes would provide interesting insights into immunomodulatory effects the particles may have on other cells. As monocytes are the precursors of macrophages and often present in the same environment[175], the ability to affect their initial differentiation and behavior could prove critical to effective immune modulation. If, through using nanoceria, monocytes themselves can be directed to differentiate directly into a pro or anti-inflammatory state, some of the aberrant immune behavior and cytokine signaling found in pro and anti-inflammatory conditions may be avoided altogether allowing for more effective treatment. Additionally, even if we cannot direct the initial differentiation, the immediate treatment of newly derived macrophages with our particle holds promise as a method to enhance our treatment efficacy.

We also primarily explored anti-inflammatory effects of nanoceria in these experiments. Though on an *in vitro* level, we have some compelling evidence that Ce^{4+} enhanced nanoceria have a reduced anti-inflammatory effect as shown in the albumin-nanoceria formulations, and we hypothesize they may have a pro-inflammatory effect based on what we saw in our preliminary SWCNT-nanoceria study *in vivo*. We need additional evidence on both an *in vitro* and an *in vivo* level to validate these findings and allow for translation. Specifically, it would make sense to explore both a pro-inflammatory condition like CIA[176] and an anti-inflammatory one like solid tumor breast cancer[55]. We would expect to see the Ce^{4+} enhanced particles enhancing the severity of the arthritis while reducing the size of the solid tumor while our Ce^{3+} enhanced particles would be expected to do the opposite. By evaluating all our particles, both pro and anti-inflammatory, in multiple conditions, we can gain a much deeper understanding of the role cerium oxide surface valence and particle substrate play in immunomodulation. These nanoceria formulations represent a new class of nanodrugs capable of being used in conditions where more traditional drug and immunotherapies are insufficient.

Only one formulation of SWCNT-nanoceria was successfully synthesized and implemented in the experiments for this chapter due to the challenges associated with its synthesis and stability during the development of the particles. However, now that one stable formulation is able to be reproducibly produced, surface valence tuned SWCNT-nanoceria could be developed with comparable Ce^{3+} to Ce^{4+} ratios to our albumin-nanoceria formulations. This would allow us to more accurately compare the effects of substrate choice on matters beyond targeting capability. For example, using a SWCNT-nanoceria formulation with comparable levels of Ce^{3+} to our most anti-inflammatory albumin-nanoceria would grant us insight into whether the use of SWCNT

enhances anti-inflammatory potential through its targeting, does not affect the overall efficacy of the nanodrug, or even reduces anti-inflammatory effect due to the inherently pro-inflammatory nature of the SWCNT. A greater understanding of the substrate effect would allow for superior particle tuning potentially including the use of novel substrates with properties of interest such as hemoglobin for long term circulation and reoxygenation of hypoxic tissues, hollow Prussian blue nanoparticles for photothermal therapy, or MMP-9 peptide-based particles for targeting.

Finally, while our *ex vivo* analysis of our mouse trial qualitatively appears to indicate efficient targeting by the SWCNT-nanoceria and anti-inflammatory effect from the albumin-nanoceria, additional *ex vivo* analysis would allow us to quantitatively back the claims made in this chapter. FACS studies on the immune population present in the paws of the mice used in our CIA model would allow for a more quantitative interpretation of the IF data presented earlier in this section. Being able to clearly distinguish between, B cells, subgroups of T cells, macrophages, monocytes, and natural killer cells would give greater insight into the overall immune activity of the treatment sites and thus the larger, not macrophage specific, immunomodulatory effect of our nanoceria formulations. Additionally, more mice are needed to be able to draw significant conclusions from the *in vivo* and *ex vivo* work which represents a promising area for further study. Power analysis indicates that each group would need 4 mice to allow for statistical analysis of CIA scoring.

3.4 Conclusions

In this study, we showed the potent immunomodulatory effect of the nanoceria synthesized in the previous chapter. *In vitro* we can clearly see that different nanoceria formulations direct

macrophage differentiation in different directions. Specifically, in the case of the albumin-nanoceria, we see that higher Ce^{3+} is associated with stronger anti-inflammatory M2-like differentiation while Ce^{4+} is associated with pro-inflammatory M1-like behavior. Additionally, we see that our formulation SWCNT-nanoceria is capable of being used as an anti-inflammatory *in vitro*. *In vivo,* our preliminary data suggests that SWCNT-nanoceria has an interesting, proinflammatory effect despite the enzymatically active ceria and anti-inflammatory *in vitro* effect. This is likely due to the inherent inflammatory properties of SWCNT and the more complex interactions that occur in the larger microenvironment of CIA. Further modulation of the SWCNT-nanoceria is needed to improve therapeutic outcomes, and further *in vivo* and *ex vivo* experiments are needed to validate the preliminary results presented here.

Chapter 4: Detection and Treatment of Endometriosis with Theranostic Nanoceria

4.1 Introduction

Endometriosis is characterized by abnormal growth of endometrial tissue outside the utopic endometrium[177]. This disease, which affects 1 in 10 reproductive aged women, can cause a variety of unpleasant symptoms[178]. Patients with endometriosis report pain, irregular periods, heavy bleeding, infertility, reduced social activity, and loss of productivity[179]. Unfortunately, endometriosis is still poorly understood and difficult to diagnose or treat. While traditional therapies including anti-inflammatories, hormone therapy, and surgery can offer some relief from symptoms, they are unable to resolve the underlying cause of the disease resulting in high rates of recurrence and a wide variety of unpleasant side effects[180, 181].

Endometriosis is best described as an estrogen dependent inflammatory condition[182]. In this disease, high levels of inflammatory cytokines are present in the tissue resulting in immune suppression and preventing appropriate immune destruction of endometrial lesions[183, 184]. In fact, the immune system plays a critical role in the disease process of endometriosis. In endometriosis, M1 pro-inflammatory macrophages, B cells, and regulatory T cells are present in unusually high numbers, and the macrophages in particular are associated with the proliferation of endometriosis and some of its most devastating effects[185-187]. Pro-inflammatory macrophages secrete proinflammatory cytokines which in turn recruit other immune cells to prolong inflammation leading to pain, heavy bleeding, and infertility[188]. However, robust populations of M2 anti-inflammatory macrophages are known to improve outcomes for patients[162]. Thus, immunomodulatory agents capable of transitioning pro-inflammatory macrophages to anti-inflammatory macrophages, like albumin-nanoceria, are uniquely poised to treat endometriosis.

STAT3 plays an active role in the development of many tissues throughout the body (Figure 16) including endometrial lesions[189, 190]. pSTAT3 specifically is associated with the high levels of estrogen that drive the development and proliferation of endometriosis[183]. For this reason, STAT inhibitors have been explored as strong candidates for the treatment of endometriosis. In fact, STAT inhibitors have been shown to reduce the prevalence and intensity of symptoms that affect the day-to-day functioning of women with this condition[191]. However, STAT3 is also critical to the proper development of early pregnancy including embryo implantation[190, 192]. For this reason, general STAT3 inhibitors are associated with infertility and pregnancy loss. Since many women of reproductive age would like to have children and infertility is already one of the common concerns of women seeking treatment for endometriosis[193], these off target effects of STAT3 inhibitors are unacceptable to many patients despite their ability to reduce disease burden. To overcome these off-target effects while still effectively treating endometriosis, a targeted STAT3 inhibitory therapy is needed.
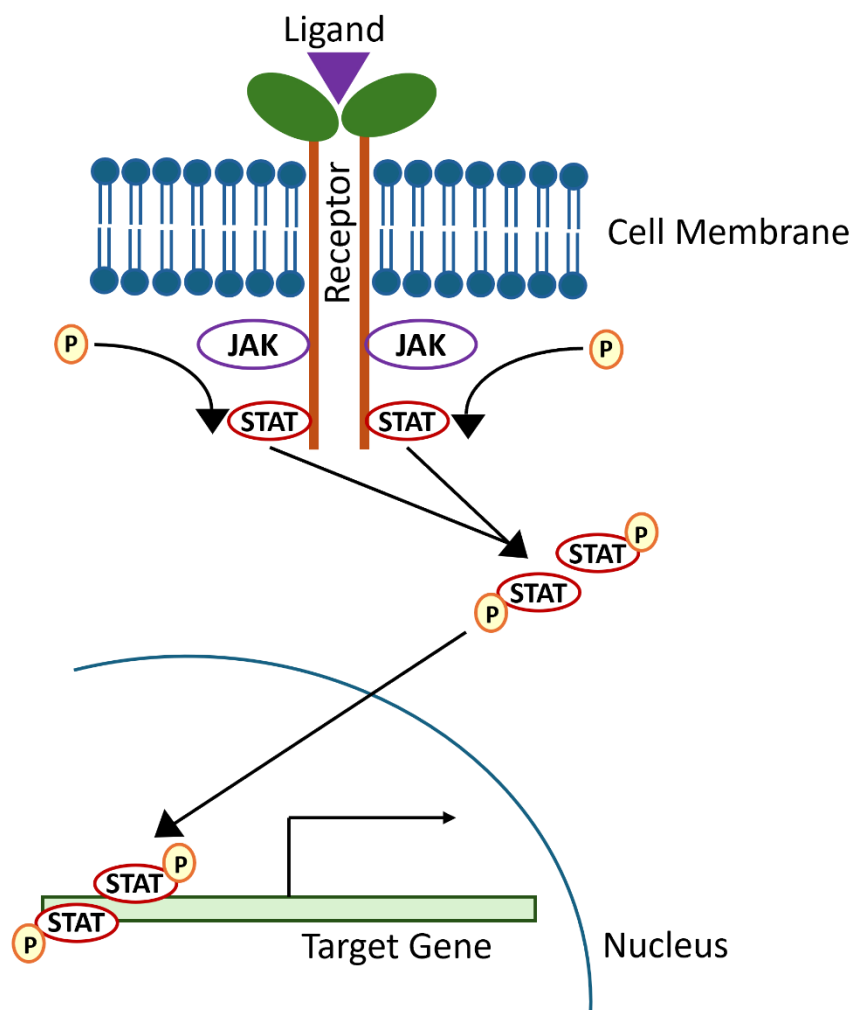
Figure 16: A schematic showing the JAK/STAT pathway in a simple way demonstrating the role that JAK has in the phosphorylation of STAT and the role that pSTAT has in gene transcription.

Nanoparticles are unique in their ability to overcome barriers to effective traditional therapies[194]. Their small size, tunable synthesis, and unique properties make them ideally suited to many applications. Nanoparticles have been employed in a wide variety of medical situations ranging from cancer therapy to antimicrobial applications to the treatment of heavy metal poisoning. In particular, albumin-nanoceria (cerium oxide nanocrystals on an albumin substrate) are a promising candidate for the treatment of endometriosis[195]. These particles, which can change enzymatic activity depending on the ratio of Ce^{3+} to Ce^{4+}, are capable of both acting as a

STAT3 inhibitor and an immunomodulatory agent[30, 140, 196, 197]. Despite these obvious strengths, however, albumin-nanoceria remains underutilized in the treatment of endometriosis. In fact, only one preclinical study on the treatment of endometriosis with nanoceria has been reported outside our group, and it relied on IP injection of nanoceria to relieve endometriosis associated oxidative stress which is impractical for clinical translation[198]. It is also critical to effectively target lesions to both enrich the dose of therapeutic nanoparticles in endometrial lesions and to prevent any off-target effects. Luckily, albumin, a common blood protein comprising around 60% of all blood proteins, accumulates in inflamed areas in the body taking advantage of the swelling and expanded interstitial fluid associated with this inflammation[158]. This allows albumin-nanoceria to effectively target sites of endometriosis in the body without the need for the inclusion of additional targeting molecules.

Thus far, the discussion has centered around the challenges associated with treating endometriosis, but diagnosis is at least as challenging than its treatment[199]. Though there are multiple options for the detection of endometriosis in theory, in practice the existing choices are long, invasive, painful, and ineffective ultimately requiring laparoscopic surgery and histology to confirm a diagnosis[200]. For this reason, finding a non-invasive and effective diagnostic for endometriosis is critical. Albumin-nanoceria could be used as such a diagnostic. These particles can be conjugated to ICG, an FDA approved NIR fluorescent dye that can also be used as a photoacoustic contrast agent, which could serve as a dual in vivo photoacoustic and ex vivo fluorescent marker for lesions as albumin-nanoceria is efficiently targeted to the lesions[91, 201]. Photoacoustic imaging, which is in the process of being translated to the clinic with early systems including the Acuity from iThera and the Imagio from Seno Medical Instruments, is

currently capable of imaging at depths of several centimeters[94]. As this technology continues to improve, it will provide a new way to identify and diagnose endometriosis. In other words, through the conjugation of ICG to the particles, we can create theranostic nanoparticles capable of both treating and diagnosing endometriosis. The work presented in this section was recently published as a co-first author paper alongside Dr. Md Rahman (University of Missouri) in the *Journal of Controlled Release* under the title "Nanoceria as a Non-Steroidal Anti-Inflammatory Drug for Endometriosis Theranostics".

4.2 Methods

4.2.1 Synthesis of Nanoparticles

4.2.1.1 Albumin-Nanoceria

The biomineralization strategy was used to synthesize albumin-nanoceria. Initially, a 20 mg/mL solution of BSA was created by stirring at 40°C. 0.5 mL of 1 mM cerium (III) nitrate was added and the resulting solution was allowed to stir for 15 min. After 15 minutes, the pH was adjusted to 8.5 by adding 2 M NaOH and 600 uL of 30% hydrogen peroxide (H_2O_2) was added immediately to catalyze the reaction. The solution should turn a clear orange color. After validating the color change, the solution was stirred for 2 hours. The albumin-nanoceria formed by this reaction was centrifugal filtration through a 100 kDa membrane at 3240 rpm and the filtrate was discarded. The remaining particle solution underwent dialysis through a 10 kDa membrane at 4°C. The final particles were stored at 4°C.

4.2.1.2 Albumin-ICG

Albumin-ICG particles were made by desolvation. A 2 mL solution of 40 mg/mL BSA and 1.5 mg/mL ICG-NHS ester (an FDA approved NIR dye) in water was prepared and stirred for 15

minutes to allow for the completed disolvation of BSA. After 15 minutes, 6 mL of ethanol was added to the stirring solution dropwise. During this process, the solution should become very cloudy and ICG should completely dissolve. The resulting solution was stirred for 30 minutes at room temperature. The resulting particles were then washed by centrifugal filtration through a 100 kDa membrane at 3240 rpm. The supernatant was collected and underwent dialysis in a 10 kDa membrane overnight at 4°C. The final product was collected and stored at 4°C.

4.2.1.3 Conjugation of ICG to Albumin-Nanoceria

A 0.5 mg/mL ICG-NHS ester (an FDA approved NIR dye) solution was prepared in water. This solution was combined with the product of 4.2.2.1 at a ratio of 1:100 ICG to albumin (mg:mg). The solution was rotated overnight at 4°C. These particles then underwent dialysis as described in 4.2.2.1. Following dialysis, excess water was removed using 100 kDa membrane centrifugal filter, and the particle product was adjusted to the desired concentration. Particles were stored at 4°C. Permanent chemical conjugation of ICG to the albumin-nanoceria was evaluated by measuring the percentage of ICG remaining in the particle solution after repeated centrifugal filtration. Particle stability in the biological environment was evaluated using a 1:10 dilution in SBF with DLS hydrodynamic diameter readings taken over the course of one week.

4.2.2 Characterization of Nanoceria

Dynamic light scattering (DLS, Zeta Sizer Nano, Malvern Instruments) measured the hydrodynamic diameter and colloidal stability of albumin-nanoceria. A 2200FS high-resolution transmission electron microscope (HRTEM, JEOL) was used to evaluate crystallinity and size of cerium-oxide nanoclusters. Samples for XPS were dried by lyophilization and XPS spectrum was acquired using an AXIS SUPRA+ system (KratosAnalytical Ltd.). Albumin concentration was

evaluated via bicinchoninic acid assay (BCA, Thermo Scientific), and ICG quantification measured by absorbance relative to a standard curve 390 nm. Cerium concentration was evaluated using inductively coupled plasma-optical emission spectroscopy (ICP-OES, Varian 710-ES Axial ICP-OES)

4.2.3 Fluorescence-Activated Cell Sorting (FACS)

J774 cells were seeded in 150 mm tissue culture dishes at $1x10^6$ cells per dish and incubated overnight at 37°C and 5% humidity. The next day, LPS and IFN-gamma (10 ng/mL) was added to the plates, other than the untreated cells which received no treatment and the anti-inflammatory cytokine control which received IL-4/IL-13 treatment (40 ng/mL each), and the cells were incubated overnight. Following incubation, cells in our experimental treatment groups were, treated with albumin-nanoceria (150 µgCe/mL), treated with 5,15 DPP (STAT3 inhibitor) (1 nmol), or treated with tofacitinib (JAK7 inhibitor) (1 mmol). All dishes ere incubated overnight. The next day, the cells were detached, stained with APC-CD80, PE-CD206, and Zombie green fixable viability dye, washed, and fixed in 4% PFA overnight at 4°C. The following day, the fixed cells were washed again, resuspended in flow buffer, and passed through a 70 µm filter prior to FACS. The fixed cells were run on an Accuri c6 flow cytometer. Data was analyzed using FCS Express analysis software.

4.2.4 Cell Viability Assay

Cell viability was assessed using a 3-(4,5-Dimethylthiazol-2-yl)-2,5-Diphenyltetrazolium Bromide (MTT) assay. Briefly, J774 cells were seeded in a 96-well plate at 50k cells/well, incubated overnight at 37°C and 5% humidity, and the following day were treated with albumin-nanoceria at 0, 5, 10, 50, 100, or 200 µg Ce/mL. After an additional overnight incubation, the supernatant

is discarded and replaced with MTT solution. Following a 4-hour incubation, the MTT solution is removed, and the resulting formazan crystals are dissolved in DMSO. Absorbance was collected using a SoftMax Pro plate reader (Molecular Devices, CA) at 570 nm. Background used for calculations was collected at 610 nm from the same plate on the same plate reader.

4.2.5 Immunofluorescence Imaging of Drug-Treated Cells

J774 cells were seeded in an 8-well slide at 50k cells/well and incubated as described above. After incubation, the cells were treated as described above in the FACS section and again incubated overnight. Then, the cells were washed to remove particles, fixed with 4% PFA at room temperature for half an hour, washed again to remove excess PFA, then blocked with 10% normal goat serum for half an hour, and finally incubated with primary antibodies (anti-CD80 and anti-Arg-1; 1:300) overnight at 4°C. The following day, they were washed to remove any unbound antibodies and incubated with secondary antibodies (1:100) for two hours at room temperature. Finally, the secondary antibodies were removed by washing. Then the cells were stained with DAPI and imaged using a Leica Thunder Microscope.

4.2.6 Tissue Collection

All animal studies were approved by IACUC of Michigan State University or the University of Missouri. *Stat3^{f/f}* (mice with two copies of the floxed gene encoding STAT3) or *Stat3^{d/d}* (having two deleted copies of the gene encoding STAT3) female and fertile *C57BL/6* male mice were bred and the presence of a vaginal plug in the morning was used to mark the gestational day 0.5 (GD 0.5). Mice were euthanized by cervical dislocation under anesthesia at GD 3.5 and 5.5, and uterine samples were collected. The tissue collected was either directly frozen at −80°C for RNA/protein extraction or fixed in 4% PFA at 4°C for histology. Whole uterine samples obtained

at GD 5.5 were photographed and weighed before fixation in 4% (vol/vol) PFA. Following the fixation, tissue was washed and embedded in OCT for cryosectioning. Using photographs, implantation sites were identified based on their visible characteristics and then counted. Implantation sites were confirmed through histological analysis.

4.2.7 Mouse Model of Endometriosis

Surgical induction of endometriosis was performed following a previously published protocol from Dr. Jae-Wook Jeong's lab at the University of Missouri involving the excision and transplantation of uterine horns from hyperestrogenic donor *Balb/c* mice into recipient mice of the same species[202].

4.2.8 Fluorescence Imaging and Immunostaining

A Nikon fluorescent dissection microscope was used alongside NIS-Elements imaging software (Nikon Instruments, Melville, NY) for fluorescence guided dissection and imaging. Tissue was sectioned at a thickness of 10 µM and placed on slides for fluorescence imaging. DAPI mounting solution (Vector Laboratories, Burlingame, CA, Cat. #H-1800) was applied to the slides to allow for cover slipping. For immunostaining, the tissue sectioned was treated with 0.3% hydrogen peroxide in methanol and washed in 1/40 Triton X-100 (Fisher Scientific, Cat. #BP151-500). The sections were blocked with 10% normal goat serum (NGS; Vector Laboratories, Cat. #S-1000) in pH 7.5 PBS and incubated with primary antibodies diluted in 10% NGS in PBS overnight at 4 °C. Specific dilutions for primary antibodies including anti-pSTAT3 (1:1000 dilution; #ab76315; Abcam), anti-F4/80 (1:800 dilution; #70076; Cell Signaling), anti-CD11c (1:250 dilution; #97585; Cell Signaling), anti-iNOS (1:100 dilution; ab15323; Abcam), Anti- ARG 1 (1:2000 dilution; #93668; Cell Signaling), anti-CD4 (1:100 dilution; #25229; Cell Signaling), anti-CD8α (1:500

dilution; #98941; Cell Signaling), and anti-NKR-P1C (1:200 dilution; ab289542; Abcam) were employed. After the incubation period, fluorescently tagged secondary antibodies were selected [anti-mouse (1:500 dilution; #BA-9200; Vector Laboratories) or anti-rabbit (1:500 dilution; #BA-1000; Vector Laboratories) conjugated to horseradish peroxidase (1:1000 dilution; #43-4324; Invitrogen) and applied before mounting and cover slipping with DAPI mounting media for imaging. Imaging procedures were conducted using PhenoImager HT (Akoya Biosciences Inc.), with whole slide contextual viewing facilitated by Phenochart 2.0.0 (Akoya Bioscience).

4.2.9 *in vivo* Imaging

Animal imaging study was approved by IACUC of Michigan State University. In vivo fluorescence imaging was performed using an IVIS imaging system (PerkinElmer, Waltham, MA) and a Pearl Trilogy NIRF imaging system (LI-COR Biosciences, Lincoln, NE) at various time points (1, 3, 6, 24 h) after intraperitoneal injection of PBS, ICG-conjugated nanoceria into our mouse model of endometriosis. The mice were kept under anesthesia with 2% isoflurane and imaged with white-lighted filter and an 800 nm filter. The regions of interest (ROI) were determined and calculated using Image J. For biodistribution, of ICG-conjugated nanoceria the mice were sacrificed 24 h after injection and the liver, spleen, heart, uterus, and ectopic lesions were removed from the body cavity. Organs were placed on a black background to reduce noise and imaged with a Pearl Trilogy NIRF imaging system. Photoacoustic imaging was performed using an MSOT imaging system (iThera Medical, Germany). Endometriosis was induced in 8-week-old female mice with dual fluorescence reports ($Pgr^{Cre/+}Rosa26^{mTmG/+}$). ICG-conjugated nanoceria (albumin–nanoceria–ICG; 480 µg/kg body weight) were injected into the model mice via tail-

vein injection. 3 hours after injection, the mice were placed in the MSOT animal holder with ultrasound gel; anesthesia (2% isoflurane and oxygen) was supplied through a breathing mask for the duration. Imaging was performed in 0.2 mm steps. All acquisition was performed using 10 averages per wavelength, with 680, 700, 730,760, 800, and 850 nm being the chosen wavelengths. Image analysis was performed in the ViewMSOT software.

4.2.10 Statistical analysis

Statistical analyses were conducted utilizing Prism9 software from GraphPad (San Diego, CA, USA). To assess the distinction between two variables, the Student's t-test was employed. For datasets involving more than two variables, one-way ANOVA was utilized, with Tukey's post hoc test applied for multiple comparisons. Statistical significance was defined as $p < 0.05$. Mean values along with standard error of the mean or standard deviations were employed to present numerical data.

4.3 Results/Discussion

To investigate the role of STAT3 in endometriosis, our murine endometriosis model was compared to a sham mouse which underwent the same procedures as the model organism without the induction of endometriosis. STAT3 was highly expressed across both conditions, however, the expression of phosphorylated-STAT3 or pSTAT3 varied dramatically. In the sham, expression of pSTAT3 was relatively low in the uterus as expected since STAT3 itself is critical for the implantation process during pregnancy (Figure 17). In the endometriosis model, on the other hand, pSTAT3 expression was elevated in the uterus ($p<0.001$) as validated by both h score and IHC (Figure 17). This, alongside prior studies[189], indicates that the activation of STAT3 is critical for the development and progression of endometriosis and may be associated with

72

some of the common symptoms of the disease including inflammation. To validate that high

levels of pro-inflammatory macrophages are present, we compared the macrophage

populations between a STAT3 knockout and a STAT3 expressing mouse. We can see clearly that

in the absence of STAT3, there are more macrophages, and these macrophages are much more

inflammatory (Figure 17). Leading us to believe that STAT3 plays a critical role in the immune

balance of the uterus.
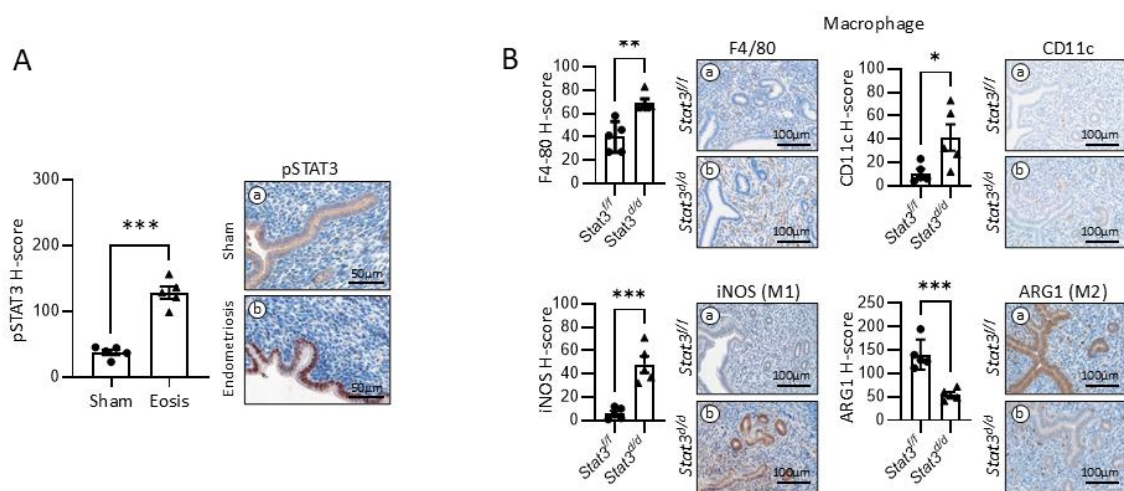
Figure 17: A) IHC showing the enhanced levels of pSTAT3 characteristic of endometriosis as compared to a sham group. (Scale Bar = 50 μm) (n=5) (*** p<0.001) Error bars represent standard error of the mean. B) IHC showing the difference in macrophage presence and subtypes with more inflammatory macrophages present in the STAT3 knockout mice indicating that STAT3 plays a critical role in the suppression of inflammation. (Scale Bar = 100 μm) (n=5) (*** p<0.001). Error bars represent standard error of the mean.

As aberrant STAT3 activation is heavily implicated in endometriosis, one treatment approach

that makes sense would be to treat the condition through blocking of the JAK/STAT pathway.

One drug that has been proposed as a potential treatment for endometriosis is the JAK inhibitor

Tofacitinib. This drug works by inhibiting JAK enzymes and preventing the transmission of

cytokine signals from the molecular environment to the STAT enzymes. This, in turn, decreases

the cellular response to inflammatory signals and reduces inflammation associated symptoms. In endometriosis, we see that treatment with Tofacitinib effectively reduces the size and prevalence of endometrial lesions in our model (Figure 22). Initially, this finding may suggest that Tofacitinib is an ideal treatment for endometriosis. However, there is a major drawback to the use of Tofacitinib in the treatment of endometriosis. Tofacitinib blocks the JAK/STAT pathway in all tissues not just in endometrial lesions. This means that the STAT3 pathway is inhibited in the utopic endometrium within the uterus leading to implantation failure and infertility. Specifically, in our mouse model we saw treatment with Tofacitinib caused complete implantation failure (Figure 22). Since a major symptom of and complaint about endometriosis is resulting infertility, any treatment that does not address this concern or, in the case of Tofacitinib, makes pregnancy even less likely is unlikely to be adopted widely in the clinical setting. Following this logic, utilizing a targeted anti-inflammatory could help overcome these concerns.

Nanoceria is a well-established NSAID within the world of nanomedicine thanks to its well characterized multi-enzymatic behavior and powerful ROS scavenging ability. To enhance its effectiveness for the treatment of endometriosis, we combined it with a biocompatible, inflammation targeting albumin protein. This was achieved through the biomineralization process wherein inorganic cerium oxide nanocrystals are deposited on albumin protein to form an organic-inorganic complex capable of withstanding the biological environment. It is known that albumin accumulates well in highly vascularized sites of inflammation such as those found in endometriosis while otherwise remaining in circulation[145]. This allows albumin-nanoceria to effectively accumulate in endometrial lesions while not accumulating in healthy uterine tissue.

To make the particles theranostic, a NIR dye known as ICG was chemically post-conjugated to the albumin-nanoceria. The dye is covalently conjugated to the particle preventing leaching in biological conditions as confirmed by both measurement of the percent ICG remaining in the particles following repeated washing steps and a weeklong stability study performed in SBF where the hydrodynamic diameter was shown to be consistent (Figure 18). The particles were found to have cerium oxide clusters of size ~5nm within a protein shell with size ~25 nm as validated by TEM (Figure 18). Size was further validated using DLS to assess hydrodynamic diameter. The particles were found to be monodisperse with a hydrodynamic diameter of 28.65 nm and a PDI of 0.471 validating the TEM results (Figure 18). Additionally, the particles exhibited mixed surface valence containing both Ce^{3+} and Ce^{4+} at a ratio of 0.54:0.46 (Figure 9) allowing them to effectively scavenge ROS as shown by the DCFDA assay for ROS scavenging (Figure 18). The enzymatic behavior of the particles was confirmed by SOD and Catalase colorimetric assays (Figure 11).
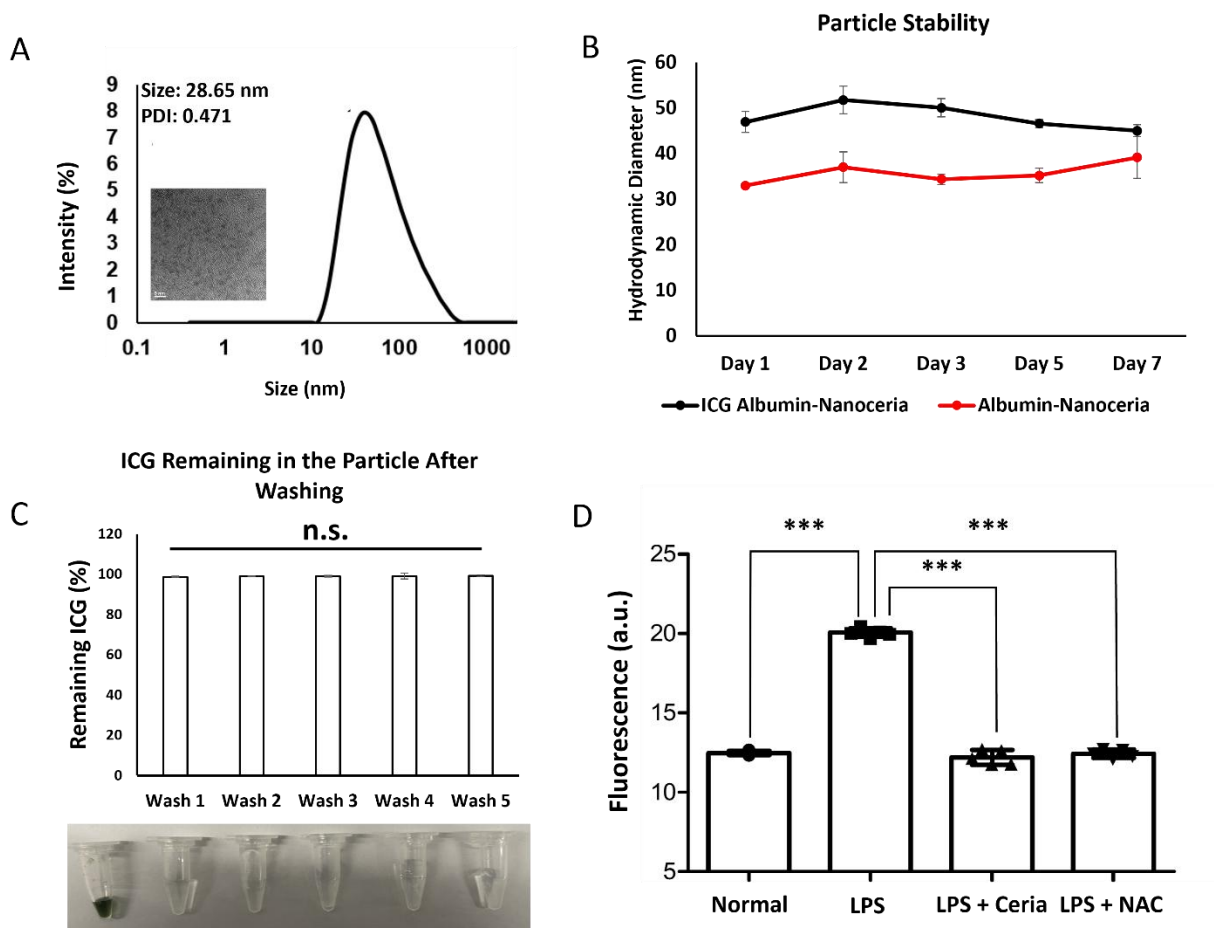
Figure 18: A) DLS data confirming the overall size and monodispersity of the particles with inlaid HRTEM showing small and highly crystalline cerium oxide nanocrystals. (Scale Bar = 5 nm) B) Particle stability studies show that over the course of 7 days in SBF neither the ICG albumin-nanoceria nor the unconjugated albumin-nanoceria degrade or change size. C) ICG conjugation study showing the covalent, highly stable conjugation of ICG to our particles. Even after 5 washes, no significant ICG has leeched out of the particles. D) Results of a DCFDA assay performed in J774 cells (n=5 wells) (*** $p<0.001$) showing that nanoceria can effectively reduce ROS. Error bars represent standard deviation.

While our albumin-nanoceria were confirmed to be small, enzymatic, and stable particles, it was critical to assess the biocompatibility of the particles prior to their use *in vitro* and *in vivo.* Nanoceria alone is associated with a variety of negative side effects ranging from cytotoxicity to neurotoxicity and genotoxicity. Thus, any new particle including cerium oxide must be carefully evaluated for biocompatibility prior to use in biomedical research.

Fortunately, our albumin-nanoceria is exceptionally biocompatible. At concentrations as high as

200 µg Ce/mL, there is no cytotoxicity or inhibition of proliferation (Figure 19). This is

meaningful when considering that the dose used in our studies is lower than the highest

concentration evaluated in the MTT assay for cell viability. To validate their safety in living

subjects, we performed a comprehensive blood panel on mice treated intraperitoneally with

albumin-nanoceria or orally with Tofacitinib overnight. Notably, we saw no differences between

the nanoceria treated groups, tofacitinib treated groups, and the control group for any of our

chosen markers. The markers included creatinine (CREA), triglycerides (TRIG), cholesterol

(CHOL), aspartate aminotransferase (AST), glucose (GLUC), calcium (CA), alanine transaminase

(ALT), total bilirubin (TBIL), blood urea nitrogen (BUN), alkaline phosphatase (ALKP), sodium

(Na), potassium (K), and chloride (Cl). AST, ALT, and ALKP were used as proxies for liver function

and CREA and BUN were used as proxies for kidney function (Figure 19).
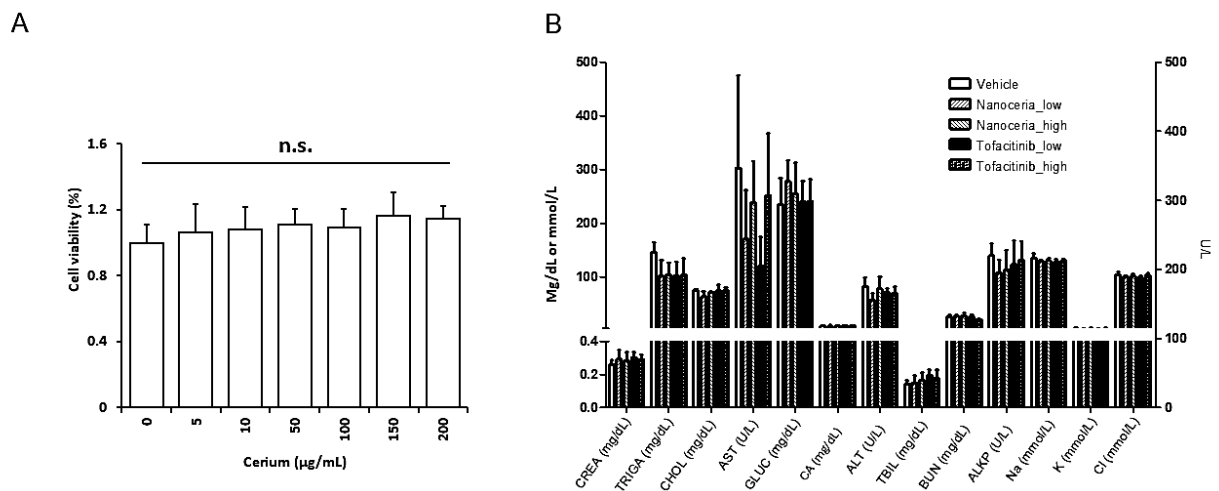
Figure 19: A) MTT assay for cell viability shows that albumin-nanoceria is not cytotoxic even at high concentrations. (n=6 wells) Error bars represent standard deviation. B) Blood chemistry results show that neither nanoceria (120 µg/kg) or (480 µg/kg) nor our control treatment tofacitinib affect kidney, liver, or metabolic function after overnight treatment as compared to a control animal (n=3 animals per treatment condition). Error bars represent standard deviation.

To evaluate the anti-inflammatory and immune modulatory effect of the albumin-nanoceria *in vitro* J774 macrophage analogue cells were used for multiple experiments. Since pro-inflammatory M1 macrophages are enhanced in endometriosis and contribute to the chronic inflammation associated with the disease, treatments ideally designed to treat endometriosis should act as potent anti-inflammatories while also helping transition local cells from M1 behavior to M2 behavior. To validate the anti-inflammatory effect of the nanoparticles, we performed a FACS experiment designed to replicate the introduction of the particles into a pro-inflammatory environment. Essentially, our particles, Tofacitinib or 5,15 DPP (a STAT inhibitor) were each used to treat pro-inflammatory J774 cells that had been induced using LPS and IFN-γ. Following treatment, the cells were fixed and stained with CD80 expression correlated with pro-inflammatory differentiation. Interestingly all three treatments were able to effectively reduce CD80 expression in activated J774 cells. However, the albumin-nanoceria performed slightly better than either of the traditional inhibitors. Additionally, the performance of the albumin-nanoceria compared to the inhibitors indicates that our particles are capable of inhibiting STAT3 activation which in turn inhibits inflammatory signaling (Figure 20).

To further validate the findings of the FACS study, we performed *in vitro* IF staining for CD80 (our pro-inflammatory marker) and Arg-1 (a well-known anti-inflammatory marker). Following the same treatments used in the flow cytometry experiments, the cells were stained with fluorophore bound antibodies and DAPI. While this experiment did validate the findings of our FACS study, there were two additional interesting findings. First, while all three treatment conditions reduced the expression of CD80, nanoceria notably enhanced the expression of Arg-1 (Figure 20). This indicates that not only are the particles reducing inflammation, but they are

also actually driving differentiation towards an M2 anti-inflammatory state. This immunomodulatory effect, which was shown in figures 13 and 14, would make them an even more potent treatment for endometriosis as M2 macrophages are associated with better outcomes and symptom reduction. Additionally, we found that the morphology of cells treated with our albumin-nanoceria is notably rounded and similar to the morphology of cells treated with anti-inflammatory cytokines. This further validates albumin-nanoceria as a potent anti-inflammatory and immunomodulatory drug.
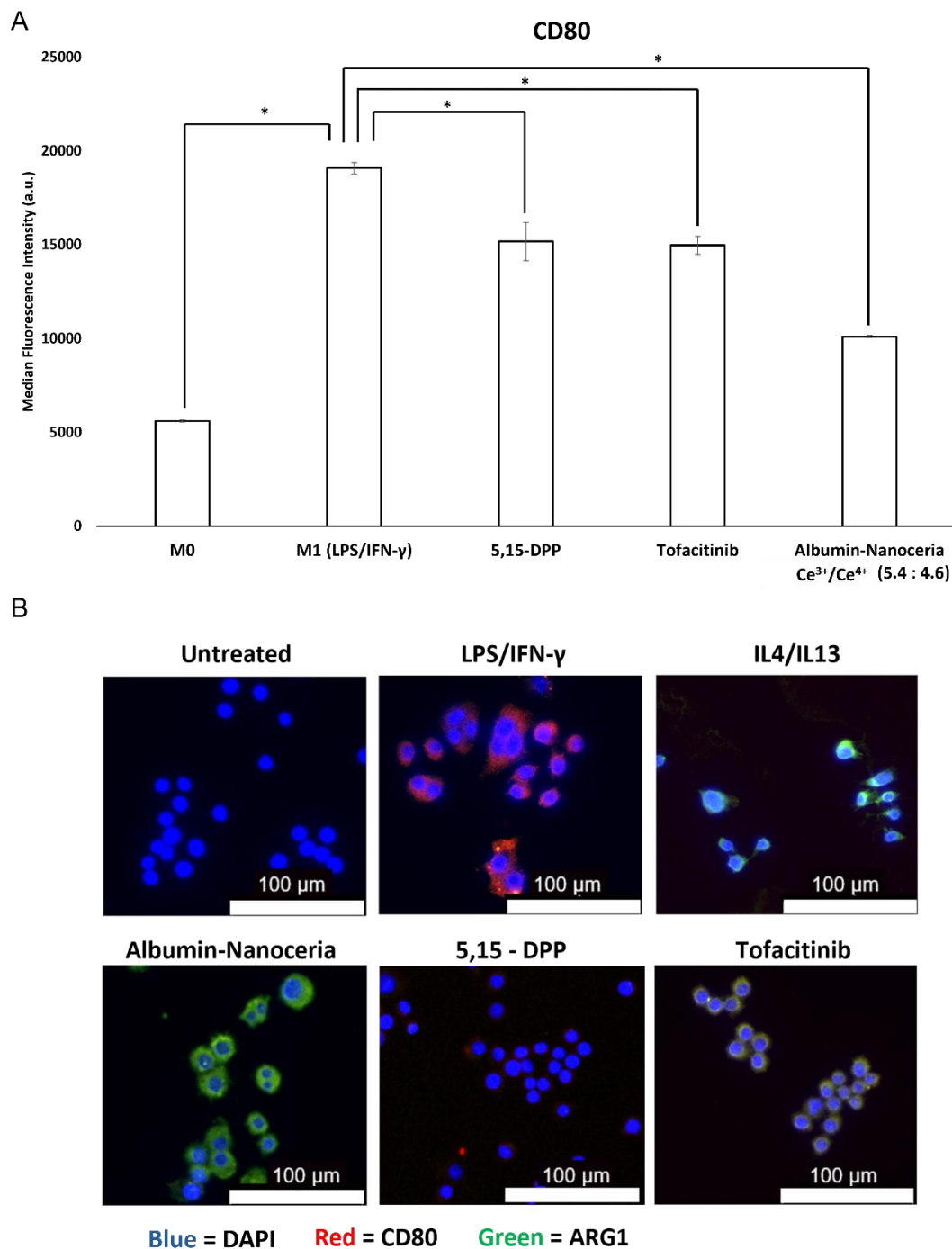
CD80

Figure 20: A) Flow cytometry data comparing the CD80 expression (correlated with M1 behavior) of cells treated with inflammatory cytokines alone to those left untreated or treated with inflammatory cytokines and particle or drug showing strong anti-inflammatory capacity of nanoceria and traditional drugs (n=3) (* p<0.05). Error bars represent standard deviation. B) IF staining showing the effects of different treatments on J774 cells with CD80 expression correlating with M1 and ARG correlating with M2. DAPI is included as a nuclear stain.

Since endometrial lesions have disorganized and leaky vasculature and a notably inflammatory environment. This disorganized and leaky vasculature is correlated with abnormally high blood flow in the endometrial regions which means we expect our particles to localize to the lesions and interact with immune cells rather than traveling to the healthy, organized uterine tissue. To validate the targeting potential of the albumin-nanoceria, ICG albumin-nanoceria was used so that localization of the particles could be easily visualized by photoacoustic and fluorescence imaging (Figure 21). Model mice were treated with these particles *via* IV. Three hours after injection, photoacoustic images were taken of the mouse with the goal of distinguishing the lesions from surrounding healthy tissue. Endogenous hemoglobin, from the excess blood flow in the lesions, and exogenous contrast provided by the nanoparticles were highly colocalized indicating strong accumulation of the particles in the endometrial lesions. To produce this model, GFP expressing uterine tissue from our model mice ($Pgr^{cre/+}Rosa26^{mTmG/+}$) was used to produce the endometrial lesions for this study. This makes it possible to detect the lesions and the uterus of our model mice through fluorescence imaging of the abdominal cavity. To validate the presence of lesions at the sites of accumulation, *in vivo* fluorescence imaging of these GFP expressing cells was performed showing lesions at the locations identified by photoacoustic imaging (Figure 21). These images confirmed the presence of nanoparticles in the lesions. After the mice were sacrificed, organs of interest including the liver, spleen, kidneys, uterus, and lesions were removed from the mouse and imaged *ex vivo* by a PEARL NIR fluorescence imager (Figure 21). The images showed a statistically significant difference in fluorescence between the lesions and the uterus with the lesions having an approximately 2.5-fold higher fluorescence than the uterus. High signal from the liver was also observed since nanoparticles administered

intravenously are known to accumulate in the liver. Finally, lesions were embedded in OCT and

sectioned for fluorescence microscopy. Resulting images, which were counterstained with DAPI,

show the presence of ICG in the lesions but not the uterus validating the targeting potential of

our particles (Figure 21).
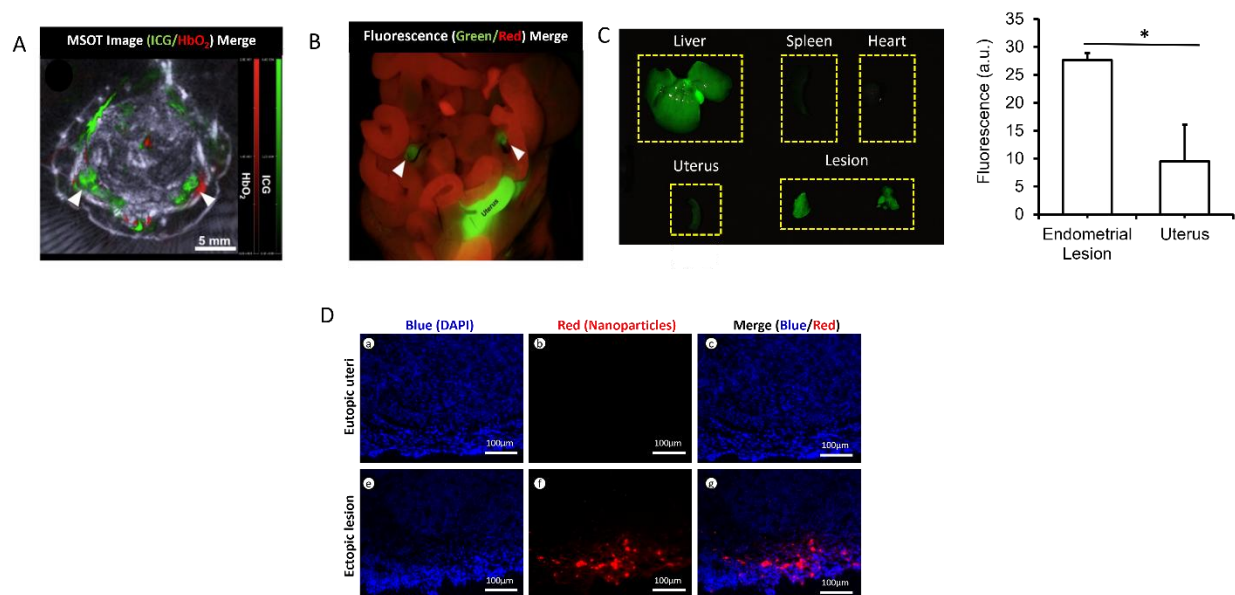
Figure 21: A) *in vivo* photoacoustic (Scale Bar = 5 mm) image showing two regions where endogenous signal from the blood and exogenous signal from the particle overlap. Regions of high blood flow are expected to be lesions due to their disorganized and leaky vasculature (n=3). B) Fluorescence imaging shows expression of the GFP expressing uterus and lesions in the mouse from A showing that there are 2 lesions in the same locations indicated by photoacoustic imaging (n=3). C) *ex vivo* NIR fluorescence imaging, facilitated by the ICG present in our particles, of key organs showing strong signals from the liver and lesions. The lesions display significantly higher signal than the uterus (n=3) (* p<0.05). Error bars represent standard deviation. D) *ex vivo* imaging of lesions stained with DAPI (blue) demonstrating that particles (red) are present in the lesions but not in the uterus. (Scale Bar = 100 μm).

Following the validation of targeting, we confirmed the effect of albumin-nanoceria on

endometriosis and infertility. Nanoceria was compared to a vehicle treatment, and the effect on

number of lesions and implantation were evaluated. Much like with the Tofacitinib, we see a

significant reduction in endometrial lesions in the mice treated with albumin-nanoceria as

compared to vehicle treated mice (Figure 22) indicating that the albumin-nanoceria is effective

at reducing the disease burden of endometriosis. Unlike the Tofacitinib, however, mice treated

with particle did not exhibit implantation failure at gestational day 5.5. Mice treated with

particle showed no statistically significant difference in number of implantation sites as

compared to the vehicle treated group (Figure 22).
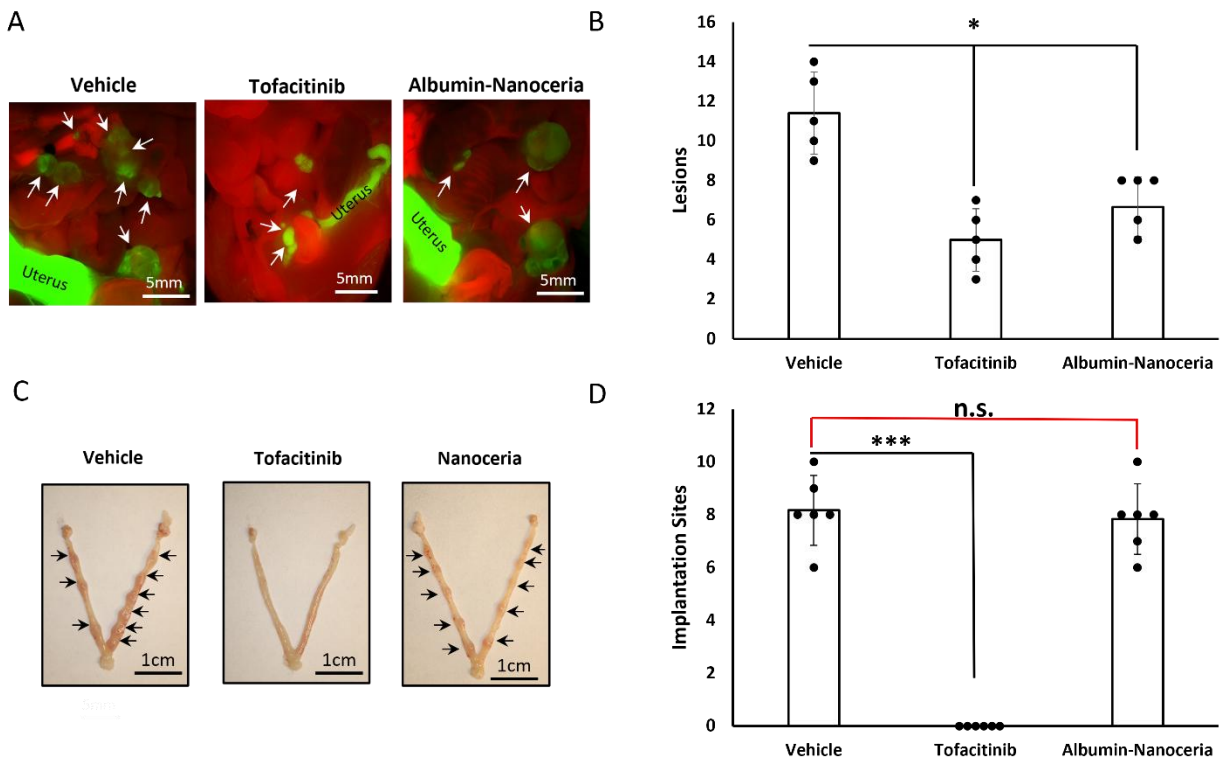
Figure 22: A) *in vivo* fluorescence imaging showing the presence of lesions in vehicle, tofacitinib, and albumin-nanoceria treated mice. (Scale bar = 5 mm) B) A graph showing statistically significant differences between the number of lesions present in the vehicle treated group and the tofacitinib or albumin-nanoceria groups (n=5) (* $p<0.05$). Error bars represent standard deviation. C) Representative *ex vivo* images of uteri with implantation sites of treatment groups at GD 5.5. (Scale bar = 1 cm) D) A graph showing a statistically significant reduction in implantation sites between vehicle treated and tofacitinib treated animals but not between vehicle and albumin-nanoceria treated cells showing that albumin-nanoceria does not influence fertility (n=6) (*** $p<0.001$). Error bars represent standard deviation.

To elucidate the mechanism of action for nanoceria in the treatment of endometriosis, we

performed IHC for a variety of markers characteristic of various immune cell populations.

Looking at the sections from a morphological perspective, we can clearly see the glands and

stroma typical of endometriosis present in our model mice. However, when we look at our immune system markers, we see a dramatic difference between the particle treated and vehicle groups. Particle treated mice express lower levels of F4/80 and CD11b (Figure 23) which can be used as a proxy for the total number of macrophages present in tissue. Despite the reduction in overall macrophages, however, while the particle treated group had lower expression of iNOS and thus lower levels of pro-inflammatory macrophages while simultaneously significantly increasing the expression of Arg-1 and thus the number of anti-inflammatory macrophages (Figure 23). This is the direct opposite of the expression shown in the endometrium of untreated model mice indicating nanoceria effectively modulates macrophages *in vivo.* We also see that the number of T cell surface markers (both CD4 and CD8α) are reduced in the uterine tissue of particle treated group (Figure 23). To validate that this effect was associated with reduction in pSTAT3 in the mice treated with albumin-nanoceria, we compared epithelial expression of pSTAT3 between the experimental and control groups. Notably, mice treated with the particles exhibited reduced epithelial expression of pSTAT3 (Figure 23) indicating the nanoceria is acting as an effective STAT inhibitor[196, 197, 203] making it a promising candidate for targeted therapy in the future.
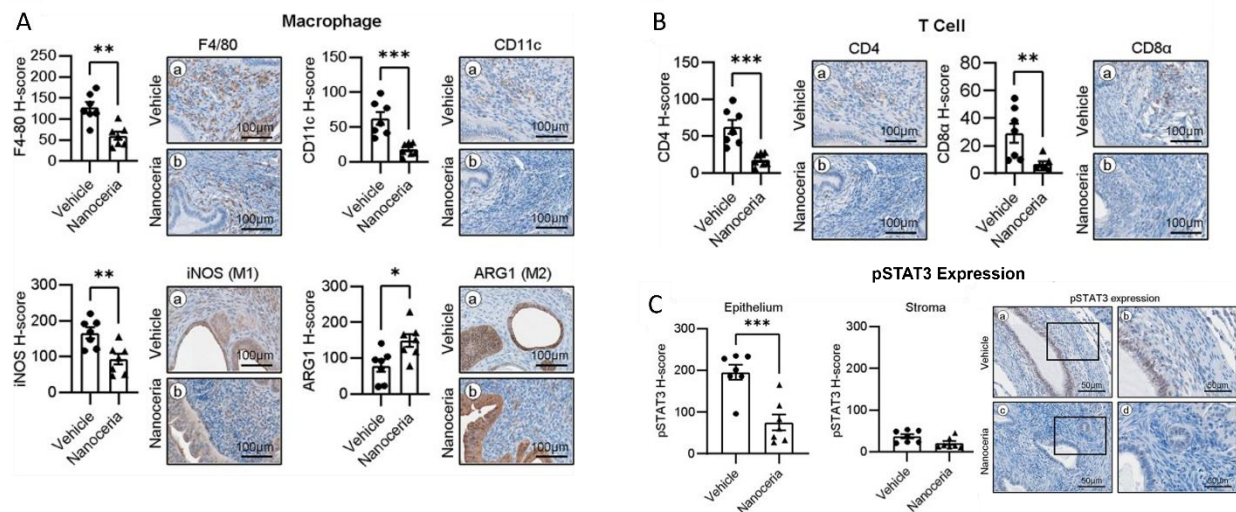
Figure 23: A) IHC Staining for the presence and phenotype of macrophages present in endometrial lesions. F4/80 and CD11c expression indicate that the overall population of macrophages found in nanoceria treated animals was lower than that of the vehicle treated animals. iNOS expression shows that the population of macrophages present is significantly less pro-inflammatory in the nanoceria treated condition while ARG1 expression indicates the population of macrophages present is significantly more anti-inflammatory (n=7 for each group) (** p<0.01). Error bars represent standard error of the mean. B) ICH staining for both CD4 and CD8α show an overall reduced T cell populations in the uterine tissue of nanoceria treated mice (n=7 for each group) (** p<0.01). C) pSTAT3 expression in the epithelium and stroma of vehicle and nanoceria treated mice show a significant reduction in epithelial pSTAT3 (n=7 for each group) (*** p<0.001). Error bars represent standard error of the mean.

This work shows the effect of nanoceria on STAT3 activation in endometriosis. Nanoceria, known for its ROS scavenging and immunomodulatory effects, acts as a STAT inhibitor in endometriosis[196, 197]. Luckily, the albumin protein shell of the particles allows them to effectively target lesions rather than indiscriminately affecting STAT activation throughout the reproductive system. This is critical to preventing implantation failure and thus infertility in those receiving treatment for endometriosis. Since STAT3 plays a critical role in the successful implantation of embryos in the uterus, any treatment that disrupts the proper activation of this enzyme can result in infertility. pSTAT3 expression is associated with disease progression and symptom

severity, so targeting the inappropriate activation of STAT3 is a promising treatment strategy for endometriosis.

Though it is well established that nanoceria is an effective anti-inflammatory, there have been remarkably few instances of its use in endometriosis. In fact, nanomedicine as a whole has been underexplored for this application. However, in recent years there has been some progress in the application of nanomedicine to endometriosis[204]. In the realm of lipid nanoparticles, methotrexate loaded particles have been effective in treating the symptoms of endometriosis in patients with deep infiltrating endometriosis[205]. Albumin-glucose oxidase particles were also investigated for their potential benefits for patients[206]. These studies are missing key exploration of whether these therapies inhibit or reverse the progression of endometriosis, however, and additionally do not discuss the effects of these nanoparticle formulations on pregnancy. Polymeric PLGA particles have been loaded with a variety of drugs including doxycycline and been shown to inhibit proliferation of endometrial cells while also reducing angiogenesis and driving the apoptosis of existing cells[207]. This approach is non-targeted, however, and thus is prone to off target effects not dissimilar to those seen in traditional STAT inhibitors. Magnetic hyperthermia driven by the presence of IONPs localized in the lesions has also been explored as an option for endometriosis treatment[36]. This technique allows for effective and targeted elimination of regions with high concentrations of particle. However, the location of endometrial lesions makes hyperthermia a risky choice. Specifically, endometrial lesions occur in the abdominal cavity and are located close to the liver. The liver takes up high levels of IONPs and thus is susceptible to damage during treatment[208, 209]. Finally, laser ablation has been explored as an alternative treatment[210]. Using particles which absorb laser light and heat up,

localized regions are heated to temperatures that result in the destruction of surrounding tissue. This approach is promising as it allows for much more precise control than other methods described in this section. However, a major limitation of laser ablation in this application is the laser's depth of penetration[211]. Limited penetration depth means that this strategy could only be employed on lesions located close to the skin or during invasive surgery. Furthermore, laser ablation is known to enhance inflammation in the treated region[212] which, in the case of endometriosis which proliferates in inflammatory conditions, may cause a rebound effect.

The ICG albumin-ceria used in this study were well suited to the application since they both provided a way of targeting endometrial lesions and an extrinsic photoacoustic contrast agent. However, further modification of the particles could serve to enhance their performance. Notably, the targeting effect seen here is a product of the tendency of albumin to accumulate withing areas with disorganized vasculature[213]. Also called the EPR effect, this method of targeting is effective but passive meaning that there is room to enhance accumulation in our tissues of interest. By using anti-VEGF antibodies, we could incorporate active targeting. VEGF is highly expressed in ectopic tissue meaning that these modified particles would directly interact with lesions[214-216]. Additionally, the existing photoacoustic contrast provided by ICG could facilitate non-invasive diagnosis of endometriosis. Photoacoustic imaging, based on a light in sound out principle, combines the sensitivity and contrast of traditional optical imaging while benefiting from enhanced imaging depth and resolution[201]. This imaging modality would make the lesions, even those located deep within the abdominal cavity, easy to visualize when they are effectively tagged by ICG conjugated nanoparticles. By enhancing our active targeting

87

strategy, we can help move diagnosis of endometriosis towards a non-invasive imaging-based strategy that is more cost effective and patient friendly.

4.4 Conclusions

ICG albumin-nanoceria is uniquely suited to the diagnosis and treatment of endometriosis due to its unique properties. While the nanoceria itself acts as an NSAID and STAT3 inhibitor, the albumin allows for lesion specific targeting preventing off target effects characteristic of traditional STAT3 inhibitors. In fact, ICG albumin-nanoceria causes a statistically significant reduction in lesions without affecting the fertility of treated mice. Additionally, the ICG allows for straightforward, non-invasive photoacoustic imaging of lesions as validated by ex vivo fluorescence imaging and histology. By acting as a theranostic and overcoming many of the side effects associated with traditional therapies and diagnostics, ICG albumin-nanoceria will provide safe alternatives and ultimately hope to the large number of reproductive aged women who suffer from this condition.

Chapter 5: Detection of Colorectal Cancer Using Fluorescent Silica Nanoprobes

5.1 Introduction

In chapter 4, we explored the benefits of using nanoparticles to allow for imaging of endometriosis which is traditionally only able to be diagnosed by exploratory surgery. Development of novel contrast agents allows us to detect conditions that otherwise may be difficult or impossible to detect using commercially available imaging systems. However, some diseases are currently screened for using well established, but imperfect protocols that can be further improved using a nanoparticle contrast agent. In chapter 4, we showed the *in vivo* benefits of using an NIR dye, ICG, as both a photoacoustic and NIR fluorescence contrast agent for sensitive imaging of lesions for noninvasive diagnosis of endometriosis. NIR fluorescence imaging can offer clinicians the ability to easily detect cancerous lesions located close to the surface with proper targeting, which would reduce the false negative results. Here, we developed a novel nanoparticle for use in fluorescent endoscopy to allow for more sensitive and specific detection of early-stage CRC. CRC is the third leading cause of cancer related death in the United States despite having an early detection survival rate of 90%[217-219]. This is due to the troubling fact that if CRC is detected after mucosal invasion, the survival rate drops to 14%[220]. For this reason, early detection is both uniquely necessary and uniquely challenging in CRC leading to the variety of available screening methods available on the market today. Screening methods range from molecular screening tools like fecal DNA testing to standard clinical imaging CT[221, 222]. However, the best known and most employed early detection method for CRC is colonoscopy[223]. Most people are familiar with colonoscopy since it is a commonly employed preventative screening recommended for those over 45 years old. The benefits of

colonoscopy are numerous. It is safe and well understood, allowing physicians to perform it effectively at large scale in the clinic. Additionally, it is real time allowing physicians to assess the characteristics of the tissue as they are rather than as they were at a fixed point in time. It also gives direct access to the tissue allowing for real time biopsy of regions of interest without invasive surgery[224]. However, there are some critical downsides to colonoscopy. First, colonoscopy does not provide any molecular information, such as protein expression, for the tissue relying instead on visual differences between healthy and diseased tissue. Second it relies on white light imaging that is typically not enhanced by contrast agents making it challenging to differentiate between similar looking early-stage cancerous lesions and healthy intestinal lining[225]. Unfortunately, colonoscopy relies completely on the ability of physicians to visually distinguish between healthy tissue and cancerous or precancerous tissue. These shortcomings can contribute to lower early-stage diagnosis even in patients who receive appropriate preventative screenings.

Fluorescence based imaging techniques have recently been gaining favor within the world of biomedical imaging. These techniques range from imaging of natively fluorescent drugs inside the body to specially designing contrast agents for different applications[226, 227]. It is not hard to see why fluorescent imaging has been widely adopted. Fluorescence imaging has excellent temporal resolution and specificity with a wide variety of fluorescent dyes and molecules available on the market covering the entire visual spectrum as well as parts of the UV and IR spectra[228, 229]. Additionally, fluorescence imaging is cost-effective and simple to perform and interpret thanks in large part to the ease of accessing machines capable of this kind of imaging[90]. The machines are common and easy to use unlike many other medical imaging

modalities. However, fluorescence imaging has some major downsides that contribute to its relatively limited clinical use in humans. First, small molecule imaging agents and dyes, including natively fluorescent drugs, are often efficiently cleared from the system and making longer imaging sessions or multiday studies impractical[37]. Additionally, fluorescence has limited ability to penetrate through water-rich biological tissues resulting in poor imaging depth in large animals[230, 231]. These challenges must be addressed for fluorescence imaging to be effectively employed in humans.

During my PhD, I developed such a contrast agent. Specifically, I developed NIR fluorescent silica nanoparticles capable of selectively targeting CRC through use of anti-CEA antibodies[37]. Silica nanoparticles were an ideal choice for this application. Silica is biocompatible with a well-established history of use in the medical field and multiple unique applications in imaging[232-234]. Additionally, these nanoparticles are straightforward to synthesize with a highly reproducible and tunable synthetic method where the size of the particles can be determined by synthesis time. Dyes can be covalently conjugated to silicate precursors and integrated directly into the nanoparticles rather than being conjugated to the surface of the particles after synthesis[235]. This allows for stable fluorescence that is not susceptible to leaching. In the case of our fluorescent silica nanoparticles, we used CF800 NIR fluorescent dye. Use of an NIR fluorescent dye allows us to take advantage of the biological transparency window: the part of the electromagnetic spectrum at which tissue and water absorb relatively low amounts of light[233]. This reduced absorbance allows imaging of NIR contrast agents at depths of up to several centimeters[236]. The surfaces of FSNs are highly modifiable allowing for enhanced biocompatibility and targeting capabilities to be integrated into the particles. This feature allows for the attachment of various

targeting molecules to the particles. For our FSNs, after PEGylation, we chose to conjugate a targeting antibody to the particle to enhance. Specifically, we chose to use anti-carcinoembryonic antigen (CEA) antibodies. CEA is an extremely common marker of CRC and high levels of CEA expression are associated with malignant lesions while healthy tissues express low levels of CEA[237-239]. This means that our antibody conjugated, PEGylated, silica nanoparticles are capable of specifically tagging malignant lesions.

Fluorescent silica nanoparticles capable of selectively targeting malignant lesions are uniquely suited for fluorescent endoscopy. The interior of the colon is comprised of epithelial lining which can take up topically applied nanoparticles[240]. When traditional colonoscopy is replaced with fluorescent endoscopy, the nanoparticles can be excited to fluoresce. In areas where lots of particles are present, such as targeted lesions, the fluorescence will be visible to the physician allowing for real time molecular detection of cancer which does not rely solely on physical differences between healthy and abnormal tissues. By eliminating the need for medical professionals to use their best judgment in CRC screenings, we can enhance the accuracy of early detection preventing needless deaths from otherwise treatable cancer. The work presented in this section was recently published as a co-first author paper alongside Dr. Seock-Jin Chung in *ACS Applied Biomaterials* under the title "Targeted Biodegradable Near-Infrared Fluorescent Nanoparticles for Colorectal Cancer Imaging."

5.2 Methods

5.2.1 Synthesis of Silica Nanoparticles

FSNs were synthesized using a modified Stöber reaction. In short, CF800-maleimide (150 µmol) was mixed overnight with (3-mercaptopropyl) trimethoxysilane (MPTMS; 2 µmol) create silane-

appended CF800 (CF800-MPTMS). Then, CF800-MPTMS was added to 2-propanol (50mL) with

ammonium hydroxide (3 mL, 28% v/v) and tetraethyl orthosilicate (1 mL, 99.999% v/v) was

added. After 30 min to 2 h of stirring the particles were centrifuged once then (10 min;10 000

rpm; 25 °C) washed once in ethanol and once in DI water. Then, the FSNs were exposed to

tetrahydrofuran (THF) which activates thiol groups and combined with thiolated poly(ethylene

glycol) (SH-PEG-COOH; 20 mg). This produced PEGylated FSN capable of further modification as

needed.

5.2.2 Characterization of Nanoparticles

Hydrodynamic diameter and zeta potential were evaluated by DLS (DLS, Zeta Sizer Nano,

Malvern Instruments). TEM was used to evaluate size and morphology (JEOL, Japan). An M5

fluorometer (Molecular Devices, SanJose, CA) was used to measure UV absorption and

fluorescent intensities of FSN. Cell images were taken with a Keyence Optical Microscope

(Keyence fluorescence microscope, Osaka, Japan). The limit of detection was determined using

a concentration curve with a threefold dilution factor on a Pearl Trilogy NIRF imaging system (LI-

COR Biosciences, Lincoln, NE).

5.2.3 Biodegradation Studies

In vitro biodegradation studies of FSNs were performed in SBF. Particles were added to SBF (pH

5) at 0.1 mg/mL FSNs then mixed at 100 rpm and 37 °C for 7 days (one week). A small amount

of degradation solution was taken out for TEM analysis on days 1, 3, and 7.

5.2.4 Cell Culture

HT29 and HCT116, human CRC lines, and CCD841coN (ATCC, Manassas, VA), a human epithelial line were used in this study. Cells were maintained in DMEM supplemented with 10% FBS and pen/strep (1%) in a humidified atmosphere containing CO_2 (5%) at 37 °C.

5.2.5 Western Blots

Total proteins were isolated from HT29 andHCT116 cells using radio-immunoprecipitation assay buffer (Sigma-Aldrich, St. Louis, MO). The proteins were loaded onto a 4−20% polyacrylamide gradient gel with sodium dodecyl sulfate (SDS). Then, after electrophoresis, the proteins were transferred to PVDF membranes (Bio-Rad, Hercules, CA) and blocked with skim milk (5%) for 1 h at room temperature. Then the membranes were incubated overnight at 4 °C with primary antibody directed at CEA (#2383S,Cell Signaling Technology, Danvers, MA; diluted 1:1000), epithelial growth factor receptor (#4267S, EGFR; Cell Signaling Technology, Danvers, MA; diluted 1:1000), vascular endothelial growth factor receptor (#ab32152, VEGFR; Abcam, Cambridge, U.K.; diluted1:500), and β-actin (#A5451, Sigma-Aldrich, St. Louis, MO; diluted 1:5000). The next day, the membranes were further incubated with horseradish peroxidase-conjugated antirabbit or antimouse IgG (Cell Signaling Technology, Danvers, MA) and the signal intensity was measured using ChemiDoc (Bio-Rad, Hercules, CA).

5.2.6 Preparation and Characterization of Antibody Conjugated Nanoparticles

PEGylated FSNs were conjugated to anti-CEA antibodies by EDC-NHS coupling reaction. Briefly, PEGylated FSNs were pelleted and resuspended in MES buffer (0.5 mol; pH 6). 1-ethyl-3-(3-(dimethylamino)propyl) carbodiimide(EDC) and sulfo-NHS were added to the solution to form NHS-esters. CEA antibodies were then added to the solution and stirred overnight. The next day,

94

CEA-FSN were washed twice in DDI water (10 min; 10 000 rpm; 25 °C) and antibody conjugation was verified by DLS.

5.2.7 Cell Viability Assay

MTT (3-(4,5-dimethylth-iazol-2-yl)-2,5-diphenyltetrazolium bromide) assay was performed to check for cytotoxicity of FSNs. HT29 cells were seeded at a density of 1×10^4 cells/well in a 96-well plate. After overnight incubation, the culture medium was replaced with fresh medium containing FSN at concentrations ranging from 0 to10 μg/mL and incubated for an additional 24 h. Following this, 10 μL of MTT (5 mg/mL in phosphate-buffered saline) was added to the wells and then incubated for 4 h followed by removal of the culture medium. Then, 100 μL of DMSO was added to each well and absorbance was measured at a wavelength of 570 nm using a microplate reader.

5.2.8 Cellular Imaging

For NIRF imaging, cells were seeded in 6-well plates at a density of 1×10^5 cells per well and incubated overnight. The following day, particles were added to cells at 10 μg/mL in DMEM and again incubated overnight. Then, the cells were washed with PBS, and a PearlTrilogy NIRF imaging system (LI-COR Biosciences, Lincoln, NE) was used to take images. For optical microscopy imaging, cells were seeded in 8-chamber slides at a density of 1×10^4 cells per chamber for 24 h. The following day, cells were treated with 10 μg/mL of FSN. After treatment, the cells were washed 3 times with PBS. The slides were mounted using Prolong Gold reagent with 4',6-diamidino-2-phenyl-indole (DAPI). Fluorescence images were taken using a Keyence imaging system with DAPI and Cy7 filters.

5.2.9 Animal Models and In Vivo Imaging

All animal studies were approved by IACUC of Michigan State University, and animal care and wellbeing throughout the study was monitored by the CAR at Michigan State University. For our xenograft models, HT29 cells (1×10^6 cells) were implanted subcutaneously in the left flank and HCT116 (1×10^6 cells) cells were implanted subcutaneously in the right flank of 8-week-old male *BALB/c-nu/nu* mice (Jackson Laboratory, Bar Harbor, ME). When the tumor volume reached 100–300 mm^3, the mice were used for NIRF imaging. For targeting studies, xenograft mice were IV injected with either CF800-labeled CEA-FSNs or PEG-FSNs (10 mg/kg) (N = 3 for each group), and NIR images were taken by a Pearl Trilogy NIRF imaging system. During the imaging sessions occurring between 0 and 48 hours post injection, mice were kept under anesthesia with 2% isoflurane, and images were taken with both white-lighted filter and 800 nm filter. The regions of interest (ROI) were analyzed with ImageJ software. For our orthotopic validation, polyposis in the rat colon (PIRC) rats with an APC gene mutation that spontaneously develop intestinal polyps were obtained from the rat resource and research center (RRRC, Columbia, MO). At six-months-old, male PIRC rats (N = 3) received CEA-FSNs (1 mg/kg) via topical application using a tube attached next to the commercial hand-held endoscope (DEPSTECH, London, U.K). At the same time, white-light endoscopy images were captured using the DEPSTECH program. After 10 minutes, PBS was applied through the tube to wash away excess particles, and the intestines were excised. NIR fluorescence images of excised tissue were collected by a Pearl Trilogy NIRF imaging system.

5.2.10 Immunofluorescence Staining in Intestine Tissues

Excised PIRC rat intestines embedded in OCT for sectioning. Sections taken on a cryostat (4 μm) from the center of the tissue were used for staining and validation. The tissue was permeabilized in PBS Triton X-100 (5%) for 5 min and blocked for 1 h at room temperature with normal goat serum diluted 1:30 in PBS. Primary antibody incubation occurred overnight at 4 °C using anti-β-catenin antibody (#8480S, Cell Signaling Technology, Danvers, MA; diluted1:1000) and anti-CEA antibody (#2383S, Cell Signaling Technology, Danvers, MA; diluted 1:1000). The following day, the slides were washed and then further stained with Alexa 488 (#A-11094, Invitrogen, Grand Island, NY; diluted 1:300) and Alexa555 conjugated secondary antibodies (#A-21422, Invitrogen, NY; diluted 1:300) and incubated for 2 h at room temperature. After this, the slides were washed and then cover slipped using Prolong Gold reagent with DAPI (#P36931,Invitrogen, Grand Island, NY). Fluorescence images were observed using a THUNDER microscopy system.

5.2.11 Statistical Analysis

Statistics were performed in GraphPad, and data is presented as means ± SDs. Statistical significances were determined using the student's unpaired t-test, and P-values of <0.05 were considered statistically significant.

5.3 Results/Discussion

Fluorescent silica nanoparticles were successfully synthesized at three different sizes (50, 100, and 200 nm) utilizing a modified Stöber reaction. As validated by TEM, particles were found to be 50 nm after 30 minutes of reaction time, 100 nm after 1 hour, and 200 nm after two hours (Figure 24). The zeta potential of the synthesized FSNs was +0.617 mV which is in line with the

expected positive charge of silica nanoparticles. This reaction included covalently conjugated CF800-MPTMS allowing for integrated fluorescence which is more stable than dye encapsulation, and PEG was conjugated to the surface utilizing thiol-thiol interaction. For CEA-FSN, anti-CEA antibodies were further conjugated to the exposed carboxylic acid group to enhance targeting capabilities. To validate the conjugation of PEG and antibodies to the surface of the particle, DLS was performed. For the 50 nm particles, the initial hydrodynamic diameter was 128 nm, the diameter after PEGylation was 224 nm, and the diameter of antibody conjugated particles was 341 nm (Figure 24). This gradual increase in size is evidence that PEGylation and antibody conjugation were successful. Interestingly, despite having nearly identical quantum yields, when compared to CF800 fluorescent dye alone, FSNs were found to exhibit 2.2 times higher fluorescence (Figure 24) making them an ideal choice for imaging in the body where background, even in the NIR region, can cause low intensity signals to be drowned out. To evaluate which FSN size was best suited to our application we determined biodegradability of FSN and uptake of FSN conjugated to PEG. Our biodegradability studies, wherein FSN of 50, 100, and 200 nm particles were suspended in SBF and stirred slowly over the course of a week with small portions being removed for TEM analysis on day 1, 3, and 7, indicate that all three sizes show notable signs of degradation by day 3. However, the only size that completely degraded within the study length was the 50 nm particles. The larger sizes remained partially intact, indicating they would take a longer time to be completely cleared from the system.
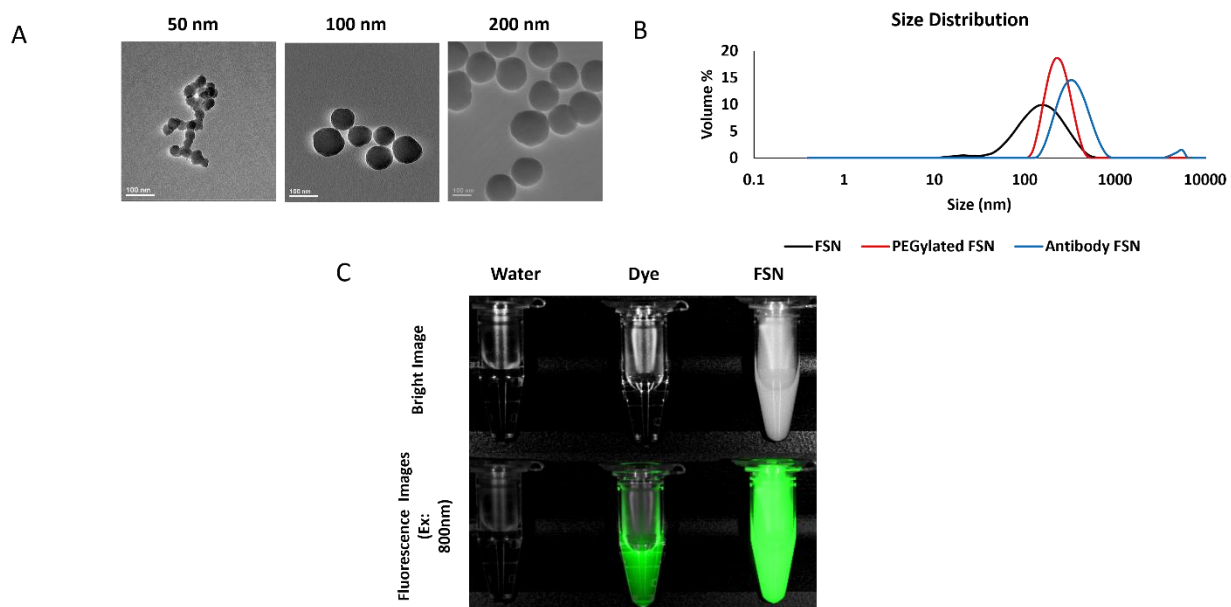
Figure 24: A) TEM images showing 50 nm, 100 nm, and 200 nm particles which were obtained through 30 min, 1 h, and 2 h reaction times. B) DLS study of unconjugated, PEGylated, and Antibody conjugated FSN showing a slight increase in hydrodynamic diameter with the addition of each additional surface modification. C) Brightfield and NIR fluorescent images showing the fluorescence intensity of water, CW800 dye alone, and our FSN. Despite having nearly identical quantum yields, the particles have 2.2 times higher intensity, making them an ideal choice for this application.

Additionally, the nanoparticle formulation enhances the targeting capability of dye as compared to dye alone. As smaller nanoparticles are typically taken up more successfully than larger particles by cells, it is not surprising that the PEGylated 50 nm particles were taken up significantly more than the 100 nm or 200 nm particles (Figure 25). Additionally, 50 nm FSN showed no toxicity to cells even at concentrations as high as 10 μg/ml. The combination of enhanced uptake and superior biodegradability makes the 50 nm particles an obvious choice for our imaging agent. However, the use of bare or PEGylated FSN would be insufficient to allow for easy detection of CRC. Specifically, targeting CRC markers is key to distinguishing malignant regions from surrounding healthy epithelium. The CRC marker chosen here, CEA, was chosen for two reasons. First, CRC is highly overexpressed in the majority of CRC. Second, it is possible to

find a CRC cell line that does not over express CEA giving us robust control to evaluate the specificity of our particles. Using Western blot (Figure 26), the expression of CEA was validated in in HT29 cells while it was confirmed that HCT116 cells do not express CEA despite both being CRC cell lines. In order to verify that our CEA-FSN were specifically targeting CEA expressing CRC cells, we performed two *in vitro* cell uptake experiments. In the first, both HT29 and HCT116 cells were treated with CEA-FSN then imaged using a PEARL NIR imager. This experiment showed that HT29 cells took up a significantly higher amount of CEA-FSNs as validated through fluorescence quantification (Figure 26). In the second, we compared the uptake of CEA-FSNs to plain FSNs in HT29 cells to validate that high uptake by the HT29 cells was due to the presence of the anti-CEA antibody rather than due to a cell line specific property. The results of this experiment show a statistically significant increase in uptake of the CEA-FSN as compared to FSN alone (Figure 26)indicating that specific targeting of CEA is responsible for the high uptake.
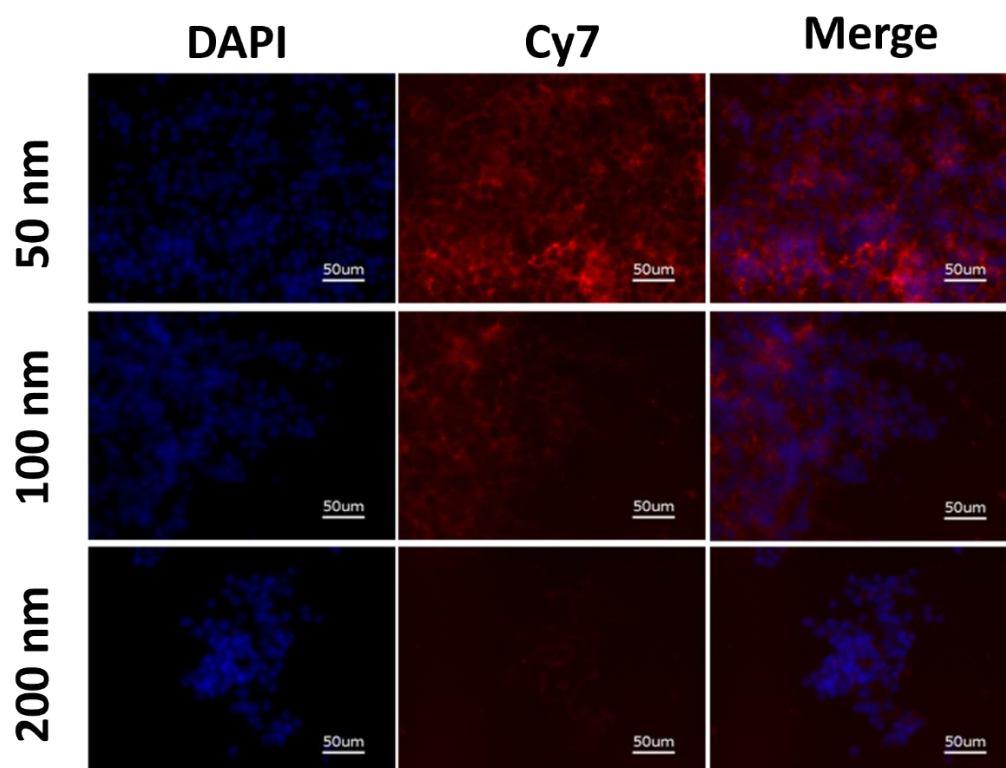
Figure 25: Size based cell uptake studies show the enhanced uptake of our 50 nm particles as compared to 100 or 200 nm FSN (Particle = Red, DAPI = Blue).
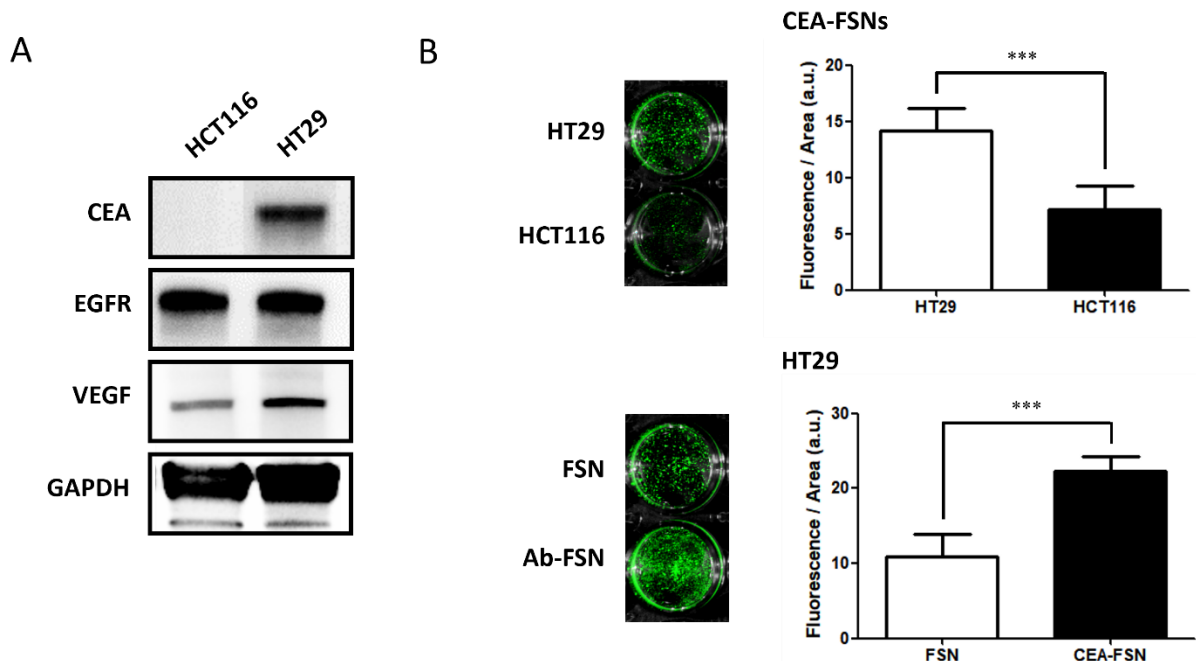
Figure 26: A) Western Blot showing the expression of CEA, EGFR, VEGF, and GAPDH in two different CRC cell lines. HCT116 cells are CEA negative while HT29 cells are CEA positive making them ideal choices to test the targeting efficacy of our CEA-FSN. B) Cell uptake experiments show that CEA expressing HT29 cells take up more CEA-FSN than HCT116 cells which do not express CEA (n=3). Additionally, CEA-FSN were taken up better than unconjugated FSN in HT29 cells (n=3) validating the antigen specific targeting (*** $p<0.001$). Error bars represent standard deviation.

To validate the *in vivo* targeting potential of FSNs, a tumor xenograft model was used (Figure 27). Specifically, a murine flank model of CRC was used where one flank contained a CEA positive HT29 tumor and the other had a CEA negative HCT116 tumor. For untargeted PEGylated FSNs we see no significant uptake in either tumor. CEA-FSNs, however, show enhanced uptake in the HT29 tumors at both 1- and 4-hours post injection (Figure 27). In fact, fluorescence is about twice as high as in the HCT116 tumor as validated by ROI analysis and is high enough to be detected and visualized through fluorescence imaging (Figure 27) pointing to a strong potential of the CEA-FSNs to be used to detect CEA expressing cells in fluorescent endoscopy.
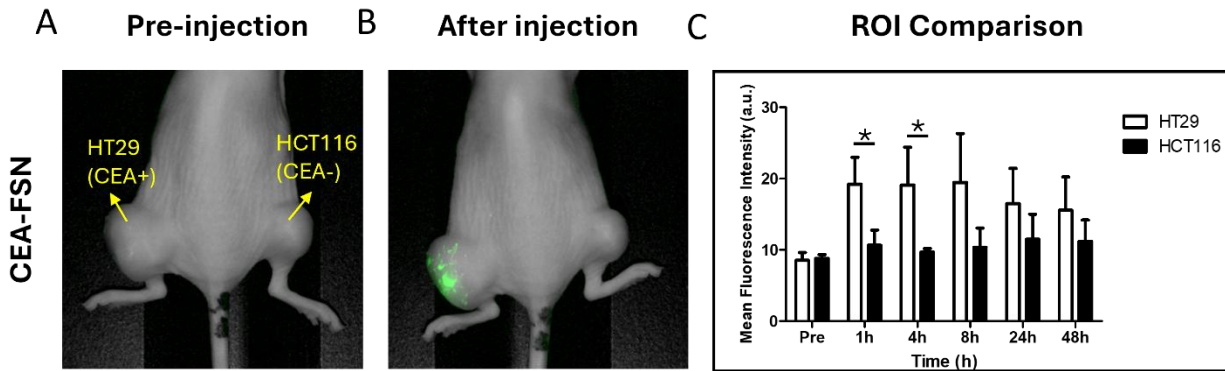
Figure 27: A) *in vivo* tumor xenograft model with an HT29 (CEA +) tumor (left) and an HCT116 (CEA -) tumor (right). B) *in vivo* NIR fluorescence imaging showing higher uptake in the HT29 tumor than in the HCT116 tumor. C) At 1 and 4 h after IV injection, NIR fluorescence is significantly higher in the HT29 tumor than the HCT116 tumor (n=3 mice) (* $p<0.05$).

To evaluate the potential use of CEA-FSNs to detect CRC polyps, PIRC rats, which spontaneously develop cancerous CRC polyps, were used. Initially, the PIRC rats received white light endoscopy, similar to traditional colonoscopy, to validate the presence of visible polyps in the intestine. Then, CEA-FSNs were applied topically to the mucosal lining. As the particles are hydrophilic and small, they are well suited to transmucosal uptake as seen in *ex vivo* NIR imaging of excised intestinal tissue (Figure 28). When compared to untreated tissue, tissue treated with particles is fluorescent, but the fluorescence is not uniform. Instead, portions of the intestine are bright while other sections have low or no signal (Figure 28). To validate that these bright spots are in fact CRC, we performed IF. After taking sections of the bright regions of the intestine, slides were stained with DAPI, a fluorescent anti-CEA antibody, and a fluorescent anti β-catenin antibody (used here as a known marker of CRC). In the resulting images, we see excellent colocalization of CEA, β-catenin, and FSNs (Figure 28) indicating both that CEA is an effective target for our particles and that the particles are localized in cancerous regions. These findings

indicate that CEA-FSNs are ideally suited to topical application and imaging during fluorescence

endoscopy.
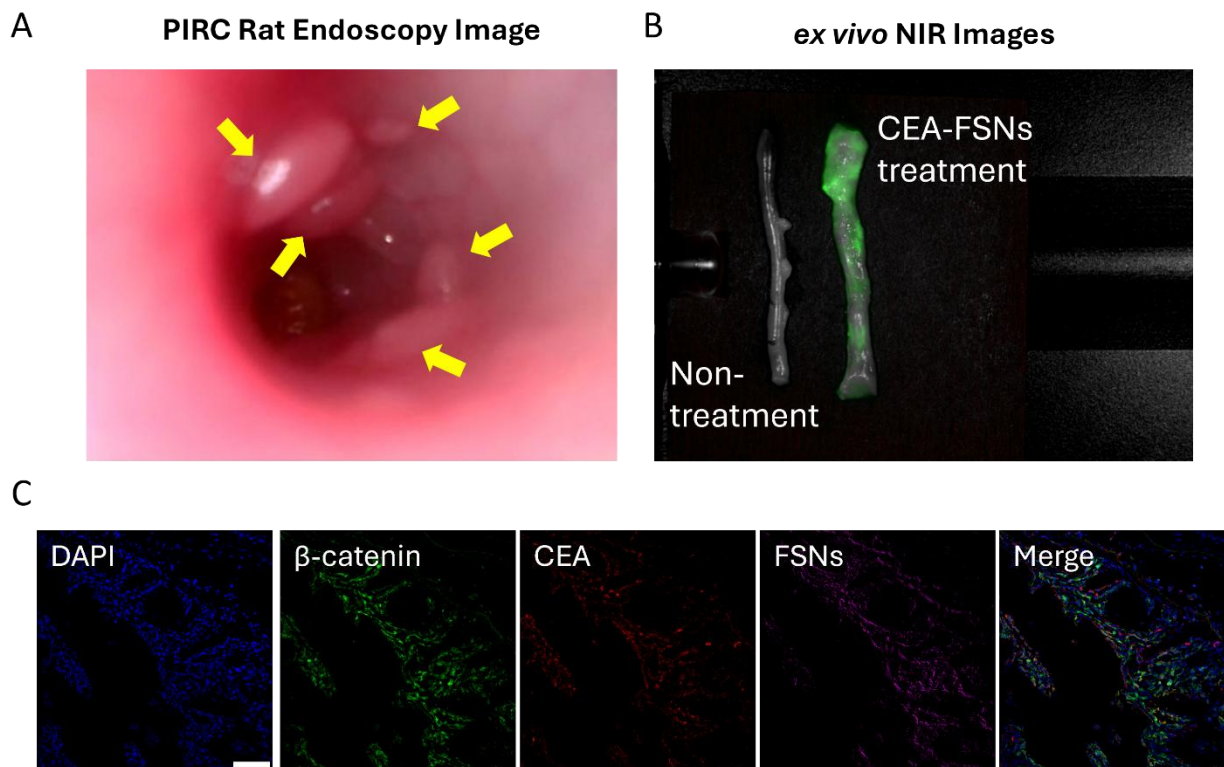
Figure 28: A) Brightfield endoscopy image of polyps in a PIRC rat colon. B) NIR fluorescence imaging of a PIRC rat colon topically treated with particles and excised after the rats were sacrificed. the treated colon, highly fluorescent areas correlate with polyps. C) To validate the findings in part B, *ex vivo* images were taken of sectioned tissue from the colon. Overlayed signal from β-catenin, CEA, and FSNs indicate that particles are highly localized to CEA expressing CRC.

The FSNs synthesized for and used in this study are uniform in size and highly monodisperse.

The 50 nm particles particularly are small and show excellent uptake and biocompatibility.

However, small nanoparticles are known to be excreted quickly especially in larger organisms

like humans[142]. Should translation of the 50 nm particles prove challenging due to the

premature clearance of the particles, two different approaches could be employed. The

simplest strategy would involve using one of our larger sized particles (either 100 nm or 200

nm). However, this strategy is likely to result in reduced uptake and biocompatibility making the

use of an alternative strategy ideal. A biocompatible nanocarrier, like albumin protein, could be used to prolong the life of the nanoparticles in the body. Albumin, as a common blood protein, is highly biocompatible and known to prolong the retention of particles in tumors[241]. It also is not known to affect the uptake of particles to tumors, making it an ideal nanocarrier for this application[242].

In the case of this study, we chose to use CF800 NIR fluorescent dye to take advantage of the biological transparency window. However, FSNs could easily be synthesized with a variety of different fluorophores. Using fluorophores with non-overlapping excitation and emission spectra alongside conjugation of particles to a variety of antibodies could allow for multiplexed, ratiometric imaging where different targets fluoresce different colors[243]. For example, antibody choice could allow us to distinguish between common and uncommon cancers which have unique molecular signatures. It could also allow for the tagging of tumor associated immune cell populations which are correlated with treatment outcomes and prognosis allowing for personalized care[244]. If we were to continue to use a single dye, however, it would make sense for us to consider the use of NIR II fluorescent dyes. While NIR dyes, like CF800, are well suited to biological applications, they are still subject to interference from tissue. In the NIR II (1000-1700nm) region, also known as the second biological window, the interference from surrounding tissue is reduced further when compared with the NIR region[245, 246]. In fact, use of NIR II dyes would allow for multi-centimeter imaging depth. At the present, however, dyes in this spectrum are rare and costly, limiting the feasibility of their use in fluorescent endoscopy applications.

While FSNs were designed with fluorescent endoscopy in mind, use of multimodal imaging may further enhance detection of CRC. For example, an integrated system capable of performing a traditional white light endoscopy alongside fluorescence imaging would allow for molecular information to appear alongside traditional colonoscopy images that physicians are familiar with. As this would augment an existing tool rather than replace it entirely, adoption would be more likely in the medical space as the benefits are obvious and the burden of entry is low. If this advanced colonoscope were capable of Raman imaging, we could achieve incredible resolution thanks to Raman's remarkable specificity. A combined scope capable of both NIR fluorescence imaging and Raman imaging combined with a contrast agent like a FSN-Raman particle would provide exceptionally detailed and useful clinical images allowing for robust early detection and superior patient outcomes[247, 248].

5.4 Conclusions

Here, CEA-FSNs were evaluated as targeted imaging probes for CRC. The particles were found to be highly uniform and monodisperse and exceptionally fluorescent while still exhibiting excellent biodegradability which makes them ideally suited to biomedical application. The CEA antibody conjugated to the particles showed remarkable targeting capabilities *in vitro, in vivo,* and *ex vivo* for both topical and IV administration allowing for easy visualization of tumor tissue. This targeting capability makes CEA-FSNs ideally suited to both early detection and resection applications. Further study of the CEA-FSNs for molecular detection during active colonoscopy is needed, however, upon completion of these studies, the use of FSNs in colonoscopy will be more widely accepted ultimately leading to clinical translation.

Chapter 6: Conclusions and Future Directions

6.1 Conclusions

The work presented in this dissertation was subdivided into 4 chapters:

1. Surface Valence and Substrate Tuned Nanoceria

2. Immunomodulatory Applications of Formulated Nanoceria

3. Detection and Treatment of Endometriosis with Theranostic Nanoceria

4. Detection of Colorectal Cancer using Fluorescent Silica Nanoprobes

Multiple nanoceria formulations were developed over the course of this work with different surface valences and substrates. Successful synthesis of these particles was validated by evaluating the size and morphology of the particles with TEM, HRTEM, and DLS. Their surface valence was evaluated by XPS, and cerium content was further evaluated and confirmed by ICP. The enzymatic behavior of these particles was validated by enzymatic assays showing characteristic SOD and catalase activity in all nano-formulations. Macrophage targeting was evaluated through a cell uptake assay. Interestingly, we see that the ratio of SOD to catalase activity is dependent on substrate indicating that different particles may have different effects on their microenvironment.

To validate these effects, *in vitro* experiments were carried out where treated J774 cells underwent FACS to evaluate the expression of CD80 proinflammatory markers and Arg-1 anti-inflammatory markers. These qualitative and quantitative experiments showed that higher ratios of Ce^{3+} to Ce^{4+} are correlated with enhanced anti-inflammatory effects while enhanced ratios of Ce^{4+} to Ce^{3+} are correlated with weaker anti-inflammatory or pro-inflammatory effects in the albumin-nanoceria. The effect of SWCNT as a substrate was observed, and greater anti-

inflammatory potential than albumin-nanoceria particles with similar surface valence was shown *in vitro*. *In vivo,* we ran a preliminary study on CIA to evaluate the anti-inflammatory efficacy of the most anti-inflammatory albumin-nanoceria and the SWCNT-nanoceria. Though further study is required to validate findings and achieve statistical significance, Ce^{3+} enhanced albumin-nanoceria appears to greatly reduce the severity of arthritis in mice indicating while SWCNT-nanoceria appears to enhance its severity. This finding was further validated by the *ex vivo* analysis showing that for the albumin-nanoceria, the population of T cells is greatly reduced while there is a robust population of macrophages. However, in the SWCNT-nanoceria group, we see an increase in T cells compared to the control indicating a more pro-inflammatory effect. Macrophages were challenging to image in the SWCNT-nanoceria condition due to quenching from the particle.

The anti-inflammatory albumin-nanoceria was then further explored as a treatment for endometriosis, a chronic inflammatory condition characterized by the growth of endometrial-like tissue outside the uterus. Traditional therapeutics for this disease come with significant side effects that can harm patients' quality of life including loss of fertility. Albumin-nanoceria, used as a treatment for endometriosis, shows similar efficacy to traditional STAT/JAK inhibitors reducing the size and number of endometrial lesions present in our mouse model. However, unlike the inhibitors, albumin-nanoceria did not affect the fertility of our mice. *Ex vivo* validation indicated that the particles acted as an efficient STAT inhibitor in the endometrial lesions without affecting normal STAT expression in the uterus accounting for both the treatment efficacy and restored fertility of the mice. This effect was due to the enhanced targeting of abnormal lesions by the albumin-nanoceria which accumulates in regions with disorganized

vasculature. We see through both *in vivo* and *ex vivo* imaging that ICG-albumin-nanoceria preferentially accumulates in lesions and there is little ICG signal detected in the uterus. This makes albumin-nanoceria an excellent candidate for the diagnosis and treatment of endometriosis.

Finally, this dissertation explored another critical application of nanoparticle imaging agents. NIR fluorescent silica nanoparticles were used as imaging agents for colorectal cancer to enhance traditional screening methods with fluorescent endoscopy. Using a straightforward synthesis, FSN were synthesized in three different sizes (50, 100, 200 nm) by varying reaction time then conjugated to PEG and anti-CEA antibodies. The 50 nm particles were shown to be the ideal choice for CRC imaging due to their complete biodegradation over the course of a week and excellent uptake by cells. These particles, when conjugated to anti-CEA antibodies, were shown to have the ability to specifically tag cells which express CEA when we compared the uptake in a CEA positive and a CEA negative CRC cell line. This finding was further validated using a tumor xenograft model where a tumor expressing CEA was implanted in one flank while a CEA negative tumor was implanted in the other. We see that, for the antibody conjugated particle, not only is fluorescence markedly higher in the CEA positive tumor, but it is also able to be easily visualized which would allow this tool to be used by surgeons. Colocalization of particles with CEA expression and cancer markers in PIRC rat models after topical application and washing shows that the particles could be applied topically during a fluorescent endoscopy to accurately tag CRC lesions. These combined factors make NIR-FSN ideal candidates for use as a contrast agent in combined white light/fluorescence endoscopy which would enhance the diagnostic potential of early CRC screenings.

6.2 Future Directions

The work presented in this dissertation provides many interesting opportunities for future research. Based on what has been presented here, I believe robust animal studies of the nanoceria in various conditions is the next crucial step in this research. Here, we have successfully demonstrated the efficacy of the formulated nanodrugs *in vitro* and in chronic inflammatory conditions including endometriosis. Further studies would allow us to confirm the anti-inflammatory effects of the studied formulations *in vivo* and would allow for further study into the effects of substrate and surface valence on the pro and anti-inflammatory immunomodulatory effects of the nanoceria. Specifically, larger scale studies in the CIA model with an N of at least 4 per group would allow for robust statistical analysis of the scoring trends for animals treated different formulations. It will be key to include multiple control groups in these experiments including a normal mouse group, a PBS treatment of CIA group, and a drug control group. Methotrexate would be an excellent choice for the drug group as it has been shown in prior studies to be an effective treatment for CIA[30]. These same experiments would also open the door to further IF staining for macrophage phenotype which, while not performed in this study would provide further insight into the macrophage modulating effect of the nanoceria *in vivo*. Following or alongside these experiments, it would also be interesting to explore the effect of the nanoceria formulation of immune privileged environments like those found in solid tumor cancers. Fortunately, our lab has a pre-established orthotopic breast cancer model that would be useful for these studies.

With regards to the FSNs for CRC imaging, the development of a pre-clinical imaging system compatible with the particles is key to their eventual clinical translation. Specifically, a

fluorescence endoscope compatible with white light imaging and particle application is necessary to fully validate the use of these particles for real time diagnosis alongside traditional colonoscopy. Though we would carry out these preliminary experiments in our PIRC rats, development of this tool would be critical to the translation of these particles to the clinic. This translation could be facilitated through a partnership with a hospital system. Confirmatory *ex vivo* studies of our particle targeting on patient samples combined with proven results with a pre-clinical fluorescent endoscope would create the possibility of clinical trials and ultimately wide scale adoption. This presents a great opportunity for collaboration with more device-focused groups and clinicians moving forward.

REFERENCES

(1) Katta, B.; Vijayakumar, C.; Dutta, S.; Dubashi, B.; Nelamangala Ramakrishnaiah, V. P. The Incidence and Severity of Patient-Reported Side Effects of Chemotherapy in Routine Clinical Care: A Prospective Observational Study. *Cureus* **2023**, *15* (4), e38301. DOI: 10.7759/cureus.38301 From NLM.

(2) Rosenblum, M. D.; Gratz, I. K.; Paw, J. S.; Abbas, A. K. Treating human autoimmunity: current practice and future prospects. *Sci Transl Med* **2012**, *4* (125), 125sr121. DOI: 10.1126/scitranslmed.3003504 From NLM.

(3) Okwundu, N.; Grossman, D.; Hu-Lieskovan, S.; Grossmann, K. F.; Swami, U. The dark side of immunotherapy. *Ann Transl Med* **2021**, *9* (12), 1041. DOI: 10.21037/atm-20-4750 From NLM.

(4) Kovacs, D.; Kovacs, P.; Eszlari, N.; Gonda, X.; Juhasz, G. Psychological side effects of immune therapies: symptoms and pathomechanism. *Curr Opin Pharmacol* **2016**, *29*, 97-103. DOI: 10.1016/j.coph.2016.06.008 From NLM.

(5) Caruso, R.; Breitbart, W. Mental health care in oncology. Contemporary perspective on the psychosocial burden of cancer and evidence-based interventions. *Epidemiol Psychiatr Sci* **2020**, *29*, e86. DOI: 10.1017/s2045796019000866 From NLM.

(6) Bayda, S.; Adeel, M.; Tuccinardi, T.; Cordani, M.; Rizzolio, F. The History of Nanoscience and Nanotechnology: From Chemical-Physical Applications to Nanomedicine. *Molecules* **2019**, *25* (1). DOI: 10.3390/molecules25010112 From NLM.

(7) Véron, O.; Blondeau, J. P.; Meneses, D. D. S.; Vignolle, C. A. Characterization of silver or copper nanoparticles embedded in Soda-lime glass after a staining process. *Surface and Coatings Technology* **2013**, *227*, 48-57.

(8) del Rio, A. P.; Castaing, J.; Aucouturier, M. Metallic nano-particles in lustre glazed ceramics from the 15th century in Seville studied by PIXE and RBS. *Nuclear Instruments and Methods in Physics Research Section B: Beam Interactions with Materials and Atoms* **2006**, *242*, 596-600.

(9) Reibold, M.; Paufler, P.; Levin, A. A.; Kochmann, W.; Pätzke, N.; Meyer, D. C. Carbon nanotubes in an ancient Damascus sabre. *Nature* **2006,** *444*

(10) Chari, C. S.; Taylor, Z. W.; Bezur, A.; Xie, S.; Faber, K. T. Nanoscale engineering of gold particles in 18th century Böttger lusters and glazes. *Proc Natl Acad Sci U S A* **2022**, *119* (18), e2120753119. DOI: 10.1073/pnas.2120753119 From NLM.

(11) Ghosal, M.; Chakraborty, A. A Comparative Study of Nano Embedments on Different Types of Cements *International Journal of Advances in Engineering & Technology* **2015**, *8* (2), 92-103.

(12) Roingeard, P. Viral detection by electron microscopy: past, present and future. *Biol Cell* **2008**, *100* (8), 491-501. DOI: 10.1042/bc20070173 From NLM.

(13) Greenfield, S.; Jones, I. L.; Berry, C. T. High-pressure plasmas as spectroscopic emission sources. *Analyst* **1964**, *89* (1064), 713-720.

(14) Siegbahn, K.; Kungl Vetenskaps-societeten i, U. ESCA; atomic, molecular and solid state structure studied by means of electron spectroscopy.

(15) Afzal, O.; Altamimi, A. S. A.; Nadeem, M. S.; Alzarea, S. I.; Almalki, W. H.; Tariq, A.; Mubeen, B.; Murtaza, B. N.; Iftikhar, S.; Riaz, N.; et al. Nanoparticles in Drug Delivery: From History to Therapeutic Applications. *Nanomaterials (Basel)* **2022**, *12* (24). DOI: 10.3390/nano12244494 From NLM.

(16) Bharti, C.; Nagaich, U.; Pal, A. K.; Gulati, N. Mesoporous silica nanoparticles in target drug delivery system: A review. *Int J Pharm Investig* **2015**, *5* (3), 124-133. DOI: 10.4103/2230-973x.160844 From NLM.

(17) Guo, X.; Zuo, X.; Zhou, Z.; Gu, Y.; Zheng, H.; Wang, X.; Wang, G.; Xu, C.; Wang, F. PLGA-Based Micro/Nanoparticles: An Overview of Their Applications in Respiratory Diseases. *Int J Mol Sci* **2023**, *24* (5). DOI: 10.3390/ijms24054333 From NLM.

(18) Yang, J.; Zeng, H.; Luo, Y.; Chen, Y.; Wang, M.; Wu, C.; Hu, P. Recent Applications of PLGA in Drug Delivery Systems. *Polymers* **2024**, *16* (18).

(19) Mehta, M.; Bui, T. A.; Yang, X.; Aksoy, Y.; Goldys, E. M.; Deng, W. Lipid-Based Nanoparticles for Drug/Gene Delivery: An Overview of the Production Techniques and Difficulties Encountered in Their Industrial Development. *ACS Materials Au* **2023**, *3* (6), 600-619.

(20) Barenholz, Y. Doxil®--the first FDA-approved nano-drug: lessons learned. *J Control Release* **2012**, *160* (2), 117-134. DOI: 10.1016/j.jconrel.2012.03.020 From NLM.

(21) Liu, Q.; Zou, J.; Chen, Z.; He, W.; Wu, W. Current research trends of nanomedicines. *Acta Pharmaceutica Sinica B* **2023**, *13* (11), 4391-4416.

(22) Dulińska-Litewka, J.; Łazarczyk, A.; Hałubiec, P.; Szafrański, O.; Karnas, K.; Karewicz, A. Superparamagnetic Iron Oxide Nanoparticles-Current and Prospective Medical Applications. *Materials (Basel)* **2019**, *12* (4). DOI: 10.3390/ma12040617 From NLM.

(23) Bakhtiary, Z.; Saei, A. A.; Hajipour, M. J.; Raoufi, M.; Vermesh, O.; Mahmoudi, M. Targeted superparamagnetic iron oxide nanoparticles for early detection of cancer: Possibilities and challenges. *Nanomedicine* **2016**, *12* (2), 287-307. DOI: 10.1016/j.nano.2015.10.019 From NLM.

(24) Li, W.; Chen, X. Gold nanoparticles for photoacoustic imaging. *Nanomedicine (Lond)* **2015**, *10* (2), 299-320. DOI: 10.2217/nnm.14.169 From NLM.

(25) Chen, Y.-S.; Zhao, Y.; Yoon, S. J.; Gambhir, S. S.; Emelianov, S. Miniature gold nanorods for photoacoustic molecular imaging in the second near-infrared optical window. *Nature Nanotechnology* **2019**, *14*, 465–472.

(26) Tay, Z. W.; Chandrasekharan, P.; Fellows, B. D.; Arrizabalaga, I. R.; Yu, E.; Olivo, M.; Conolly, S. M. Magnetic Particle Imaging: An Emerging Modality with Prospects in Diagnosis, Targeting and Therapy of Cancer. *Cancers (Basel)* **2021**, *13* (21). DOI: 10.3390/cancers13215285 From NLM.

(27) Vogel, P.; Markert, J.; Rückert, M. A.; Herz, S.; Keßler, B.; Dremel, K.; Althoff, D.; Weber, M.; Buzug, T. M.; Bley, T. A.; et al. Magnetic Particle Imaging meets Computed Tomography: first simultaneous imaging. *Sci Rep* **2019**, *9* (1), 12627. DOI: 10.1038/s41598-019-48960-1 From NLM.

(28) Arbabi, A.; Spencer Noakes, L.; Vousden, D.; Dazai, J.; Spring, S.; Botelho, O.; Keshavarzian, T.; Mattingly, M.; Ellegood, J. E.; Nutter, L. M. J.; et al. Multiple-mouse magnetic resonance imaging with cryogenic radiofrequency probes for evaluation of brain development. *Neuroimage* **2022**, *252*, 119008. DOI: 10.1016/j.neuroimage.2022.119008 From NLM.

(29) Huang, C.; Dong, H.; Su, Y.; Wu, Y.; Narron, R.; Yong, Q. Synthesis of Carbon Quantum Dot Nanoparticles Derived from Byproducts in Bio-Refinery Process for Cell Imaging and In Vivo Bioimaging. *Nanomaterials (Basel)* **2019**, *9* (3). DOI: 10.3390/nano9030387 From NLM.

(30) Kalashnikova, I.; Chung, S.-J.; Nafiujjaman, M.; Hill, M. L.; Siziba, M. E.; Contag, C. H.; Kim, T. Ceria-based nanotheranostic agent for rheumatoid arthritis. *Theranostics* **2020**, *10* (26), 11863-11880. DOI: 10.7150/thno.49069.

(31) Wu, L. C.; Zhang, Y.; Steinberg, G.; Qu, H.; Huang, S.; Cheng, M.; Bliss, T.; Du, F.; Rao, J.; Song, G.; et al. A Review of Magnetic Particle Imaging and Perspectives on Neuroimaging. *AJNR Am J Neuroradiol* **2019**, *40* (2), 206-212. DOI: 10.3174/ajnr.A5896 From NLM.

(32) Beaucage, K. L.; Pollmann, S. I.; Sims, S. M.; Dixon, S. J.; Holdsworth, D. W. Quantitative in vivo micro-computed tomography for assessment of age-dependent changes in murine whole-body composition. *Bone Rep* **2016**, *5*, 70-80. DOI: 10.1016/j.bonr.2016.04.002 From NLM.

(33) Carniato, F.; Gatti, G.; Vittoni, C.; Katsev, A. M.; Guidotti, M.; Evangelisti, C.; Bisio, C. More Efficient Prussian Blue Nanoparticles for an Improved Caesium Decontamination from Aqueous Solutions and Biological Fluids. *Molecules* **2020**, *25* (15). DOI: 10.3390/molecules25153447 From NLM.

(34) Rybka, M.; Mazurek, Ł.; Konop, M. Beneficial Effect of Wound Dressings Containing Silver and Silver Nanoparticles in Wound Healing-From Experimental Studies to Clinical Practice. *Life (Basel)* **2022**, *13* (1). DOI: 10.3390/life13010069 From NLM.

(35) Liao, S.; Yue, W.; Cai, S.; Tang, Q.; Lu, W.; Huang, L.; Qi, T.; Liao, J. Improvement of Gold Nanorods in Photothermal Therapy: Recent Progress and Perspective. *Front Pharmacol* **2021**, *12*, 664123. DOI: 10.3389/fphar.2021.664123 From NLM.

(36) Park, Y.; Demessie, A. A.; Luo, A.; Taratula, O. R.; Moses, A. S.; Do, P.; Campos, L.; Jahangiri, Y.; Wyatt, C. R.; Albarqi, H. A.; et al. Targeted Nanoparticles with High Heating Efficiency for the Treatment of Endometriosis with Systemically Delivered Magnetic Hyperthermia. *Small* **2022**, *18* (24), e2107808. DOI: 10.1002/smll.202107808 From NLM.

(37) Chung, S. J.; Hadrick, K.; Nafiujjaman, M.; Apu, E. H.; Hill, M. L.; Nurunnabi, M.; Contag, C. H.; Kim, T. Targeted Biodegradable Near-Infrared Fluorescent Nanoparticles for Colorectal Cancer Imaging. *ACS Appl Bio Mater* **2024**. DOI: 10.1021/acsabm.4c00072 From NLM.

(38) Li, L.; Jiang, W.; Luo, K.; Song, H.; Lan, F.; Wu, Y.; Gu, Z. Superparamagnetic iron oxide nanoparticles as MRI contrast agents for non-invasive stem cell labeling and tracking. *Theranostics* **2013**, *3* (8), 595-615. DOI: 10.7150/thno.5366 From NLM.

(39) Goldmann, E.; Górski, M.; Klemczak, B. Recent Advancements in Carbon Nano-Infused Cementitious Composites. *Materials (Basel)* **2021**, *14* (18). DOI: 10.3390/ma14185176 From NLM.

(40) Netea, M. G.; Balkwill, F.; Chonchol, M.; Cominelli, F.; Donath, M. Y.; Giamarellos-Bourboulis, E. J.; Golenbock, D.; Gresnigt, M. S.; Heneka, M. T.; Hoffman, H. M.; et al. A guiding map for inflammation. *Nature Immunology* **2017**, *18*, 826–831.

(41) Furman, D.; Campisi, J.; Verdin, E.; Carrera-Bastos, P.; Targ, S.; Franceschi, C.; Ferrucci, L.; Gilroy, D. W.; Fasano, A.; Miller, G. W.; et al. Chronic inflammation in the etiology of disease across the life span. *Nature Medicine* **2019**, *25*, 1822–1832.

(42) Theoharides, T. C.; Alysandratos, K. D.; Angelidou, A.; Delivanis, D. A.; Sismanopoulos, N.; Zhang, B.; Asadi, S.; Vasiadi, M.; Weng, Z.; Miniati, A.; et al. Mast cells and inflammation. *Biochim Biophys Acta* **2012**, *1822* (1), 21-33. DOI: 10.1016/j.bbadis.2010.12.014 From NLM.

(43) Margraf, A.; Lowell, C. A.; Zarbock, A. Neutrophils in acute inflammation: current concepts and translational implications. *Blood* **2022**, *139* (14), 2130–2144.

(44) Megha, K. B.; Joseph, X.; Akhil, V.; Mohanan, P. V. Cascade of immune mechanism and consequences of inflammatory disorders. *Phytomedicine* **2021**, *91*, 153712. DOI: 10.1016/j.phymed.2021.153712 From NLM.

(45) Seder, R. A.; Ahmed, R. Similarities and differences in CD4+ and CD8+ effector and memory T cell generation. *Nature Immunology* **2003**, *4*, 835–842.

(46) Catalán, D.; Mansilla, M. A.; Ferrier, A.; Soto, L.; Oleinika, K.; Aguillón, J. C.; Aravena, O. Immunosuppressive Mechanisms of Regulatory B Cells. *Front Immunol* **2021**, *12*, 611795. DOI: 10.3389/fimmu.2021.611795 From NLM.

(47) Wang, Y.; Xu, J.; Zhang, X.; Wang, C.; Huang, Y.; Dai, K. TNF-α-induced LRG1 promotes angiogenesis and mesenchymal stem cell migration in the subchondral bone during osteoarthritis. *Cell Death Dis* **2017**, *8* (3), e2715. DOI: 10.1038/cddis.2017.129 From NLM.

(48) Venetsanopoulou, A. I.; Alamanos, Y.; Voulgari, P. V.; Drosos, A. A. Epidemiology and Risk Factors for Rheumatoid Arthritis Development. *Mediterr J Rheumatol* **2023**, *34* (4), 404-413. DOI: 10.31138/mjr.301223.eaf From NLM.

(49) Raharja, A.; Mahil, S. K.; Barker, J. N. Psoriasis: a brief overview. *Clin Med (Lond)* **2021**, *21* (3), 170-173. DOI: 10.7861/clinmed.2021-0257 From NLM.

(50) Henein, M. Y.; Vancheri, S.; Longo, G.; Vancheri, F. The Role of Inflammation in Cardiovascular Disease. *Int J Mol Sci* **2022**, *23* (21). DOI: 10.3390/ijms232112906 From NLM.

(51) George, L.; Brightling, C. E. Eosinophilic airway inflammation: role in asthma and chronic obstructive pulmonary disease. *Ther Adv Chronic Dis* **2016**, *7* (1), 34-51. DOI: 10.1177/2040622315609251 From NLM.

(52) Cornwell, C. R.; Hsu, J.; Tompkins, L. K.; Pennington, A. F.; Flanders, W. D.; Sircar, K. Clinical outcomes among hospitalized US adults with asthma or chronic obstructive pulmonary disease, with or without COVID-19. *J Asthma* **2022**, *59* (12), 2509-2519. DOI: 10.1080/02770903.2021.2018703 From NLM.

(53) Indicators of Environmental Health Disparites: Childhood Asthma Prevalence. EPA.gov, 2023.

(54) Sartori, A. C.; Vance, D. E.; Slater, L. Z.; Crowe, M. The impact of inflammation on cognitive function in older adults: implications for healthcare practice and research. *J Neurosci Nurs* **2012**, *44* (4), 206-217. DOI: 10.1097/JNN.0b013e3182527690 From NLM.

(55) Chen, Y.; Song, Y.; Du, W.; Gong, L.; Chang, H.; Zou, Z. Tumor-associated macrophages: an accomplice in solid tumor progression. *Journal of Biomedical Science* **2019**, *26* (1). DOI: 10.1186/s12929-019-0568-z.

(56) Dropulic, L. K.; Lederman, H. M. Overview of Infections in the Immunocompromised Host. *Microbiol Spectr* **2016**, *4* (4). DOI: 10.1128/microbiolspec.DMIH2-0026-2016 From NLM.

(57) Cryer, B.; Feldman, M. Cyclooxygenase-1 and cyclooxygenase-2 selectivity of widely used nonsteroidal anti-inflammatory drugs. *Am J Med* **1998**, *104* (5), 413-421. DOI: 10.1016/s0002-9343(98)00091-6 From NLM.

(58) Ohashi, N.; Kohno, T. Analgesic Effect of Acetaminophen: A Review of Known and Novel Mechanisms of Action. *Front Pharmacol* **2020**, *11*, 580289. DOI: 10.3389/fphar.2020.580289 From NLM.

(59) Murphy, P. B.; Kasotakis, G.; Haut, E. R.; Miller, A.; Harvey, E.; Hasenboehler, E.; Higgins, T.; Hoegler, J.; Mir, H.; Cantrell, S.; et al. Efficacy and safety of non-steroidal anti-inflammatory drugs (NSAIDs) for the treatment of acute pain after orthopedic trauma: a practice management guideline from the Eastern Association for the Surgery of Trauma and the Orthopedic Trauma Association. *Trauma Surg Acute Care Open* **2023**, *8* (1), e001056. DOI: 10.1136/tsaco-2022-001056 From NLM.

(60) Ghlichloo, I.; Gerriets, V. *Nonsteroidal Anti-Inflammatory Drugs*. StatPearls Publishing, 2023. (accessed 2025).

(61) Agrawal, S.; Khazaeni, B. *Acetaminophen Toxicity*. StatPearls Publishing, 2023. (accessed 2025).

(62) Bindu, S.; Mazumder, S.; Bandyopadhyay, U. Non-steroidal anti-inflammatory drugs (NSAIDs) and organ damage: A current perspective. *Biochem Pharmacol* **2020**, *180*, 114147. DOI: 10.1016/j.bcp.2020.114147 From NLM.

(63) Shagufta; Ahmad, I.; Panda, G. Quest for steroidomimetics: Amino acids derived steroidal and nonsteroidal architectures. *European Journal of Medicinal Chemistry* **2017**, *133*, 139-151.

(64) Hodgens, A.; Sharman, T. *Corticosteroids*. StatPearls Publishing, 2023. (accessed 2025).

(65) Harvey, J.; Lax, S. J.; Lowe, A.; Santer, M.; Lawton, S.; Langan, S. M.; Roberts, A.; Stuart, B.; Williams, H. C.; Thomas, K. S. The long-term safety of topical corticosteroids in atopic dermatitis: A systematic review. *Skin Health Dis* **2023**, *3* (5), e268. DOI: 10.1002/ski2.268 From NLM.

(66) Finnikin, S. J.; Wilcock, J.; Edwards, P. J. Presentation and management of insect bites in out-of-hours primary care: a descriptive study. *BMJ Open* **2023**, *13* (9), e070636. DOI: 10.1136/bmjopen-2022-070636 From NLM.

(67) Coondoo, A.; Phiske, M.; Verma, S.; Lahiri, K. Side-effects of topical steroids: A long overdue revisit. *Indian Dermatol Online J* **2014**, *5* (4), 416-425. DOI: 10.4103/2229-5178.142483 From NLM.

(68) Jones, C. J.; Morris, K. J.; Jayson, M. I. Prednisolone inhibits phagocytosis by polymorphonuclear leucocytes via steroid receptor mediated events. *Ann Rheum Dis* **1983**, *42* (1), 56-62. DOI: 10.1136/ard.42.1.56 From NLM.

(69) Manthorpe, R.; Hansen, T. M.; Junker, P.; Lorenzen, I.; Utne, H. E. Prednisone effect on microvascular permeability in patients with inflammatory rheumatic diseases. *Scand J Rheumatol* **1979**, *8* (3), 139-141. DOI: 10.3109/03009747909114445 From NLM.

(70) Price, D.; Castro, M.; Bourdin, A.; Fucile, S.; Altman, P. Short-course systemic corticosteroids in asthma: striking the balance between efficacy and safety. *Eur Respir Rev* **2020**, *29* (155). DOI: 10.1183/16000617.0151-2019 From NLM.

(71) Boers, M.; Hartman, L.; Opris-Belinski, D.; Bos, R.; Kok, M. R.; Da Silva, J. A.; Griep, E. N.; Klaasen, R.; Allaart, C. F.; Baudoin, P.; et al. Low dose, add-on prednisolone in patients with rheumatoid arthritis aged 65+: the pragmatic randomised, double-blind placebo-controlled GLORIA trial. *Ann Rheum Dis* **2022**, *81* (7), 925-936. DOI: 10.1136/annrheumdis-2021-221957 From NLM.

(72) Yasir, M.; Goyal, A.; Sonthalia, S. *Corticosteroid Adverse Effects*. StatPearls Publishing, 2023. (accessed 2025).

(73) Manubolu, S.; Nwosu, O. Exogenous Cushing's syndrome secondary to intermittent high dose oral prednisone for presumed asthma exacerbations in the setting of multiple emergency department visits. *Journal of Clinical and Translational Endocrinology: Case Reports* **2017**, *6*, 4-8.

(74) Manjiani, D.; Paul, D. B.; Kunnumpurath, S.; Kaye, A. D.; Vadivelu, N. Availability and utilization of opioids for pain management: global issues. *Ochsner J* **2014**, *14* (2), 208-215. From NLM.

(75) Slater, D.; Kunnathil, S.; McBride, J.; Koppala, R. Pharmacology of nonsteroidal antiinflammatory drugs and opioids. *Semin Intervent Radiol* **2010**, *27* (4), 400-411. DOI: 10.1055/s-0030-1267855 From NLM.

(76) Dydyk, A. M.; Jain, N. K.; Gupta, M. *Opioid Use Disorder*. StatPearls Publishing, 2024. (accessed 2025).

(77) Lyle Cooper, R.; Thompson, J.; Edgerton, R.; Watson, J.; MacMaster, S. A.; Kalliny, M.; Huffman, M. M.; Juarez, P.; Mathews-Juarez, P.; Tabatabai, M.; et al. Modeling dynamics of fatal opioid overdose by state and across time. *Prev Med Rep* **2020**, *20*, 101184. DOI: 10.1016/j.pmedr.2020.101184 From NLM.

(78) Awate, S.; Babiuk, L. A.; Mutwiri, G. Mechanisms of action of adjuvants. *Front Immunol* **2013**, *4*, 114. DOI: 10.3389/fimmu.2013.00114 From NLM.

(79) Apostólico Jde, S.; Lunardelli, V. A.; Coirada, F. C.; Boscardin, S. B.; Rosa, D. S. Adjuvants: Classification, Modus Operandi, and Licensing. *J Immunol Res* **2016**, *2016*, 1459394. DOI: 10.1155/2016/1459394 From NLM.

(80) Dong, P.; Gewirtz, D. A. Editorial: Risks and Benefits of Adjuvants to Cancer Therapies. *Front Oncol* **2022**, *12*, 913626. DOI: 10.3389/fonc.2022.913626 From NLM.

(81) Esfahani, K.; Roudaia, L.; Buhlaiga, N.; Del Rincon, S. V.; Papneja, N.; Miller, W. H., Jr. A review of cancer immunotherapy: from the past, to the present, to the future. *Curr Oncol* **2020**, *27* (Suppl 2), S87-s97. DOI: 10.3747/co.27.5223 From NLM.

(82) Pavón-Romero, G. F.; Parra-Vargas, M. I.; Ramírez-Jiménez, F.; Melgoza-Ruiz, E.; Serrano-Pérez, N. H.; Teran, L. M. Allergen Immunotherapy: Current and Future Trends. *Cells* **2022**, *11* (2). DOI: 10.3390/cells11020212 From NLM.

(83) Allen, L. A.; Dayan, C. M. Immunotherapy for type 1 diabetes. *Br Med Bull* **2021**, *140* (1), 76-90. DOI: 10.1093/bmb/ldab027 From NLM.

(84) Boswell, L.; Casals, G.; Blanco, J.; Jiménez, A.; Aya, F.; de Hollanda, A.; Halperin, I.; Arance, A. M.; Mora, M.; Hanzu, F. A. Onset of fulminant type 1 diabetes mellitus following hypophysitis after discontinuation of combined immunotherapy. A case report. *J Diabetes Investig* **2021**, *12* (12), 2263-2266. DOI: 10.1111/jdi.13604 From NLM.

(85) Ventola, C. L. Cancer Immunotherapy, Part 3: Challenges and Future Trends. *P t* **2017**, *42* (8), 514-521. From NLM.

(86) Han, X.; Xu, K.; Taratula, O.; Farsad, K. Applications of nanoparticles in biomedical imaging. *Nanoscale* **2019**, *11* (3), 799-819. DOI: 10.1039/c8nr07769j From NLM.

(87) Haustein, E.; Schwille, P. Trends in fluorescence imaging and related techniques to unravel biological information. *Hfsp j* **2007**, *1* (3), 169-180. DOI: 10.2976/1.2778852 From NLM.

(88) Chen, F.; Ehlerding, E. B.; Cai, W. Theranostic nanoparticles. *J Nucl Med* **2014**, *55* (12), 1919-1922. DOI: 10.2967/jnumed.114.146019 From NLM.

(89) Estelrich, J.; Sánchez-Martín, M. J.; Busquets, M. A. Nanoparticles in magnetic resonance imaging: from simple to dual contrast agents. *Int J Nanomedicine* **2015**, *10*, 1727-1741. DOI: 10.2147/ijn.s76501 From NLM.

(90) Refaat, A.; Yap, M. L.; Pietersz, G.; Walsh, A. P. G.; Zeller, J.; del Rosal, B.; Wang, X.; Peter, K. In vivo fluorescence imaging: success in preclinical imaging paves the way for clinical applications. *Journal of Nanobiotechnology* **2022**, *20*.

(91) Dai, Z. Y.; Shen, C.; Mi, X. Q.; Pu, Q. The primary application of indocyanine green fluorescence imaging in surgical oncology. *Front Surg* **2023**, *10*, 1077492. DOI: 10.3389/fsurg.2023.1077492 From NLM.

(92) Frangioni, J. V. In vivo near-infrared fluorescence imaging. *Curr Opin Chem Biol* **2003**, *7* (5), 626-634. DOI: 10.1016/j.cbpa.2003.08.007 From NLM.

(93) Riksen, J. J. M.; Nikolaev, A. V.; van Soest, G. Photoacoustic imaging on its way toward clinical utility: a tutorial review focusing on practical application in medicine. *J Biomed Opt* **2023**, *28* (12), 121205. DOI: 10.1117/1.jbo.28.12.121205 From NLM.

(94) Steinberg, I.; Huland, D. M.; Vermesh, O.; Frostig, H. E.; Tummers, W. S.; Gambhir, S. S. Photoacoustic clinical imaging. *Photoacoustics* **2019**, *14*, 77-98. DOI: 10.1016/j.pacs.2019.05.001 From NLM.

(95) Su, J. L.; Wang, B.; Wilson, K. E.; Bayer, C. L.; Chen, Y. S.; Kim, S.; Homan, K. A.; Emelianov, S. Y. Advances in Clinical and Biomedical Applications of Photoacoustic Imaging. *Expert Opin Med Diagn* **2010**, *4* (6), 497-510. DOI: 10.1517/17530059.2010.529127 From NLM.

(96) Hill, M. L.; Chung, S. J.; Woo, H. J.; Park, C. R.; Hadrick, K.; Nafiujjaman, M.; Kumar, P. P. P.; Mwangi, L.; Parikh, R.; Kim, T. Exosome-Coated Prussian Blue Nanoparticles for Specific Targeting and Treatment of Glioblastoma. *ACS Appl Mater Interfaces* **2024**, *16* (16), 20286-20301. DOI: 10.1021/acsami.4c02364 From NLM.

(97) Link, S.; Burda, C.; Nikoobakht, B.; El-Sayed, M. A. Laser-Induced Shape Changes of Colloidal Gold Nanorods Using Femtosecond and Nanosecond Laser Pulses. *The Journal of Physical Chemistry B* **2000**, *104* (26).

(98) Deinavizadeh, M.; Kiasat, A. R.; Shafiei, M.; Sabaeian, M.; Mirzajani, R.; Zahraei, S. M.; Khalili, F.; Shao, M.; Wu, A.; Makvandi, P.; et al. Synergistic chemo-photothermal therapy using gold nanorods supported on thiol-functionalized mesoporous silica for lung cancer treatment. *Scientific Reports* **2024**, *14*.

(99) Zhang, W. H.; Hu, X. X.; Zhang, X. B. Dye-Doped Fluorescent Silica Nanoparticles for Live Cell and In Vivo Bioimaging. *Nanomaterials (Basel)* **2016**, *6* (5). DOI: 10.3390/nano6050081 From NLM.

(100) Liu, J.; Liu, Z.; Pang, Y.; Zhou, H. The interaction between nanoparticles and immune system: application in the treatment of inflammatory diseases. *Journal of Nanobiotechnology* **2022**, *20*.

(101) Mitchell, M. J.; Billingsley, M. M.; Haley, R. M.; Wechsler, M. E.; Peppas, N. A.; Langer, R. Engineering precision nanoparticles for drug delivery. *Nat Rev Drug Discov* **2021**, *20* (2), 101-124. DOI: 10.1038/s41573-020-0090-8 From NLM.

(102) Joudeh, N.; Linke, D. Nanoparticle classification, physicochemical properties, characterization, and applications: a comprehensive review for biologists. *J Nanobiotechnology* **2022**, *20* (1), 262. DOI: 10.1186/s12951-022-01477-8 From NLM.

(103) Kothamasu, P.; Kanumur, H.; Ravur, N.; Maddu, C.; Parasuramrajam, R.; Thangavel, S. Nanocapsules: the weapons for novel drug delivery systems. *Bioimpacts* **2012**, *2* (2), 71-81. DOI: 10.5681/bi.2012.011 From NLM.

(104) Dos Santos da Silva, A.; Dos Santos, J. H. Z. Stöber method and its nuances over the years. *Adv Colloid Interface Sci* **2023**, *314*, 102888. DOI: 10.1016/j.cis.2023.102888 From NLM.

(105) Harun, S. N.; Ahmad, H.; Lim, H. N.; Chia, S. L.; Gill, M. R. Synthesis and Optimization of Mesoporous Silica Nanoparticles for Ruthenium Polypyridyl Drug Delivery. *Pharmaceutics* **2021**, *13* (2). DOI: 10.3390/pharmaceutics13020150 From NLM.

(106) Suk, J. S.; Xu, Q.; Kim, N.; Hanes, J.; Ensign, L. M. PEGylation as a strategy for improving nanoparticle-based drug and gene delivery. *Adv Drug Deliv Rev* **2016**, *99* (Pt A), 28-51. DOI: 10.1016/j.addr.2015.09.012 From NLM.

(107) Andrade, S.; Ramalho, M. J.; Loureiro, J. A.; Pereira, M. C. Liposomes as biomembrane models: Biophysical techniques for drug-membrane interaction studies. *Journal of Molecular Liquids* **2021**, *334*.

(108) Liu, P.; Chen, G.; Zhang, J. A Review of Liposomes as a Drug Delivery System: Current Status of Approved Products, Regulatory Environments, and Future Perspectives. *Molecules* **2022**, *27* (4). DOI: 10.3390/molecules27041372 From NLM.

(109) Khan, A. A.; Allemailem, K. S.; Almatroodi, S. A.; Almatroudi, A.; Rahmani, A. H. Recent strategies towards the surface modification of liposomes: an innovative approach for different clinical applications. *3 Biotech* **2020**, *10* (4), 163. DOI: 10.1007/s13205-020-2144-3 From NLM.

(110) Deshpande, P. P.; Biswas, S.; Torchilin, V. P. Current trends in the use of liposomes for tumor targeting. *Nanomedicine (Lond)* **2013**, *8* (9), 1509-1528. DOI: 10.2217/nnm.13.118 From NLM.

(111) Elumalai, K.; Srinivasan, S.; Shanmugam, A. Review of the efficacy of nanoparticle-based drug delivery systems for cancer treatment. *Biomedical Technology* **2024**, *5*, 109-122.

(112) Anselmo, A. C.; Mitragotri, S. A Review of Clinical Translation of Inorganic Nanoparticles. *Aaps j* **2015**, *17* (5), 1041-1054. DOI: 10.1208/s12248-015-9780-2 From NLM.

(113) DeNardo, G. L.; DeNardo, S. J. Update: Turning the heat on cancer. *Cancer Biother Radiopharm* **2008**, *23* (6), 671-680. DOI: 10.1089/cbr.2008.0591 From NLM.

(114) Glazer, E. S.; Curley, S. A. The ongoing history of thermal therapy for cancer. *Surg Oncol Clin N Am* **2011**, *20* (2), 229-235, vii. DOI: 10.1016/j.soc.2010.11.001 From NLM.

(115) Russell, P.; Hagemeyer, C. E.; Esser, L.; Voelcker, N. H. Theranostic nanoparticles for the management of thrombosis. *Theranostics* **2022**, *12* (6), 2773-2800. DOI: 10.7150/thno.70001 From NLM.

(116) Sahli, C.; Moya, S. E.; Lomas, J. S.; Gravier-Pelletier, C.; Briandet, R.; Hémadi, M. Recent advances in nanotechnology for eradicating bacterial biofilm. *Theranostics* **2022**, *12* (5), 2383-2405. DOI: 10.7150/thno.67296 From NLM.

(117) Zhang, Y.; Zhan, X.; Xiong, J.; Peng, S.; Huang, W.; Joshi, R.; Cai, Y.; Liu, Y.; Li, R.; Yuan, K.; et al. Temperature-dependent cell death patterns induced by functionalized gold nanoparticle photothermal therapy in melanoma cells. *Scientific Reports* **2018**, *8*.

(118) Rock, K. L.; Kono, H. The inflammatory response to cell death. *Annu Rev Pathol* **2008**, *3*, 99-126. DOI: 10.1146/annurev.pathmechdis.3.121806.151456 From NLM.

(119) Zhuang, J.; Holay, M.; Park, J. H.; Fang, R. H.; Zhang, J.; Zhang, L. Nanoparticle Delivery of Immunostimulatory Agents for Cancer Immunotherapy. *Theranostics* **2019**, *9* (25), 7826-7848. DOI: 10.7150/thno.37216 From NLM.

(120) Nsairat, H.; Khater, D.; Sayed, U.; Odeh, F.; Al Bawab, A.; Alshaer, W. Liposomes: structure, composition, types, and clinical applications. *Heliyon* **2022**, *8* (5), e09394. DOI: 10.1016/j.heliyon.2022.e09394 From NLM.

(121) Schwendener, R. A. Liposomes as vaccine delivery systems: a review of the recent advances. *Ther Adv Vaccines* **2014**, *2* (6), 159-182. DOI: 10.1177/2051013614541440 From NLM.

(122) Tretiakova, D. S.; Vodovozova, E. L. Liposomes as Adjuvants and Vaccine Delivery Systems. *Biochem (Mosc) Suppl Ser A Membr Cell Biol* **2022**, *16* (1), 1-20. DOI: 10.1134/s1990747822020076 From NLM.

(123) Tenchov, R.; Bird, R.; Curtze, A. E.; Zhou, Q. Lipid Nanoparticles–From Liposomes to mRNA Vaccine Delivery, a Landscape of Research Diversity and Advancement. *ACS Nano* **2021**, *15* (11), 16982-17015. DOI: 10.1021/acsnano.1c04996 From NLM.

(124) Pöyhönen, L.; Bustamante, J.; Casanova, J. L.; Jouanguy, E.; Zhang, Q. Life-Threatening Infections Due to Live-Attenuated Vaccines: Early Manifestations of Inborn Errors of Immunity. *J Clin Immunol* **2019**, *39* (4), 376-390. DOI: 10.1007/s10875-019-00642-3 From NLM.

(125) Deshwal, A.; Saxena, K.; Sharma, G.; Rajesh; Sheikh, F. A.; Seth, C. S.; Tripathi, R. M. Nanozymes: A comprehensive review on emerging applications in cancer diagnosis and

therapeutics. *Int J Biol Macromol* **2024**, *256* (Pt 1), 128272. DOI: 10.1016/j.ijbiomac.2023.128272 From NLM.

(126) Kurup, C. P.; Ahmed, M. U. Nanozymes towards Personalized Diagnostics: A Recent Progress in Biosensing. *Biosensors (Basel)* **2023**, *13* (4). DOI: 10.3390/bios13040461 From NLM.

(127) Zhang, L.; Zhu, J.; Hong, W.; Li, G. Highly sensitive electrochemical detection of cholesterol based on Au-Pt NPs/PAMAM-ZIF-67 nanomaterials. *Anal Sci* **2024**, *40* (1), 37-45. DOI: 10.1007/s44211-023-00427-0 From NLM.

(128) Li, Q.; Liu, Y.; Dai, X.; Jiang, W.; Zhao, H. Nanozymes Regulate Redox Homeostasis in ROS-Related Inflammation. *Front Chem* **2021**, *9*, 740607. DOI: 10.3389/fchem.2021.740607 From NLM.

(129) Huang, X.; He, D.; Pan, Z.; Luo, G.; Deng, J. Reactive-oxygen-species-scavenging nanomaterials for resolving inflammation. *Mater Today Bio* **2021**, *11*, 100124. DOI: 10.1016/j.mtbio.2021.100124 From NLM.

(130) Saifi, M. A.; Seal, S.; Godugu, C. Nanoceria, the versatile nanoparticles: Promising biomedical applications. *Journal of Controlled Release* **2021**, (338), 164-189.

(131) Estevez, A. Y.; Erlichman, J. S. The potential of cerium oxide nanoparticles (nanoceria) for neurodegenerative disease therapy. *Nanomedicine (Lond)* **2014**, *9* (10), 1437-1440. DOI: 10.2217/nnm.14.87 From NLM.

(132) Kim, C. K.; Kim, T.; Choi, I. Y.; Soh, M.; Kim, D.; Kim, Y. J.; Jang, H.; Yang, H. S.; Kim, J. Y.; Park, H. K.; et al. Ceria nanoparticles that can protect against ischemic stroke. *Angew Chem Int Ed Engl* **2012**, *51* (44), 11039-11043. DOI: 10.1002/anie.201203780 From NLM.

(133) Ren, X.; Chen, D.; Wang, Y.; Li, H.; Zhang, Y.; Chen, H.; Li, X.; Huo, M. Nanozymes-recent development and biomedical applications. *Journal of Nanobiotechnology* **2022**, *20* (92).

(134) P, N. N.; Mehla, S.; Begum, A.; Chaturvedi, H. K.; Ojha, R.; Hartinger, C.; Plebanski, M.; Bhargava, S. K. Smart Nanozymes for Cancer Therapy: The Next Frontier in Oncology. *Adv Healthc Mater* **2023**, *12* (25), e2300768. DOI: 10.1002/adhm.202300768 From NLM.

(135) *Cerium*. Royal Society of Chemistry, 2025. (accessed 2025).

(136) Charbgoo, F.; Ahmad, M. B.; Darroudi, M. Cerium oxide nanoparticles: green synthesis and biological applications. *Int J Nanomedicine* **2017**, *12*, 1401-1413. DOI: 10.2147/ijn.s124855 From NLM.

(137) Xu, C.; Qu, X. Cerium oxide nanoparticle: a remarkably versatile rare earth nanomaterial for biological applications. *NPG Asia Materials* **2014**, *6* (3), e90-e90. DOI: 10.1038/am.2013.88.

(138) Gangopadhyay, S.; Frolov, D. D.; Masunov, A. E.; Seal, S. Structure and properties of cerium oxides in bulk and nanoparticulate forms. **2014**, *584*, 199-208.

(139) Hirst, S. M.; Karakoti, A. S.; Tyler, R. D.; Sriranganathan, N.; Seal, S.; Reilly, C. M. Anti-inflammatory properties of cerium oxide nanoparticles. *Small* **2009**, *5* (24), 2848-2856. DOI: 10.1002/smll.200901048 From NLM.

(140) Rajeshkumar, S.; Naik, P. Synthesis and biomedical applications of Cerium oxide nanoparticles – A Review. *Biotechnology Reports* **2018**, *17*, 1-5. DOI: https://doi.org/10.1016/j.btre.2017.11.008.

(141) Yokel, R. A.; Hussain, S.; Garantziotis, S.; Demokritou, P.; Castranova, V.; Cassee, F. R. The Yin: An adverse health perspective of nanoceria: uptake, distribution, accumulation, and mechanisms of its toxicity. *Environ Sci Nano* **2014**, *1* (5), 406-428. DOI: 10.1039/c4en00039k From NLM.

(142) Soo Choi, H.; Liu, W.; Misra, P.; Tanaka, E.; Zimmer, J. P.; Itty Ipe, B.; Bawendi, M. G.; Frangioni, J. V. Renal clearance of quantum dots. *Nature Biotechnology* **2007**, *25* (10), 1165-1170. DOI: 10.1038/nbt1340.

(143) Younis, A.; Chu, D.; Li, S. Cerium Oxide Nanostructures and their Applications. InTech, 2016.

(144) Wu, B.; Wang, J.; Chen, Y.; Fu, Y. Inflammation-Targeted Drug Delivery Strategies via Albumin-Based Systems. *ACS Biomater. Sci. Eng.* **2024**, *10*, 743-761.

(145) Moman, R.; Gupta, N.; Varacallo, M. *Physiology, Albumin*. NIH, 2022. (accessed 2024 4/26/24).

(146) Spada, A.; Emami, J.; Tuszynski, J. A.; Lavasanifar, A. The Uniqueness of Albumin as a Carrier in Nanodrug Delivery. *Mol Pharm* **2021**, *18* (5), 1862-1894. DOI: 10.1021/acs.molpharmaceut.1c00046 From NLM.

(147) Qu, N.; Song, K.; Ji, Y.; Liu, M.; Chen, L.; Lee, R. J.; Teng, L. Albumin Nanoparticle-Based Drug Delivery Systems. *Int J Nanomedicine* **2024**, *19*, 6945-6980. DOI: 10.2147/ijn.s467876 From NLM.

(148) *Nanotubes and Carbon Fibers*. 2022. (accessed 12/7/2022).

(149) Zhang, Y.; Bai, Y.; Yan, B. Functionalized carbon nanotubes for potential medicinal applications. *Drug Discov Today* **2010**, *15* (11-12), 428-435. DOI: 10.1016/j.drudis.2010.04.005 From NLM.

(150) Robinson, J. T.; Hong, G.; Liang, Y.; Zhang, B.; Yaghi, O. K.; Dai, H. In vivo fluorescence imaging in the second near-infrared window with long circulating carbon nanotubes capable of ultrahigh tumor uptake. *J Am Chem Soc* **2012**, *134* (25), 10664-10669. DOI: 10.1021/ja303737a From NLM.

(151) Kobayashi, N.; Izumi, H.; Morimoto, Y. Review of toxicity studies of carbon nanotubes. *J Occup Health* **2017**, *59* (5), 394-407. DOI: 10.1539/joh.17-0089-RA From NLM.

(152) Jin, H.; Heller, D. A.; Sharma, R.; Strano, M. S. Size-Dependent Cellular Uptake and Expulsion of Single-Walled Carbon Nanotubes: Single Particle Tracking and a Generic Uptake Model for Nanoparticles. *ACS Nano* **2009**, *3* (1), 149-158.

(153) Chattopadhyay, J.; de Jesus Cortez, F.; Chakraborty, S.; Slater, N. K. H.; Billups, W. E. Synthesis of Water-Soluble PEGylated Single-Walled Carbon Nanotubes. *Chemistry of Materials* **2006**, *18* (25).

(154) Smith, B. R.; Ghosn, E. E. B.; Rallapalli, H.; Prescher, J. A.; Larson, T.; Herzenberg, L. A.; Gambhir, S. S. Selective uptake of single-walled carbon nanotubes by circulating monocytes for enhanced tumour delivery. *Nature Nanotechnology* **2014**, *9* (6), 481-487. DOI: 10.1038/nnano.2014.62.

(155) Singh, K. R.; Nayak, V.; Sarkar, T.; Singh, R. P. Cerium oxide nanoparticles: properties, biosynthesis and biomedical application. *RSC Adv* **2020**, *10* (45), 27194-27214. DOI: 10.1039/d0ra04736h From NLM.

(156) Bai, Y.; Li, Y.; Tian, L. Advanced Biological Applications of Cerium Oxide Nanozymes in Disease Related to Oxidative Damage. *ACS Omega* **2024**, *9* (8), 8601-8614. DOI: 10.1021/acsomega.3c03661 From NLM.

(157) Baktur, R.; Patel, H.; Kwon, S. Effect of exposure conditions on SWCNT-induced inflammatory response in human alveolar epithelial cells. *Toxicol In Vitro* **2011**, *25* (5), 1153-1160. DOI: 10.1016/j.tiv.2011.04.001 From NLM.

(158) Sheng, Z.; Hu, D.; Zheng, M.; Zhao, P.; Liu, H.; Gao, D.; Gong, P.; Gao, G.; Zhang, P.; Ma, Y.; et al. Smart human serum albumin-indocyanine green nanoparticles generated by programmed assembly for dual-modal imaging-guided cancer synergistic phototherapy. *ACS Nano* **2014**, *8* (12), 12310-12322. DOI: 10.1021/nn5062386 From NLM.

(159) Zanganeh, S.; Li, H.; Kumavor, P. D.; Alqasemi, U.; Aguirre, A.; Mohammad, I.; Stanford, C.; Smith, M. B.; Zhu, Q. Photoacoustic imaging enhanced by indocyanine green-conjugated single-wall carbon nanotubes. *J Biomed Opt* **2013**, *18* (9), 096006. DOI: 10.1117/1.jbo.18.9.096006 From NLM.

(160) De la Zerda, A.; Zavaleta, C.; Keren, S.; Vaithilingam, S.; Bodapati, S.; Liu, Z.; Levi, J.; Smith, B. R.; Ma, T. J.; Oralkan, O.; et al. Carbon nanotubes as photoacoustic molecular imaging agents in living mice. In *Nat Nanotechnol*, Vol. 3; 2008; pp 557-562.

(161) Hong, G.; Dai, H. In Vivo Fluorescence Imaging in the Second Near-Infrared Window Using Carbon Nanotubes. *Methods Mol Biol* **2016**, *1444*, 167-181. DOI: 10.1007/978-1-4939-3721-9_15 From NLM.

(162) Chen, S.; Saeed, A.; Liu, Q.; Jiang, Q.; Xu, H.; Xiao, G. G.; Rao, L.; Duo, Y. Macrophages in immunoregulation and therapeutics. *Signal Transduct Target Ther* **2023**, *8* (1), 207. DOI: 10.1038/s41392-023-01452-1 From NLM.

(163) Zhang, Y.; Zou, J.; Chen, R. An M0 macrophage-related prognostic model for hepatocellular carcinoma. *BMC Cancer* **2022**, *22*

(164) Yunna, C.; Mengru, H.; Lei, W.; Weidong, C. Macrophage M1/M2 polarization. *Eur J Pharmacol* **2020**, *877*, 173090. DOI: 10.1016/j.ejphar.2020.173090 From NLM.

(165) Murray, P. J. Macrophage Polarization. *Annu Rev Physiol* **2017**, *79*, 541-566. DOI: 10.1146/annurev-physiol-022516-034339 From NLM.

(166) Wu, Y.; Yang, Z.; Cheng, K.; Bi, H.; Chen, J. Small molecule-based immunomodulators for cancer therapy. *Acta Pharm Sin B* **2022**, *12* (12), 4287-4308. DOI: 10.1016/j.apsb.2022.11.007 From NLM.

(167) Duan, Z.; Luo, Y. Targeting macrophages in cancer immunotherapy. *Signal Transduction and Targeted Therapy* **2021**, *6* (1). DOI: 10.1038/s41392-021-00506-6 (accessed 2023-02-09T16:21:20).

(168) Ruiz, R.; Kirk, A. D. Long-Term Toxicity of Immunosuppressive Therapy. In *Transplantation of the Liver*, Copyright © 2015 Elsevier Inc. All rights reserved., 2015; pp 1354-1363.

(169) Li, J.; Wen, J.; Li, B.; Li, W.; Qiao, W.; Shen, J.; Jin, W.; Jiang, X.; Yeung, K. W. K.; Chu, P. K. Valence State Manipulation of Cerium Oxide Nanoparticles on a Titanium Surface for Modulating Cell Fate and Bone Formation. *Adv Sci (Weinh)* **2018**, *5* (2), 1700678. DOI: 10.1002/advs.201700678 From NLM.

(170) Corsi, F.; Deidda Tarquini, G.; Urbani, M.; Bejarano, I.; Traversa, E.; Ghibelli, L. The Impressive Anti-Inflammatory Activity of Cerium Oxide Nanoparticles: More than Redox? *Nanomaterials (Basel)* **2023**, *13* (20). DOI: 10.3390/nano13202803 From NLM.

(171) Qu, C.; Wang, L.; He, J.; Tan, J.; Liu, W.; Zhang, S.; Zhang, C.; Wang, Z.; Jiao, S.; Liu, S.; et al. Carbon nanotubes provoke inflammation by inducing the pro-inflammatory genes IL-1β and IL-6. *Gene* **2012**, *493* (1), 9-12. DOI: 10.1016/j.gene.2011.11.046 From NLM.

(172) Pinals, R. L.; Yang, D.; Lui, A.; Cao, W.; Landry, M. P. Corona Exchange Dynamics on Carbon Nanotubes by Multiplexed Fluorescence Monitoring. *J Am Chem Soc* **2020**, *142* (3), 1254-1264. DOI: 10.1021/jacs.9b09617 From NLM.

(173) Andreu, N.; Phelan, J.; de Sessions, P. F.; Cliff, J. M.; Clark, T. G.; Hibberd, M. L. Primary macrophages and J774 cells respond differently to infection with Mycobacterium tuberculosis. *Sci Rep* **2017**, *7*, 42225. DOI: 10.1038/srep42225 From NLM.

(174) Herb, M.; Schatz, V.; Hadrian, K.; Hos, D.; Holoborodko, B.; Jantsch, J.; Brigo, N. Macrophage variants in laboratory research: most are well done, but some are RAW. *Front Cell Infect Microbiol* **2024**, *14*, 1457323. DOI: 10.3389/fcimb.2024.1457323 From NLM.

(175) Yang, J.; Zhang, L.; Yu, C.; Yang, X. F.; Wang, H. Monocyte and macrophage differentiation: circulation inflammatory monocyte as biomarker for inflammatory diseases. *Biomark Res* **2014**, *2* (1), 1. DOI: 10.1186/2050-7771-2-1 From NLM.

(176) Brand, D. D.; Latham, K. A.; Rosloniec, E. F. Collagen-induced arthritis. *Nature Protocols* **2007**, *2* (5), 1269-1275. DOI: 10.1038/nprot.2007.173.

(177) Vercellini, P.; Viganò, P.; Somigliana, E.; Fedele, L. Endometriosis: pathogenesis and treatment. *Nat Rev Endocrinol* **2014**, *10* (5), 261-275. DOI: 10.1038/nrendo.2013.255 From NLM.

(178) Ellis, K.; Munro, D.; Clarke, J. Endometriosis Is Undervalued: A Call to Action. *Front Glob Womens Health* **2022**, *3*, 902371. DOI: 10.3389/fgwh.2022.902371 From NLM.

(179) Zondervan Krina, T.; Becker Christian, M.; Missmer Stacey, A. Endometriosis. *New England Journal of Medicine* **2020**, *382*.

(180) Chapron, C.; Marcellin, L.; Borghese, B.; Santulli, P. Rethinking mechanisms, diagnosis and management of endometriosis. *Nat Rev Endocrinol* **2019**, *15* (11), 666-682. DOI: 10.1038/s41574-019-0245-z From NLM.

(181) Guo, S. W. Recurrence of endometriosis and its control. *Hum Reprod Update* **2009**, *15* (4), 441-461. DOI: 10.1093/humupd/dmp007 From NLM.

(182) Zou, G.; Wang, J.; Xu, X.; Xu, P.; Zhu, L.; Yu, Q.; Peng, Y.; Guo, X.; Li, T.; Zhang, X. Cell subtypes and immune dysfunction in peritoneal fluid of endometriosis revealed by single-cell RNA-sequencing. *Cell & Bioscience* **2021**, *11*.

(183) Yoo, J. Y.; Jeong, J. W.; Fazleabas, A. T.; Tayade, C.; Young, S. L.; Lessey, B. A. Protein Inhibitor of Activated STAT3 (PIAS3) Is Down-Regulated in Eutopic Endometrium of Women with Endometriosis. *Biol Reprod* **2016**, *95* (1), 11. DOI: 10.1095/biolreprod.115.137158 From NLM.

(184) Vallvé-Juanico, J.; Houshdaran, S.; Giudice, L. C. The endometrial immune environment of women with endometriosis. *Hum Reprod Update* **2019**, *25* (5), 564-591. DOI: 10.1093/humupd/dmz018 From NLM.

(185) Le, N.; Cregger, M.; Fazleabas, A.; Braundmeier-Fleming, A. Effects of endometriosis on immunity and mucosal microbial community dynamics in female olive baboons. *Sci Rep* **2022**, *12* (1), 1590. DOI: 10.1038/s41598-022-05499-y From NLM.

(186) Slabe, N.; Meden-Vrtovec, H.; Verdenik, I.; Kosir-Pogacnik, R.; Ihan, A. Cytotoxic T-Cells in Peripheral Blood in Women with Endometriosis. *Geburtshilfe Frauenheilkd* **2013**, *73* (10), 1042-1048. DOI: 10.1055/s-0033-1350702 From NLM.

(187) Zhang, D.; Yu, Y.; Duan, T.; Zhou, Q. The role of macrophages in reproductive-related diseases. *Heliyon* **2022**, *8* (11), e11686. DOI: 10.1016/j.heliyon.2022.e11686 From NLM.

(188) Kobayashi, H.; Imanaka, S. Understanding the molecular mechanisms of macrophage polarization and metabolic reprogramming in endometriosis: A narrative review. *Reprod Med Biol* **2022**, *21* (1), e12488. DOI: 10.1002/rmb2.12488 From NLM.

(189) Kim, B. G.; Yoo, J. Y.; Kim, T. H.; Shin, J. H.; Langenheim, J. F.; Ferguson, S. D.; Fazleabas, A. T.; Young, S. L.; Lessey, B. A.; Jeong, J. W. Aberrant activation of signal transducer and activator of transcription-3 (STAT3) signaling in endometriosis. *Hum Reprod* **2015**, *30* (5), 1069-1078. DOI: 10.1093/humrep/dev050 From NLM.

(190) Nakamura, H.; Kimura, T.; Koyama, S.; Ogita, K.; Tsutsui, T.; Shimoya, K.; Taniguchi, T.; Koyama, M.; Kaneda, Y.; Murata, Y. Mouse model of human infertility: transient and local inhibition of endometrial STAT-3 activation results in implantation failure. *FEBS Lett* **2006**, *580* (11), 2717-2722. DOI: 10.1016/j.febslet.2006.04.029 From NLM.

(191) Kotlyar, A. M.; Mamillapalli, R.; Flores, V. A.; Taylor, H. S. Tofacitinib alters STAT3 signaling and leads to endometriosis lesion regression. *Mol Hum Reprod* **2021**, *27* (4). DOI: 10.1093/molehr/gaab016 From NLM.

(192) Lee, J. H.; Kim, T. H.; Oh, S. J.; Yoo, J. Y.; Akira, S.; Ku, B. J.; Lydon, J. P.; Jeong, J. W. Signal transducer and activator of transcription-3 (Stat3) plays a critical role in implantation via progesterone receptor in uterus. *Faseb j* **2013**, *27* (7), 2553-2563. DOI: 10.1096/fj.12-225664 From NLM.

(193) Bulletti, C.; Coccia, M. E.; Battistoni, S.; Borini, A. Endometriosis and infertility. *J Assist Reprod Genet* **2010**, *27* (8), 441-447. DOI: 10.1007/s10815-010-9436-1 From NLM.

(194) Luo, L.; Zhou, H.; Wang, S.; Pang, M.; Zhang, J.; Hu, Y.; You, J. The Application of Nanoparticle-Based Imaging and Phototherapy for Female Reproductive Organs Diseases. *Small* **2024**, *20* (41), e2207694. DOI: 10.1002/smll.202207694 From NLM.

(195) Huang, Y.; Guo, X.; Wu, Y.; Chen, X.; Feng, L.; Xie, N.; Shen, G. Nanotechnology's frontier in combatting infectious and inflammatory diseases: prevention and treatment.

(196) Asano, S.; Arvapalli, R.; Manne, N. D.; Maheshwari, M.; Ma, B.; Rice, K. M.; Selvaraj, V.; Blough, E. R. Cerium oxide nanoparticle treatment ameliorates peritonitis-induced diaphragm dysfunction. *Int J Nanomedicine* **2015**, *10*, 6215-6225. DOI: 10.2147/ijn.s89783 From NLM.

(197) Manne, N. D.; Arvapalli, R.; Nepal, N.; Shokuhfar, T.; Rice, K. M.; Asano, S.; Blough, E. R. Cerium oxide nanoparticles attenuate acute kidney injury induced by intra-abdominal infection in Sprague-Dawley rats. *J Nanobiotechnology* **2015**, *13*, 75. DOI: 10.1186/s12951-015-0135-z From NLM.

(198) Chaudhury, K.; Babu, K. N.; Singh, A. K.; Das, S.; Kumar, A.; Seal, S. Mitigation of endometriosis using regenerative cerium oxide nanoparticles. *Nanomedicine* **2013**, *9* (3), 439-448. DOI: 10.1016/j.nano.2012.08.001 From NLM.

(199) Saunders, P. T. K.; Whitaker, L. H. R.; Horne, A. W. Endometriosis: Improvements and challenges in diagnosis and symptom management. *Cell Rep Med* **2024**, *5* (6), 101596. DOI: 10.1016/j.xcrm.2024.101596 From NLM.

(200) Gratton, S. M.; Choudhry, A. J.; Vilos, G. A.; Vilos, A.; Baier, K.; Holubeshen, S.; Medor, M. C.; Mercier, S.; Nguyen, V.; Chen, I. Diagnosis of Endometriosis at Laparoscopy: A Validation Study Comparing Surgeon Visualization with Histologic Findings. *J Obstet Gynaecol Can* **2022**, *44* (2), 135-141. DOI: 10.1016/j.jogc.2021.08.013 From NLM.

(201) Han, S.; Lee, D.; Kim, S.; Kim, H. H.; Jeong, S.; Kim, J. Contrast Agents for Photoacoustic Imaging: A Review Focusing on the Wavelength Range. *Biosensors (Basel)* **2022**, *12* (8). DOI: 10.3390/bios12080594 From NLM.

(202) Yoo, J.-Y.; Kim, T. H.; Shin, J.-H.; Marquardt, R. M.; Müller, U.; Fazleabas, A. T.; Young, S. L.; Lessey, B. A.; Yoon, H.-G.; Jeong, J.-W. Loss of MIG-6 results in endometrial progesterone resistance via ERBB2. *Nature Communications* **2022**, *13*.

(203) Selvaraj, V.; Nepal, N.; Rogers, S.; Manne, N. D.; Arvapalli, R.; Rice, K. M.; Asano, S.; Fankhanel, E.; Ma, J. J.; Shokuhfar, T.; et al. Inhibition of MAP kinase/NF-kB mediated signaling and attenuation of lipopolysaccharide induced severe sepsis by cerium oxide nanoparticles. *Biomaterials* **2015**, *59*, 160-171. DOI: 10.1016/j.biomaterials.2015.04.025 From NLM.

(204) Moses, A. S.; Demessie, A. A.; Taratula, O.; Korzun, T.; Slayden, O. D. Nanomedicines for Endometriosis: Lessons Learned from Cancer Research. *Small* **2021**, *17* (7), e2004975. DOI: 10.1002/smll.202004975 From NLM.

(205) Avila-Tavares, R.; Gibran, L.; Brito, L. G. O.; Tavoni, T. M.; Gonçalves, M. O.; Baracat, E. C.; Maranhão, R. C.; Podgaec, S. Pilot study of treatment of patients with deep infiltrative

endometriosis with methotrexate carried in lipid nanoparticles. *Arch Gynecol Obstet* **2024**, *309* (2), 659-667. DOI: 10.1007/s00404-023-07246-8 From NLM.

(206) Zhu, S.; Zhang, J.; Xue, N.; Zhu, X.; Li, F.; Dai, Q.; Qing, X.; Chen, D.; Liu, X.; Wei, Z.; et al. Highly specific neutrophil-mediated delivery of albumin nanoparticles to ectopic lesion for endometriosis therapy. *J Nanobiotechnology* **2023**, *21* (1), 81. DOI: 10.1186/s12951-023-01831-4 From NLM.

(207) Yuan, M.; Ding, S.; Meng, T.; Lu, B.; Shao, S.; Zhang, X.; Yuan, H.; Hu, F. Effect of A-317491 delivered by glycolipid-like polymer micelles on endometriosis pain. *Int J Nanomedicine* **2017**, *12*, 8171-8183. DOI: 10.2147/ijn.s146569 From NLM.

(208) Zhang, Y. N.; Poon, W.; Tavares, A. J.; McGilvray, I. D.; Chan, W. C. W. Nanoparticle-liver interactions: Cellular uptake and hepatobiliary elimination. *J Control Release* **2016**, *240*, 332-348. DOI: 10.1016/j.jconrel.2016.01.020 From NLM.

(209) Feng, Q.; Liu, Y.; Huang, J.; Chen, K.; Huang, J.; Xiao, K. Uptake, distribution, clearance, and toxicity of iron oxide nanoparticles with different sizes and coatings. *Scientific Reports* **2018**, *8*.

(210) Moses, A. S.; Taratula, O. R.; Lee, H.; Luo, F.; Grenz, T.; Korzun, T.; Lorenz, A. S.; Sabei, F. Y.; Bracha, S.; Alani, A. W. G.; et al. Nanoparticle-Based Platform for Activatable Fluorescence Imaging and Photothermal Ablation of Endometriosis. *Small* **2020**, *16* (18), e1906936. DOI: 10.1002/smll.201906936 From NLM.

(211) Aldalawi, A. A.; Suardi, N.; Ahmed, N. M.; Al-Farawn, M. A. S.; Dheyab, M. A.; Jebur, W. I.; Kadhim, F. J. Comparison of Wavelength-Dependent Penetration Depth of 532 nm and 660 nm Lasers in Different Tissue Types. *J Lasers Med Sci* **2023**, *14*, e28. DOI: 10.34172/jlms.2023.28 From NLM.

(212) Bown, S. Phototherapy of tumors. *World Journal of Surgery* **1983**, *7* (6), 700-709.

(213) Joris, I.; Cuénoud, H. F.; Doern, G. V.; Underwood, J. M.; Majno, G. Capillary leakage in inflammation. A study by vascular labeling. *Am J Pathol* **1990**, *137* (6), 1353-1363. From NLM.

(214) Rocha, A. L.; Reis, F. M.; Taylor, R. N. Angiogenesis and endometriosis. *Obstet Gynecol Int* **2013**, *2013*, 859619. DOI: 10.1155/2013/859619 From NLM.

(215) van den Berg, L. L.; Crane, L. M.; van Oosten, M.; van Dam, G. M.; Simons, A. H.; Hofker, H. S.; Bart, J. Analysis of biomarker expression in severe endometriosis and determination of possibilities for targeted intraoperative imaging. *Int J Gynaecol Obstet* **2013**, *121* (1), 35-40. DOI: 10.1016/j.ijgo.2012.10.025 From NLM.

(216) Machado, D. E.; Berardo, P. T.; Palmero, C. Y.; Nasciutti, L. E. Higher expression of vascular endothelial growth factor (VEGF) and its receptor VEGFR-2 (Flk-1) and metalloproteinase-9

(MMP-9) in a rat model of peritoneal endometriosis is similar to cancer diseases. *J Exp Clin Cancer Res* **2010**, *29* (1), 4. DOI: 10.1186/1756-9966-29-4 From NLM.

(217) Siegel, R. L.; Miller, K. D.; Jemal, A. Cancer statistics, 2016. *CA Cancer J Clin* **2016**, *66* (1), 7-30. DOI: 10.3322/caac.21332 From NLM.

(218) Bibbins-Domingo, K.; Grossman, D. C.; Curry, S. J.; Davidson, K. W.; Epling, J. W., Jr.; García, F. A. R.; Gillman, M. W.; Harper, D. M.; Kemper, A. R.; Krist, A. H.; et al. Screening for Colorectal Cancer: US Preventive Services Task Force Recommendation Statement. *Jama* **2016**, *315* (23), 2564-2575. DOI: 10.1001/jama.2016.5989 From NLM.

(219) Rex, D. K.; Johnson, D. A.; Anderson, J. C.; Schoenfeld, P. S.; Burke, C. A.; Inadomi, J. M. American College of Gastroenterology guidelines for colorectal cancer screening 2009 [corrected]. *Am J Gastroenterol* **2009**, *104* (3), 739-750. DOI: 10.1038/ajg.2009.104 From NLM.

(220) Wang, J.; Li, S.; Liu, Y.; Zhang, C.; Li, H.; Lai, B. Metastatic patterns and survival outcomes in patients with stage IV colon cancer: A population-based analysis. *Cancer Med* **2020**, *9* (1), 361-373. DOI: 10.1002/cam4.2673 From NLM.

(221) Ginnerup Pedersen, B.; Rosenkilde, M.; Christiansen, T. E.; Laurberg, S. Extracolonic findings at computed tomography colonography are a challenge. *Gut* **2003**, *52* (12), 1744-1747. DOI: 10.1136/gut.52.12.1744 From NLM.

(222) Imperiale, T. F.; Ransohoff, D. F.; Itzkowitz, S. H.; Levin, T. R.; Lavin, P.; Lidgard, G. P.; Ahlquist, D. A.; Berger, B. M. Multitarget stool DNA testing for colorectal-cancer screening. *N Engl J Med* **2014**, *370* (14), 1287-1297. DOI: 10.1056/NEJMoa1311194 From NLM.

(223) Howard, R.; Machado-Aranda, D. Frailty as a Predictor of Colonoscopic Procedural Risk: Robust Associations from Fragile Patients. In *Dig Dis Sci*, Vol. 63; 2018; pp 3159-3160.

(224) Gimeno-García, A. Z.; Quintero, E. Role of colonoscopy in colorectal cancer screening: Available evidence. *Best Practice & Research Clinical Gastroenterology* **2023**, *66* (101838).

(225) Lee, J. H.; Wang, T. D. Molecular endoscopy for targeted imaging in the digestive tract. *Lancet Gastroenterol Hepatol* **2016**, *1* (2), 147-155. DOI: 10.1016/s2468-1253(16)30027-9 From NLM.

(226) Wang, J. H.; Endsley, A. N.; Green, C. E.; Matin, A. C. Utilizing native fluorescence imaging, modeling and simulation to examine pharmacokinetics and therapeutic regimen of a novel anticancer prodrug. *BMC Cancer* **2016**, *16*, 524. DOI: 10.1186/s12885-016-2508-6 From NLM.

(227) Li, W.; Kaminski Schierle, G. S.; Lei, B.; Liu, Y.; Kaminski, C. F. Fluorescent Nanoparticles for Super-Resolution Imaging. *Chemical Reviews* **2022**, *122* (15), 12495–12543.

(228) Chen, K.; Yan, R.; Xiang, L.; Xu, K. Excitation spectral microscopy for highly multiplexed fluorescence imaging and quantitative biosensing. *Light: Science and Applications* **2021**, *10*

(229) Kasaragod, D. K.; Aizawa, H. Deep ultraviolet fluorescence microscopy of three-dimensional structures in the mouse brain. *Scientific Reports* **2022**, *13*.

(230) Marshall, M. V.; Rasmussen, J. C.; Tan, I. C.; Aldrich, M. B.; Adams, K. E.; Wang, X.; Fife, C. E.; Maus, E. A.; Smith, L. A.; Sevick-Muraca, E. M. Near-Infrared Fluorescence Imaging in Humans with Indocyanine Green: A Review and Update. *Open Surg Oncol J* **2010**, *2* (2), 12-25. DOI: 10.2174/1876504101002010012 From NLM.

(231) Faris, F.; Thorniley, M.; Wickramasinghe, Y.; Houston, R.; Rolfe, P.; Livera, N.; Spencer, A. Non-invasive in vivo near-infrared optical measurement of the penetration depth in the neonatal head. *Clin Phys Physiol Meas* **1991**, *12* (4), 353-358. DOI: 10.1088/0143-0815/12/4/005 From NLM.

(232) Mérian, J.; Gravier, J.; Navarro, F.; Texier, I. Fluorescent nanoprobes dedicated to in vivo imaging: from preclinical validations to clinical translation. *Molecules* **2012**, *17* (5), 5564-5591. DOI: 10.3390/molecules17055564 From NLM.

(233) Morozova, S.; Alikina, M.; Vinogradov, A.; Pagliaro, M. Silicon Quantum Dots: Synthesis, Encapsulation, and Application in Light-Emitting Diodes. *Front Chem* **2020**, *8*, 191. DOI: 10.3389/fchem.2020.00191 From NLM.

(234) Chen, F.; Hableel, G.; Zhao, E. R.; Jokerst, J. V. Multifunctional nanomedicine with silica: Role of silica in nanoparticles for theranostic, imaging, and drug monitoring. *Journal of Colloid and Interface Science* **2018**, *521*, 261-279.

(235) Gubala, V.; Giovannini, G.; Kunc, F.; Monopoli, M. P.; Moore, C. J. Dye-doped silica nanoparticles: synthesis, surface chemistry and bioapplications. *Cancer Nanotechnology* **2020**, *11*

(236) Cao, J.; Zhu, B.; Zheng, K.; He, S.; Meng, L.; Song, J.; Yang, H. Recent Progress in NIR-II Contrast Agent for Biological Imaging. *Front. Bioeng. Biotechnol.* **2020**, *7*

(237) Ozawa, H.; Kotake, K.; Hosaka, M.; Hirata, A.; Nakagawa, Y.; Fujita, S.; Sugihara, K. Incorporation of serum carcinoembryonic antigen levels into the prognostic grouping system of colon cancer. *Int J Colorectal Dis* **2017**, *32* (6), 821-829. DOI: 10.1007/s00384-017-2772-1 From NLM.

(238) Becerra, A. Z.; Probst, C. P.; Tejani, M. A.; Aquina, C. T.; González, M. G.; Hensley, B. J.; Noyes, K.; Monson, J. R.; Fleming, F. J. Evaluating the Prognostic Role of Elevated Preoperative Carcinoembryonic Antigen Levels in Colon Cancer Patients: Results from the National Cancer

Database. *Ann Surg Oncol* **2016**, *23* (5), 1554-1561. DOI: 10.1245/s10434-015-5014-1 From NLM.

(239) Hall, C.; Clarke, L.; Pal, A.; Buchwald, P.; Eglinton, T.; Wakeman, C.; Frizelle, F. A Review of the Role of Carcinoembryonic Antigen in Clinical Practice. *Ann Coloproctol* **2019**, *35* (6), 294-305. DOI: 10.3393/ac.2019.11.13 From NLM.

(240) TM, M. W.; Ng, K. W.; Lau, W. M.; Khutoryanskiy, V. V. Silica Nanoparticles in Transmucosal Drug Delivery. *Pharmaceutics* **2020**, *12* (8). DOI: 10.3390/pharmaceutics12080751 From NLM.

(241) An, F. F.; Zhang, X. H. Strategies for Preparing Albumin-based Nanoparticles for Multifunctional Bioimaging and Drug Delivery. *Theranostics* **2017**, *7* (15), 3667-3689. DOI: 10.7150/thno.19365 From NLM.

(242) Stehle, G.; Wunder, A.; Schrenk, H. H.; Hartung, G.; Heene, D. L.; Sinn, H. Albumin-based drug carriers: comparison between serum albumins of different species on pharmacokinetics and tumor uptake of the conjugate. *Anticancer Drugs* **1999**, *10* (8), 785-790. From NLM.

(243) Lim, Y. T.; Kim, S.; Nakayama, A.; Stott, N. E.; Bawendi, M. G.; Frangioni, J. V. Selection of quantum dot wavelengths for biomedical assays and imaging. *Mol Imaging* **2003**, *2* (1), 50-64. DOI: 10.1162/15353500200302163 From NLM.

(244) Galon, J.; Costes, A.; Sanchez-Cabo, F.; Kirilovsky, A.; Mlecnik, B.; Lagorce-Pagès, C.; Tosolini, M.; Camus, M.; Berger, A.; Wind, P.; et al. Type, density, and location of immune cells within human colorectal tumors predict clinical outcome. *Science* **2006**, *313* (5795), 1960-1964. DOI: 10.1126/science.1129139 From NLM.

(245) Liu, L.; Wang, S.; Zhao, B.; Pei, P.; Fan, Y.; Li, X.; Zhang, F. Er(3+) Sensitized 1530 nm to 1180 nm Second Near-Infrared Window Upconversion Nanocrystals for In Vivo Biosensing. *Angew Chem Int Ed Engl* **2018**, *57* (25), 7518-7522. DOI: 10.1002/anie.201802889 From NLM.

(246) Cao, J.; Zhu, B.; Zheng, K.; He, S.; Meng, L.; Song, J.; Yang, H. Recent Progress in NIR-II Contrast Agent for Biological Imaging. *Journal of Nanobiotechnology* **2022**, *20*.

(247) Kim, Y. I.; Jeong, S.; Jung, K. O.; Song, M. G.; Lee, C. H.; Chung, S. J.; Park, J. Y.; Cha, M. G.; Lee, S. G.; Jun, B. H.; et al. Simultaneous Detection of EGFR and VEGF in Colorectal Cancer using Fluorescence-Raman Endoscopy. *Sci Rep* **2017**, *7* (1), 1035. DOI: 10.1038/s41598-017-01020-y From NLM.

(248) Wang, Y. W.; Reder, N. P.; Kang, S.; Glaser, A. K.; Liu, J. T. C. Multiplexed Optical Imaging of Tumor-Directed Nanoparticles: A Review of Imaging Systems and Approaches. *Nanotheranostics* **2017**, *1* (4), 369-388. DOI: 10.7150/ntno.21136 From NLM.

APPENDIX 1: ACHIEVEMENTS OF NOTE

AWARDS AND FELLOWSHIPS

Fitch H. Beach Award for Outstanding Graduate Research	**Spring 2025**
Biomedical Engineering Department Fellowship	**Fall 2024 and Spring 2025**
Graduate Travel Fellowship	**Fall 2024**
GLAMS Molecular Imaging Poster Award	**Summer 2024**
MSU College of Engineering Summer Fellowship	**Summer 2024**
Nucleate Michigan Semi-Finalist	**Summer 2024**
MSU Student Venture Capital Fund Competition Winner	**Spring 2024**
3rd place 3-minute thesis	**Spring 2024**
Dissertation Completion Fellowship	**Spring 2024**
Quentin Whitsitt Graduate Student Leadership Award	**Spring 2024**
Academic Achievement Withrow Fellowship Award	**Spring 2022**
ACS Local Chapter Travel Award	**Fall 2022**
Best Medical Device Concept in MSU Biodesign	**Spring 2021**
Engineering Distinguished Fellowship	**Fall 2020**

PUBLICATIONS

1. P. P. Kumar[†]; S. J. Chung[†]; **K. Hadrick**; M. L. Hill; M. Lee; and T. Kim[*]. Noninvasive Detection and Thermal Ablation Therapy of Endometriosis Using Silica-Coated Gold Nanorods (Submitted)

2. P. P. Kumar; M. Nafiujjaman; A. Makela; **K. Hadrick**; M. L. Hill; M. Lee; and T. Kim[*]. Development of Iron Oxide Nanochains as a Sensitive Magnetic Particle Imaging Tracer for Cancer Detection. *ACS Applied Materials and Interfaces* (Accepted)

3. M. S Rahman[†]; **K. Hadrick**[†]; S. J. Chung; I. Carley; J. Y. Yoo; S. Nahar; T. H. Kim; T. Kim*; and J. W. Jeong[*]. Nanoceria as a non-steroidal anti-inflammatory drug for endometriosis theranostics. *Journal of Controlled Release* **2025**, (378) 1015-1029

4. M. L. Hill; S.J. Chung; H. J. Woo; C Park; **K. Hadrick**; M. Nafiujjaman; P. P. Kumar; L. Mwangi; R. Parikh; and T. Kim[*]. Exosome-Coated Prussian Blue Nanoparticles for Specific Targeting and Treatment of Glioblastoma. *ACS Applied Materials and Interfaces* **2024**, 16(16) 20286-20301

5. S. J. Chung[†]; **K. Hadrick**[†]; M. Nafiujjaman[†]; E. H. Apu; M. L. Hill; M Nunrunnabi; C. H. Contag; and T. Kim[*]; Targeted Biodegradable Near-Infrared Fluorescent Nanoparticles for Colorectal Cancer Imaging *ACS Applied Bio Materials* **2024**, 7(12) 7861–7870

6. H. J. Woo; **K. Hadrick**; and T. Kim[*]. Thermally Induced Morphological and Structural Transformations on Eu $^{2+}$/Eu $^{3+}$ - Coactivated Calcium Silicate Nanophosphors. *ACS Applied Optical Materials* **2024**, 2(3) 445-452

7. H. J. Woo; S. J. Chung; M. L. Hill; **K. Hadrick;** and T. Kim[*]. Europium-Doped Calcium Silicate Nanoparticles as High-Quantum Yield Red-Emitting Phosphors. *ACS Applied Nanomaterials* **2023**, 6(11) 9884-9891

8. A. Vilkins[*], **K. Hadrick**, M. Hakun, C. O'Hern, and S. Sanchez. Enhancing Laparoscopic Education with Use of LaparAssist, a Hands-Free Device Designed to Direct Learners on a Laparoscopic Monitor. *Journal of Minimally Invasive Gynecology* **2022**, 27(11) S110-S111

9. R. M. Marquardt; M. Nafiujjaman; T. H. Kim; S. J. Chung; **K. Hadrick**; T. Kim*; and J. W. Jeong[*]. A Mouse Model of Endometriosis with Nanoparticle Labeling for In Vivo Photoacoustic Imaging. *Reproductive Sciences* **2022**, 29(10) 2947-2959

[†] These authors contributed equally to the work

* Corresponding author

PRESENTATIONS

1. MSU Fitch H. Beach Presentation: **K. Hadrick**, Engineering of an Immunomodulative Nanodrug for Theranostics and Biomedical Applications, East Lansing, MI USA, April 2025 (Oral)

2. HFH Cancer Symposium: S. J. Chung, **K. Hadrick**, M Nafiujjaman, E. H. Apu, M. L. Hill, M. Nunrunnabi, C. H. Contag, and T. Kim, Targeted Biodegradable Near-Infrared Fluorescent Nanoparticles for Colorectal Cancer Imaging, Detroit, MI USA, November 2024 (Poster)

3. BMES 2024: S. J. Chung, **K. Hadrick**, M Nafiujjaman, E. H. Apu, M. L. Hill, M. Nunrunnabi, C. H. Contag, and T. Kim, Targeted Biodegradable Near-Infrared Fluorescent Nanoparticles for Colorectal Cancer Imaging, Baltimore, MD USA, October 2024 (Oral)

4. GLAMS Poster Presentation: S. J. Chung, **K. Hadrick**, M Nafiujjaman, E. H. Apu, M. L. Hill, M. Nunrunnabi, C. H. Contag, and T. Kim, Targeted Biodegradable Near-Infrared Fluorescent Nanoparticles for Colorectal Cancer Imaging, Holland, MI USA, June 2024 (Poster)

5. Nucleate Midwest Pitch Competition: **K. Hadrick**, C. O'Hern, and S. Sanchez, LaparAssist, Chicago, IL USA, May 2024 (Oral)

6. Engineering Graduate Research Symposium 3-minute Thesis: **K. Hadrick**, M. L. Hill, I. Carley, I. Kalashnikova, and T. Kim, Engineered Nanoceria for Macrophage Modulation, East Lansing, MI USA, April 2024 (Oral)

7. Graduate Research Symposium: **K. Hadrick**, M. L. Hill, I. Carley, I. Kalashnikova, and T. Kim, Engineered Nanoceria for Macrophage Modulation, East Lansing, MI USA, March 2024 (Oral)

8. Graduate Research Symposium 3-minute Thesis: **K. Hadrick**, M. L. Hill, I. Carley, I. Kalashnikova, and T. Kim, Engineered Nanoceria for Macrophage Modulation, East Lansing, MI USA, March 2024 (Oral)

9. IQ Research Day: S. J. Chung, **K. Hadrick**, M Nafiujjaman, E. H. Apu, M. L. Hill, M. Nunrunnabi, C. H. Contag, and T. Kim, Targeted Biodegradable Near-Infrared Fluorescent Nanoparticles for Colorectal Cancer Imaging, East Lansing, MI USA, February 2024 (Poster)

10. Biomedical Engineering Society Meeting: **K. Hadrick**, M. L. Hill, I. Carley, I. Kalashnikova, and T. Kim, Engineered Nanoceria with Tuned Surface Valence for Macrophage Modulation, Seattle, WA USA, October 2023 (Oral)

11. MSU Immunology Research Symposium: **K. Hadrick**, I. Carley, S. Chung, M. L. Hill, H. Woo, I. Kalashnikova, and T. Kim Synthesis of Albumin-Nanoceria with Controlled Valence State and Its Effects on Macrophage Differentiation, East Lansing, MI September 2023 (Poster)

12. Engineering Graduate Research Symposium: **K. Hadrick**, I. Carley, S. Chung, M. L. Hill, H. Woo, I. Kalashnikova, and T. Kim Synthesis of Albumin-Nanoceria with Controlled Valence State and Its Effects on Macrophage Differentiation, East Lansing, MI USA, May 2023 (Poster)

13. MSU Imaging Symposium: **K. Hadrick**, I. Carley, S. Chung, M. L. Hill, H. Woo, I. Kalashnikova, and T. Kim Synthesis of Albumin-Nanoceria with Controlled Valence State and Its Effects on Macrophage Differentiation, East Lansing, MI USA, May 2023 (Poster)

14. Nanomedicine Symposium: Materials and Applications: **K. Hadrick**, I. Carley, S. Chung, M. L. Hill, H. Woo, I. Kalashnikova, and T. Kim Synthesis of Albumin-Nanoceria with Controlled Valence State and Its Effects on Macrophage Differentiation, East Lansing, MI USA, May 2023 (Poster)

15. IQ Research Day: **K. Hadrick**, I. Carley, S. Chung, M. L. Hill, H. Woo, I. Kalashnikova, and T. Kim Synthesis of Albumin-Nanoceria with Controlled Valence State and Its Effects on Macrophage Differentiation, East Lansing, MI USA, April 2023 (Poster)

16. MSU Graduate Academic Conference: **K. Hadrick**, Engineered Nanoceria for Immune Modulation, East Lansing, MI USA, April 2023 (Oral)

17. MSU 3 Minute Thesis Competition: **K. Hadrick**, Controlling Albumin-Nanoceria to Control the Immune System, East Lansing, MI USA, March 2023 (Oral)

18. Engineering the Future of Human Health Collaborative Research Symposium: **K. Hadrick**, I. Carley, S. Chung, M. L. Hill, H. Woo, I. Kalashnikova, and T. Kim Synthesis of Albumin Nanoceria with Controlled Valence State and Its Effects on Macrophage Differentiation, Grand Rapids, MI USA, March 2023 (Poster)

19. American Association of Gynecologic Laparoscopists Global Conference on Minimally Invasive Gynecological Surgery: A. Vilkins, **K. Hadrick**, M. Hakun, C. O'Hern, and S. Sanchez, Enhancing Laparoscopic Education with Use of LaparAssist, a Hands-Free Device Designed to Direct Learners on a Laparoscopic Monitor, Aurora, CO USA, December 2022 (Poster)

20. American Chemical Society Meeting: **K. Hadrick**, I. Carley, M. Hill, I. Kalashnikova, and T. Kim, Catalyst-dependent synthesis of albumin-nanoceria to control particle valence state and macrophage differentiation, Chicago, IL USA, August 2022 (Oral)

21. MSU Engineering Graduate Research Symposium: **K. Hadrick**, M. Nafiujjaman, M. L. Hill, C. Park, H. Woo, and T. Kim, Development of Iron Oxide Nanochains for Cancer Imaging with Magnetic Particle Imaging, East Lansing, MI USA, April 2022 (Poster)

22. HFH + MSU Translational Oncology Research Symposium: **K. Hadrick**, M. Nafiujjaman, M. L. Hill, C. Park, H.Woo, and T. Kim Development of Iron Oxide Nanochains for Cancer Imaging with Magnetic Particle Imaging, East Lansing, MI USA, November 2021 (Poster)

23. World Molecular Imaging Congress: **K. Hadrick**, M. Nafiujjaman, M. L. Hill, C. Park, H.Woo, and T. Kim Development of Iron Oxide Nanochains as Sensitive Magnetic Particle Imaging Agents, Miami, FL USA (virtual), October 2021 (oral)

APPENDIX 2: ALTERNATE METHODS ATTEMPTED

Albumin-Nanoceria pH and Catalyst Variations: In the synthesis of albumin nanoceria, pHs from 2-12 were used with and without the addition of hydrogen peroxide in an attempt to create a wider variety of particle subtypes. pHs 2-5 and 12 resulted in large aggregates rather than nanoparticles, pHs 6 and 7 failed to form nanocrystalline cerium oxide that was detectable by HRTEM, and pH 10 too similar to pH 8.5 and pH 11 results to be a useful intermediary for these experiments. The addition of hydrogen peroxide either further destabilized the particles or forced them to be Ce^{3+} dominant, so we used the particles synthesized at pH 8.5 for their superior stability.

Albumin-Nanoceria Reaction Timing: Early on, reactions were run for 15 minutes, 1 hour, 2 hours, 4 hours, and overnight to see if particle yield or quality could be improved. 15 minute and 1 hour synthesis conditions resulted in lower cerium detected in the particles by ICP indicating that this reaction time was insufficient to allow for biomineralization. 2 and 4 hours showed similar amounts of cerium, but the 2-hour particles showed superior stability and smaller size. The overnight reaction produced a foamy albumin aggregate rather than nanoparticles. This motivated the use of the 2-hour reaction time.

SWCNT PEGylation Trials: DSPE-PEG was selected for use with the SWCNT due to its ability to solubilize the hydrophobic SWCNT through hydrophobic interaction between the PEG and the SWCNT. Early on, many ratios of PEG to SWCNT were explored. 1:1, 1:5, 1:10, and 1:50 were tested. The 1:1 ratio was insufficient to solubilize the SWCNT resulting in a thick, black solution with many SWCNT aggregates that were too large to be taken up by a micropipette. 1:5, 1:10, and 1:50 ratios all solubilized the SWCNT, however, it was clear that we were removing excess

PEG during washing for the 1:10 and 1:50 conditions, so we chose 1:5 moving forward.

Additionally, sonication time was found to be very important to the successful, stable

PEGylation of the particles. Under-sonication and over-sonication both resulted in the

aggregation of particles with under-sonication also resulting in nanotubes that were too long to

safely use in living organisms. When 2, 4-, 6-, 12-, and 16-hour sonication times (after the

combining of PEG and SWCNT) were explored, 6 hours of sonication produced the most uniform

and stable particles of appropriate size.

Temperature For Nanoceria Formulations: Due to the delicate nature of the substrates used in

the production of the nanoceria formulations presented here, care must be taken to prevent

damage to the substrate while still allowing for efficient formation of cerium-oxide nanocrystals.

For both albumin and SWCNT, room temperature, 40°C, 60°C, and 80°C were evaluated. Colder

and hotter temperatures were excluded due to the reduced reaction rate at low temperature

and the boiling point of water being 100°C. For both the albumin and SWCNT, 40°C proved to be

the idea temperature to perform synthesis. At room temperature, the reaction was less

vigorous resulting in a less Ce dense particle. At higher temperatures, we start to see the

albumin protein denaturing and appearing cooked and the SWCNT begin to aggregate.

FSN Reaction Time: Three sizes of FSN were used in Chapter 5, however, two others were also

created with reaction times of 15 minutes and 3 hours respectively. The particles with the 15-

minute reaction time were smaller than 50 nm but were more polydisperse and had a less

uniform, rounded shape. This combined with the tendency of small particles to be efficiently

cleared led us to exclude them from the study. The particles with a 3-hour reaction time were

around 300 nm and were simply too large to be of interest for our studies.